AD NUMBER

AD911497

NEW LIMITATION CHANGE

TO

Approved for public release, distribution unlimited

FROM

Distribution authorized to U.S. Gov't. agencies only; Test and Evaluation; JUL 1973. Other requests shall be referred to Army Safeguard Systems Command, Attn: SSC-WES, Huntsville, AL 35807.

AUTHORITY

USASSC ltr, 2 May 1974

GULF RADIATION TECHNOLOGY

Gulf-RT-C12566

EFFECTS OF IONIZING RADIATION ON TANTALUM CAPACITORS

Subtask Final Report

Prepared for
BELL LABORATORIES
under
Contract 606258

army Safeguard System
Comd attn SSC-WES
Huntsville, Ala 35807

March 30, 1973

GULF RADIATION TECHNOLOGY
A DIVISION OF GULF ENERGY & ENVIRONMENTAL SYSTEMS COMPANY
P.O. BOX 608, SAN DIEGO, CALIFORNIA 92112

GULF RADIATION TECHNOLOGY

Gulf-RT-C12566

EFFECTS OF IONIZING RADIATION ON TANTALUM CAPACITORS

Work done by:
Project Staff

Report written by:
T. Flanagan

Bell Laboratories
Contract 606258
Rad Tech Project 0301

March 30, 1973

GULF RADIATION TECHNOLOGY
A DIVISION OF GULF ENERGY & ENVIRONMENTAL SYSTEMS COMPANY
P.O. BOX 608, SAN DIEGO, CALIFORNIA 92112

CONTENTS

TABLES

FIGURES

FIGURES (Cont'd)

FIGURES (Cont'd)

1. INTRODUCTION

When tantalum capacitors are irradiated with ionizing radiation, electrons and holes are excited into mobile states. The excess mobile carriers in the tantalum and the MnO_2 contacts quickly recombine, but the excess carriers in the Ta_2O_5 dielectric persist for some time in mobile states. The effects and time histories of the excess carriers produced by the irradiation of tantalum capacitors have been studied previously (Ref. 1). The radiation induced discharge of tantalum capacitors with several volts initial bias have been explained by a radiation-induced conductivity mechanism in the Ta_2O_5 dielectric. In recent work (Ref. 1, 8), the explanation was extended to include the radiation-induced voltage buildup across initially unbiased tantalum capacitors by considering equilibrium band-bending in the Ta_2O_5 caused by the work function difference between the tantalum and the manganese dioxide counterelectrode. Experiments at Bell Laboratories using low dose rates and at Gulf Radiation Technology using a pulsed linear accelerator have verified a proposed model.

To obtain parameter characterizations on a population of capacitors and to define the variability of response within the population, this proposed model has been applied to capacitors under a variety of conditions in the present work. The present study is concerned with dry slug tantalum capacitors with working voltage between 6 and 50 volts. Except for two experiments discussed in the next section, capacitors were not reverse-biased. The temperature range of interest was from 25 to 85°C.

The purposes of this study were to:

1. Provide methods for the radiation characterization of tantalum capacitors.
2. Perform parametric studies to measure the applicable responses of capacitors under those conditions of interest to the Safeguard system.

3. To provide methods to eliminate maverick capacitors from the populations of Safeguard system capacitors.
4. To provide a circuit model with appropriate parameters for tantalum capacitor responses.

This report describes the results of current effort on these four points.

Summary and Conclusions

1. Mavericks

Maverick radiation response in capacitors is caused by charge injection and storage within the oxide. While there are always sufficient traps to store charge in the oxide, for most capacitors significant injection of charge does not occur at the electrodes when bias of the correct polarity is applied. In a few capacitors, one or both electrodes do not block adequately and charge can be injected and trapped in the Ta_2O_5. Ionizing radiation releases this trapped charge, and the charge can then move under the influence of the built-in bias plus the space-charge field, producing an anomalously large zero-bias radiation transient. Capacitors which can readily store charge can be eliminated from the population by application of the appropriate electrical screen. Once a population has been screened, indications are that the introduction rate of maverick capacitors under normal use conditions, including a screening dose of radiation, is about the same as the failure rate due to aging.

Proscription: The only way found to produce mavericks with high frequency of occurrance in the laboratory is through the application of reverse bias. Thus, the application of significant reverse bias to single capacitors to be used in low-bias applications or to back-to-back pairs is to be avoided, in both manufacture and checkout of circuits.

2. Back-to-Back Pairs

The model of the back-to-back pair response as the sum of two single-capacitor responses agrees with the results obtained; there are no synergistic effects in the ionized response. The pair response is nonlinear in dose, with decreasing response per unit dose for increasing doses. It is concluded that, for cases within reasonable limits of feasibility, screening at low doses is appropriate.

3. Parametric Studies

The capacitor response is dependent on the dose deposited in the Ta_2O_5 and is independent of spectrum. The response per unit dose is linear in the applied voltage over the range of voltages of interest. The response per unit dose is larger for larger working-voltage capacitors, and the temperature dependence of the response is also larger for larger-working-voltage capacitors. The voltage on a capacitor without recharge decays exponentially or slightly slower with the dose.

4. Circuit Models

Circuit models using current generators of various complexities are derived from the experimental data. The delayed components are described in terms of the external load. A load independent model appears possible but was not pursued under the present program.

2. EXPERIMENTS

The capacitors examined in this program all conformed to the general requirements for solid electrolyte tantalum capacitors incorporated into Safeguard system drawings (Ref. 2). Sprague, Kemet, and Mallory capacitors were examined. Since the Mallory capacitors became available only late in the study, most testing was performed on the Sprague and Kemet capacitors.

The ionization testing of Ta_2O_5 capacitors was performed using 4.5-μsec pulses of electrons of 35 to 40 MeV energy from the Gulf Rad Tech Linear Accelerator (Linac) as an ionizing source. The experimental arrangement for the radiation experiments is diagrammed in Figure 1. In Figure 1 the beam enters from the left, passes through a collimator with a secondary emission foil beam intensity monitor, and is scattered to provide uniform illumination of the sample. For calibration, a thin calorimeter is placed at the sample position and the dose from this calorimeter is placed at the sample position and the dose from this calorimeter is compared with the foil monitor signal, which is recorded for each Linac pulse during the test.

Two separate test fixtures were employed during the course of the experiments, and while the test fixture used in the latter portion of the experiments had a larger sample carrying capacity, both test fixtures were quite similar. Hence, only the latter fixture will be described.

The capacitors to be tested were mounted on fiberglass wheels which can hold up to 60 parallel-pair capacitors or 36 back-to-back pairs. The wheel was mounted in a vacuum chamber which contains a drive mechanism for positioning the wheel and electrical contact and switching mechanisms to bring leads from the sample under test out to the measuring circuitry. The schematic of the measuring circuit is shown in Figure 2. Figures 3 and 4 show methods of installing the capacitors on the wheel. The

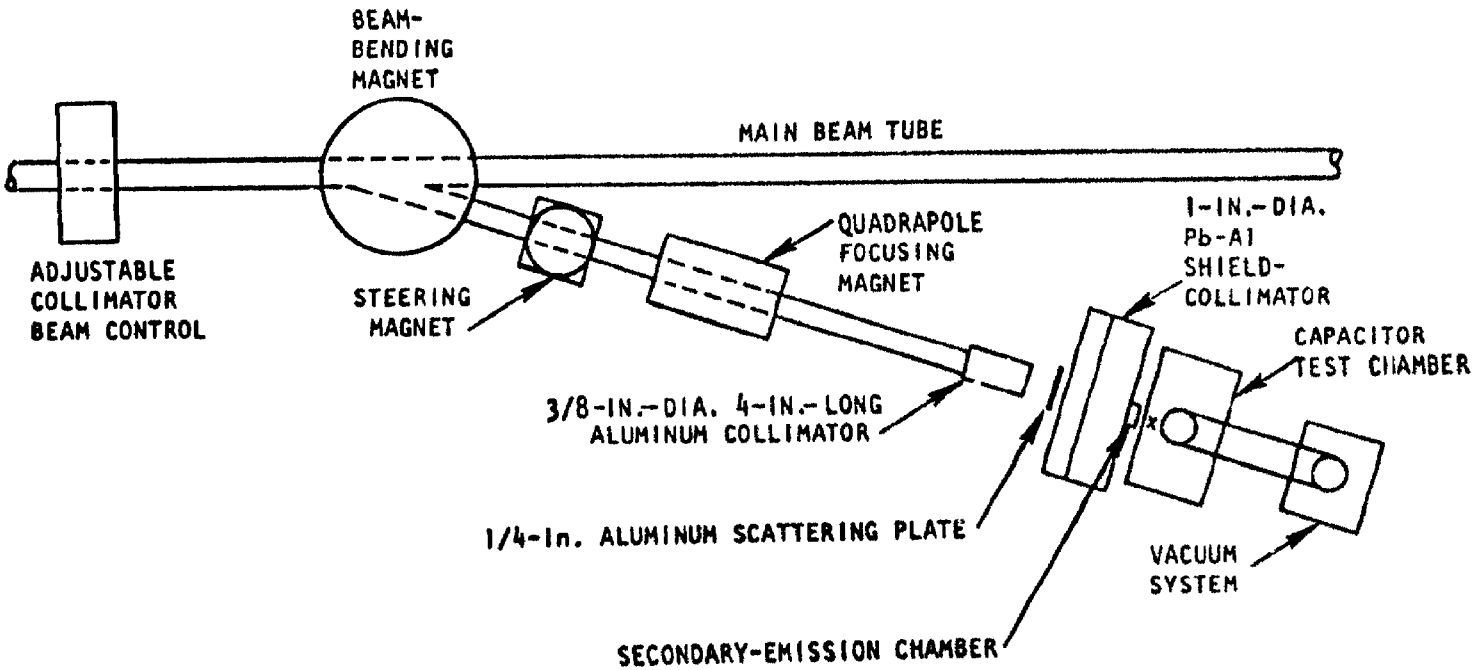

Figure 1. Test configuration during testing of Ta_2O_5 capacitors

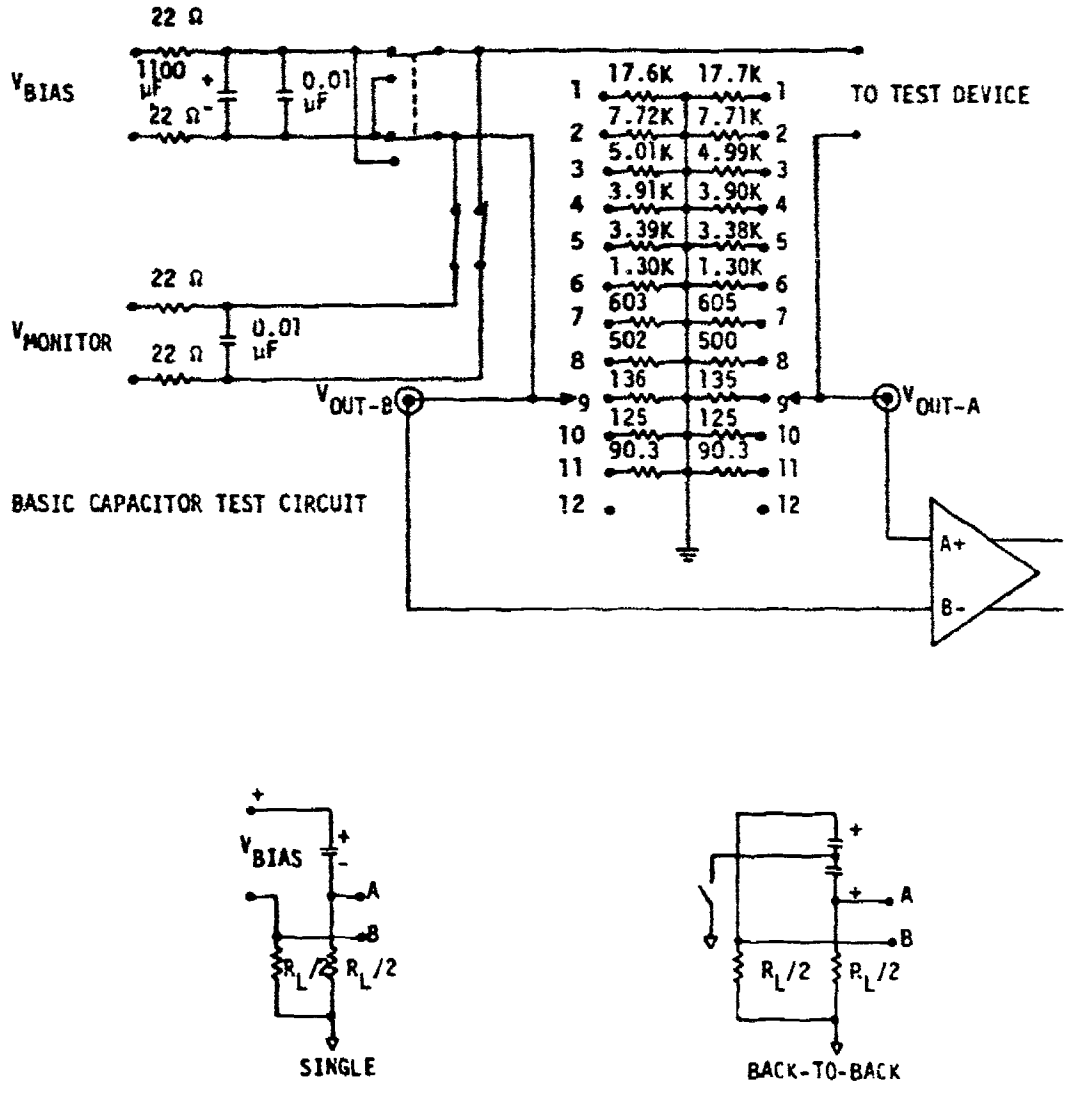

RT-02086

Figure 2. Schematic of capacitor test circuit and simplified diagrams of test circuits

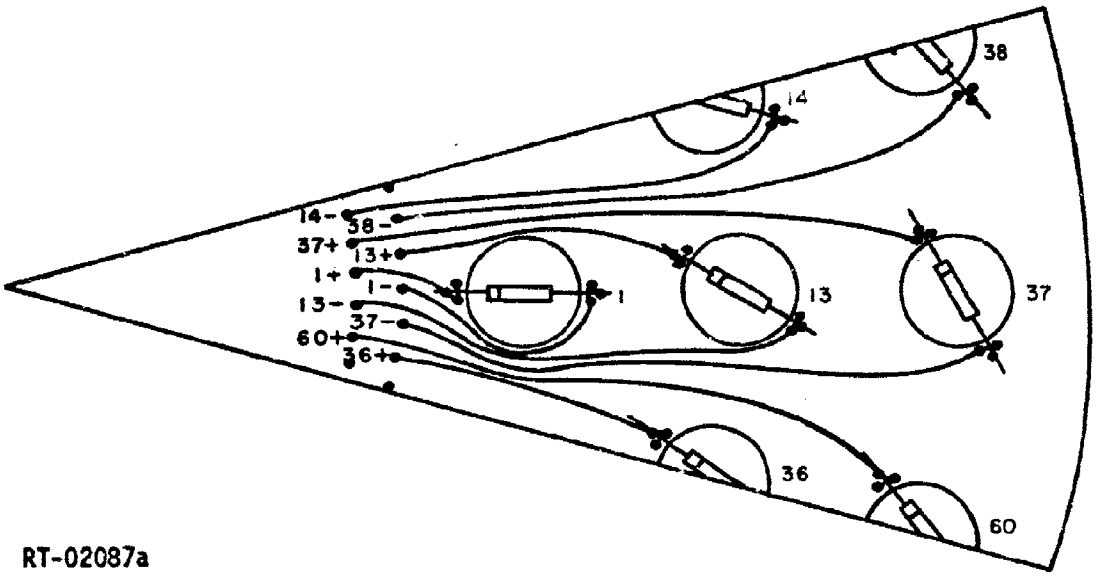

RT-02087a

Figure 3. Capacitor positioning for biased single capacitor tests

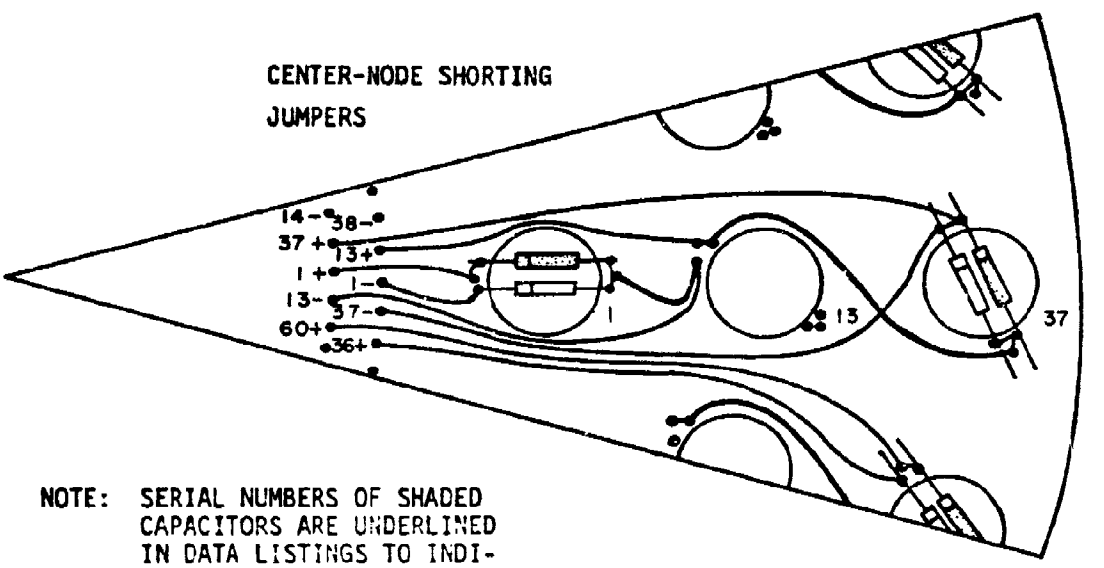

NOTE: SERIAL NUMBERS OF SHADED CAPACITORS ARE UNDERLINED IN DATA LISTINGS TO INDICATE CAPACITOR TIED TO -B AMPLIFIER UNIT.

RT-02088

Figure 4. Capacitor positioning for back-to-back pairs

position of the wheel can be remotely selected to position any of the capacitors in front of the Linear accelerator beam. The entire vacuum chamber can be heated from room temperature to above 85°C. The temperature is monitored with a copper constantan thermocouple mounted inside the chamber in position to contact the test wheel. The vacuum is monitored with a thermocouple gauge. A more complete description of the test and test procedures is given in Appendix A of this report.

3. THE SEARCH FOR MAVERICKS

During previous studies of capacitors, it was noted that a certain percentage of capacitors produced zero-bias responses which were larger than expected on the basis of the statistical distribution of response. Capacitors with large responses outside the distribution of normal capacitors were dubbed mavericks. Since it is desirable to eliminate mavericks from the capacitor population, initial efforts in this study devoted to

1. Characterizing the mechanism for a maverick behavior, and
2. Examining ways in which mavericks could be eliminated from the populations.

The most likely mechanism for maverick behavior is charge stored in the oxide of the capacitor. The charge can be subsequently released by irradiation. To test this hypothesis, 180 capacitors were obtained and examined for their zero-bias response. In the 180 capacitors, there were 30 each 6.8-μF, 6-W.V., and 50-W.V. Sprague, Kemet, and Mallory capacitors. All were measured at 25°C. The results are shown in the statistical plots in Figures 5, 6, and 7. As can be seen from these plots, no mavericks appeared in these populations; a single statistical distribution is noted for each population, with the possible exception of the 50-W.V. Mallory capacitors. Hence, for capacitors as received from the manufacturer, there is a low frequency of maverick capacitors.

During some tests of circuit boards, McDonnell Douglas Corporation noted a response which indicated a capacitor peak response of about 20 mV per krad with a decay time of about 3 times the RC time constant of the circuit. If this behavior was due to the storage of charge within the oxide, then it should be producible artificially in a laboratory by inducing space-charge polarization of the dielectric.

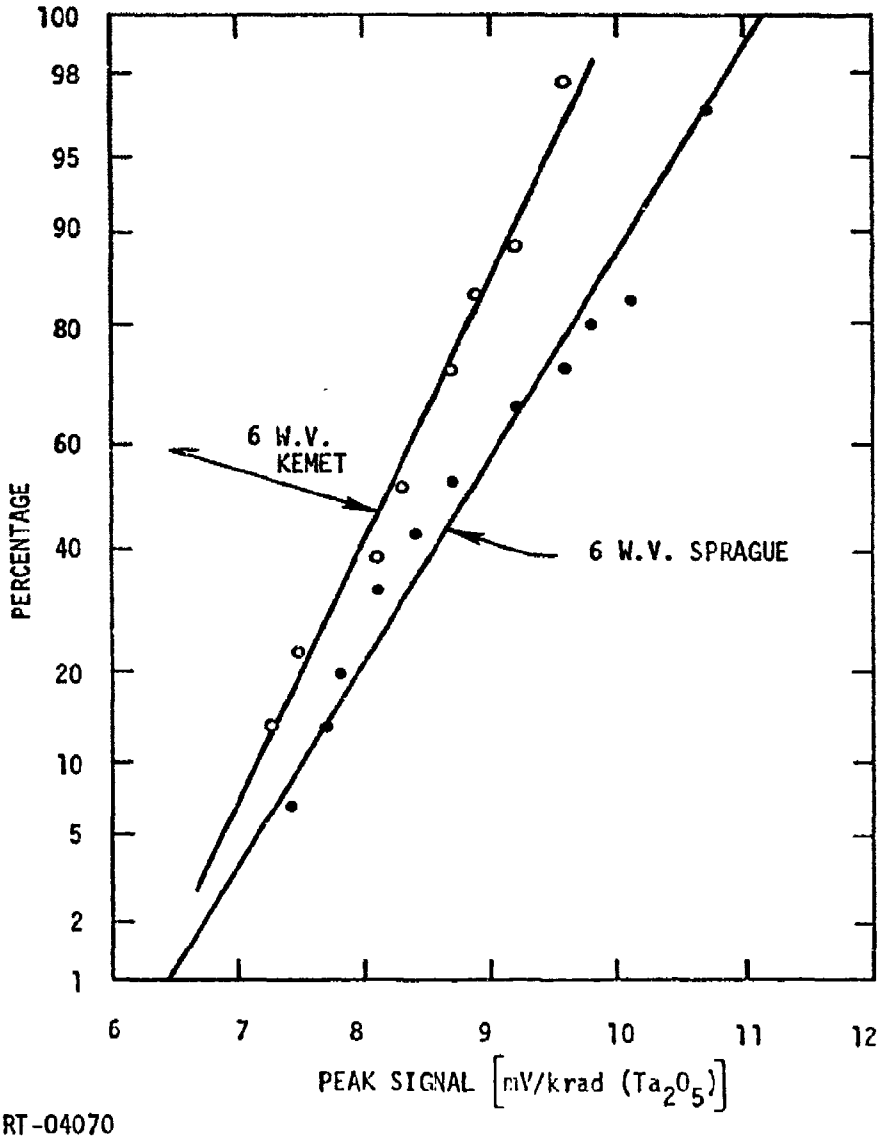

Figure 5. Cumulative frequency distribution for zero bias responses in 6-W.V. Sprague and Kemet capacitors

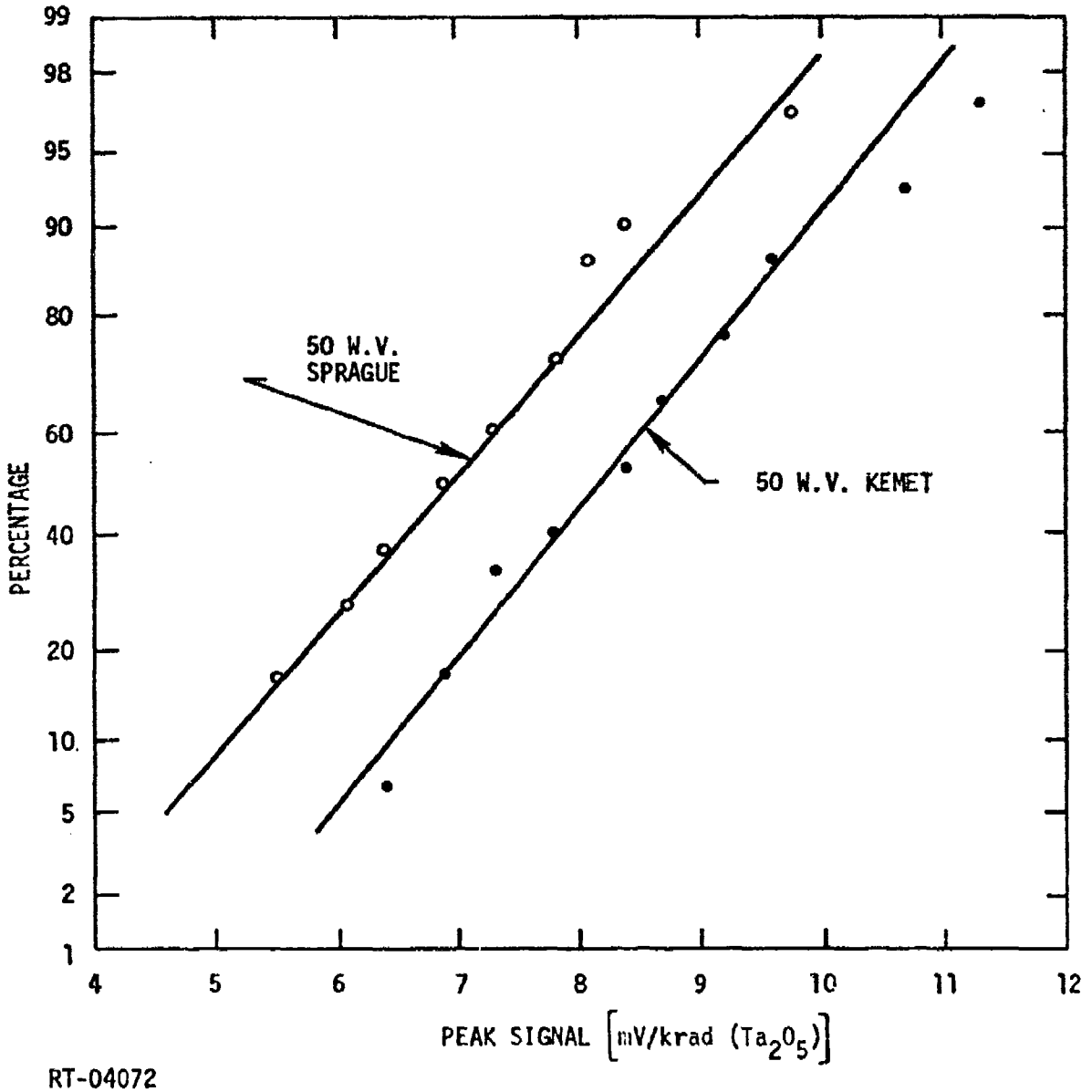

Figure 6. Cumulative frequency distribution for zero bias responses in 50-W.V. Sprague and Kemet capacitors

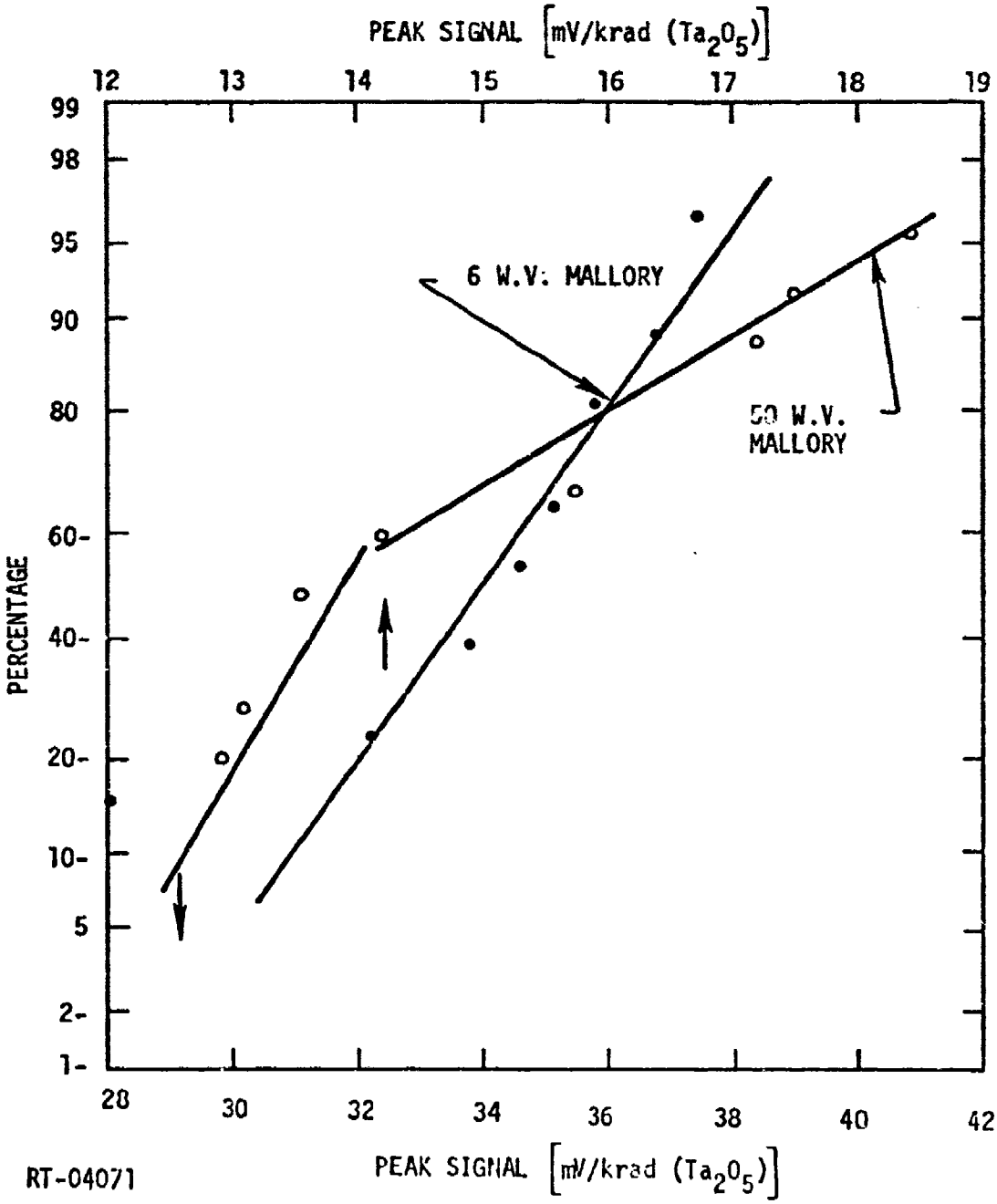

Figure 7. Cumulative frequency distribution for zero bias response in 6- and 50-W.V. Mallory capacitors

3.1 SPACE-CHARGE POLARIZATION STUDIES

Space-charge polarization phenomena are observed in many samples as a result of radiation-induced conductivity measurements. With a constant bias on the sample and successive radiation pulses applied to the sample, lower current pulses pass through the measuring circuit. After the bias is removed, subsequent radiation pulses cause a current flow in the circuit opposite in direction to that observed with the bias applied. The effect is due to a space-charge field induced inside the sample during irradiation. This induced field tends to cancel the applied field. Such an effect has been observed in various photoconductors and is known by workers in the field as persistent internal polarization.

Persistent internal polarization and the creation of space charges can be understood in terms of the model developed in previous work and is based on the development of a nonuniformity in the trapped charges (Ref. 3). It is assumed that the radiation field generates excess holes and electrons uniformly through the insulator. Radiation will also excite some electrons in the metal contacts. However, since the thermalization time in metals is usually much shorter than the recombination time in insulators, metal contacts are assumed to remain at thermal equilibrium. When a voltage is applied across the capacitor, the free electrons in the insulator move toward the positive electrode, and holes move toward the negative electrode until they become trapped or recombine. In the bulk of the insulator, electrons and holes that are removed from one region are replaced by others flowing in from adjacent regions; thus, the densities and the bulk of the insulator remain essentially uniform. Because the electrodes are assumed to be in thermal equilibrium, the density of electrons in the metal above the conduction band in the insulator is less than the density of electrons in the conduction band of the insulator. Therefore, electrons that move away from the negative electrode are not completely replaced by electrons from the metal. The electron density in the insulator is partially depleted near the negative electrode, and the hole density is partially

depleted near the positive electrode. This nonumiform density of free carriers causes nonuniform trapping of charges and, therefore, polarization. Thus, in this model, the effective high-resistivity barrier and the nonuniformity of carriers are direct consequences of the difference between thermalization time in the metal contacts and the recombination lifetime in the insulator.

The decrease in current with radiation, i.e., with polarization, results from the depletion of the carriers near the contact. At time zero, the electric field and the free carrier density are constant across the capacitor which results in a certain current. As the asymetric distribution of trapped charges develops, the electric field becomes nonuniform; i.e., the field becomes larger near the contacts and smaller near the bulk, thus keeping the same total voltage across the sample. Therefore, the field is large where the carrier density is small and vice versa. The net result is a decrease in current until an equilibrium condition is achieved.

Thus, by irradiating with a constant applied bias, charges can be created in the insulator and stored there for long periods of time. Once the stored charge is there, it should respond the same as a charge injected by other means. The working hypothesis is that maverick behavior is caused by space charge trapped in the oxide which has been released by radiation. Hence, a series of experiments were conducted in which space-charge polarization was purposely created within a capacitor, (1) to examine the relaxation of this charge under irradiation, and (2) to correlate this with maverick response.

The first experiments used 50-W.V. capacitors with a 45-volt bias. When 200 krad was accumulated in the sample, a 20% response decrease was noted. This indicated that a space-charge polarization field was building up in the sample. Further irradiation did not result in a greater decrease, indicating that an equilibrium was obtained. With the 6-W.V. capacitors, about 10% decrease in the peak response was noted for 500 krad, indicating a much lower space-charge field. In general, the 6-W.V. capacitors showed much lower space-charge polarization effects. The release of the space charge is observed by reducing the applied bias to zero and observing the response under further pulsing. The 6-W.V.

capacitors showed only a slight decrease in the zero-bias signal as a result of polarization, and the normal zero-bias signal was quickly regained as the radiation continued. The results on the 50-W.V. capacitor are shown in Figure 8. After 250 krad at zero bias, a Sprague 50-W.V. capacitor (478) was returned to zero bias and irradiated at zero bias. The response (with the anode grounded) is shown as Record 365 in Figure 8. Note the initial positive voltage build-up across the capacitor followed by a rapid swing negative to a peak at around 2.3 mV/krad. The response decays with the time constant of about 2000 μsec. Note that this signal indicates a space-charge release apposite in direction to the normal charge release from these capacitors. The response with successive pulsing is shown in Figure 8, and the normal zero-bias signal is ultimately achieved. Further irradiation produced no further changes in the zero-bias signal (Record 401) unless enough dose is accumulated to cause damage in the capacitor.

These experiments were sumulated with the computer model developed in previous studies (Ref. 1) and the results are shown in Figure 9. A 50-W.V. capacitor was modeled in the computer simulation with a 100-ohm load. The upper curve shows the response calculated for a 45-volt bias and 40 krad/pulse. Fifty pulses were then applied to the simulated capacitor in the model at 45-volt bias. Following this, a radiation pulse at zero bias was applied to the capacitor, yielding curve 2 in Figure 9. Note that the qualitative behavior of the experimental results with the initial positive swing and the larger time constant is reproduced by the model. With further adjustments of the values of the transport parameters used in the simulation, the theoretical and the experimental data would have agreed more closely; but since the primary object of this study was to identify mechanisms, detailed quantitative modeling was not carried further. The simulation indicates that the space-charge polarization phenomenon in the tantalum capacitors is due to trapped charge in the oxide, as hypothesized at the beginning of the study, and that the trapped-charge release has the characteristics of a maverick response.

Thus, if maverick capacitors are those which have built-in space-charge fields to trapped charge, the question is: How did they get that

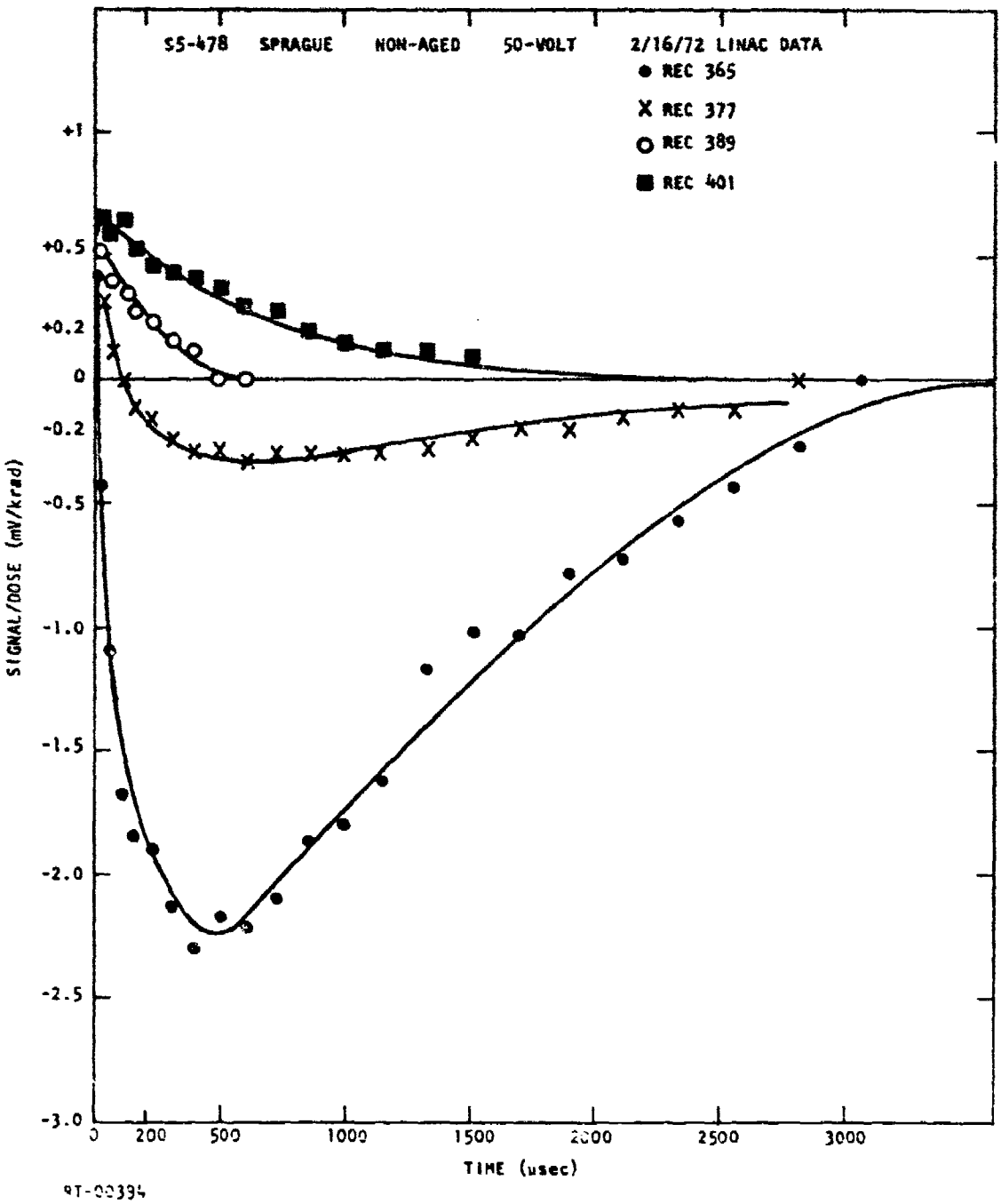

Figure 8. Space charge relaxation polarization relaxation with accumulated dose for a 50-W.V. capacitor

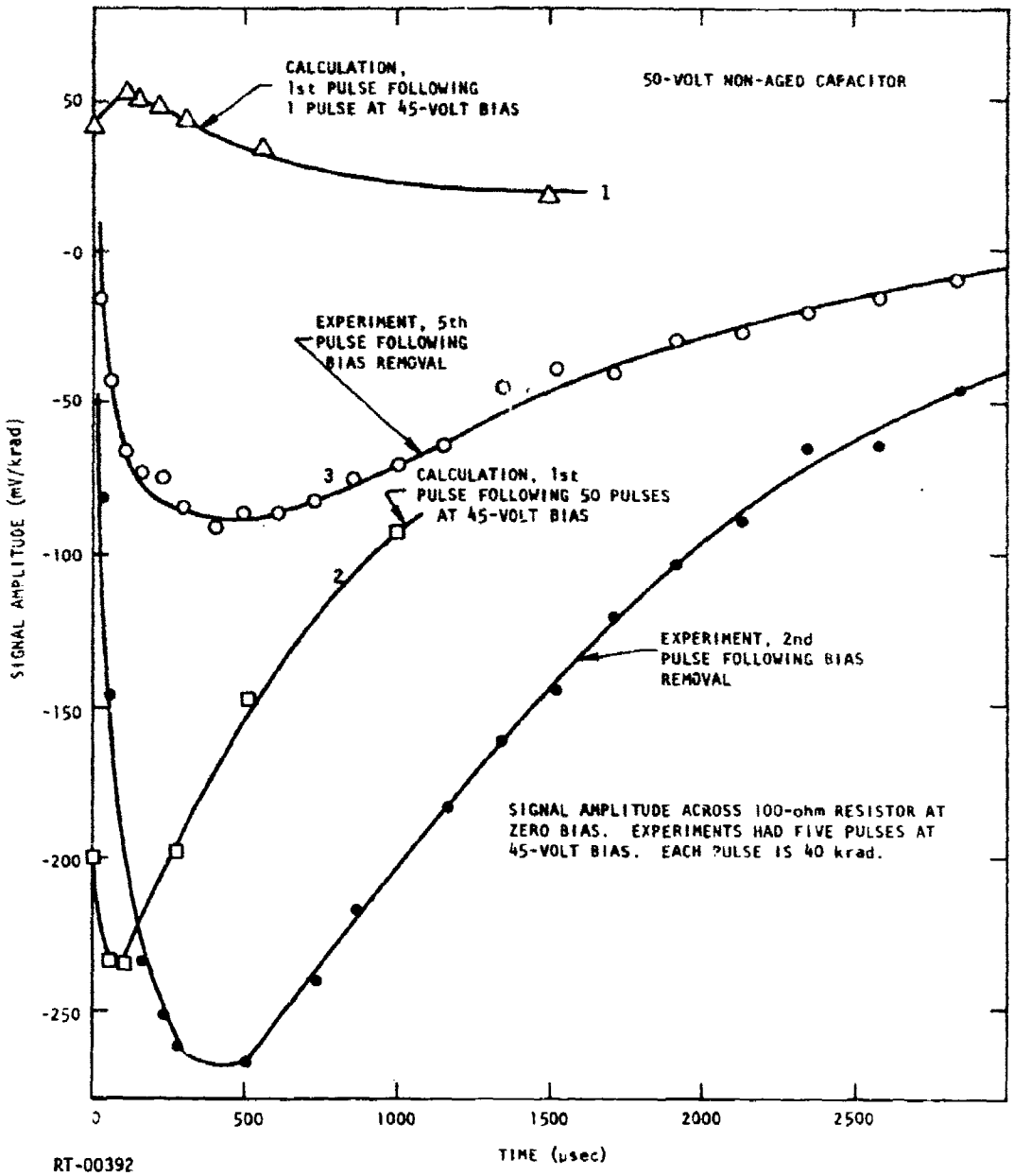

Figure 9. Results of calculations of space-charge build-up and relaxation

way? Since there are plenty of trapping states in any Ta capacitor, a mechanism which allows relatively easier injection in some capacitors must account for mavericks.

It has been known for some time that voltage and temperature stresses on a tantalum capacitor increase the leakage current. Voltage and temperature stresses are applied to graded-reliability tantalum capacitors to determine the failure rates for a given population. Capacitors from a given lot are aged until the failure rate drops below a specified level (Ref. 4). This implies that some capacitors are near the end of their life when they are shipped, and may leave some capacitors more susceptible to charge-storage effects than others. To test this hypothesis, four 6-W.V. and four 50-W.V. capacitors were aged at a bias of 1.63 times the rated W.V. at 85°C for 4 hours. This is equivalent to a normal usage of 40,000 hours. These capacitors were then tested for change in capacitance and in leakage resistance, and were found to be acceptable. The capacitors were then shorted for 24 hours before being tested at Linac.

The radiation response of these capacitors and eight unaged control capacitors were examined at zero bias and with applied voltage at 25°C. Seven of the aged capacitors showed only minor differences in their response, both with and without bias, compared to the unaged capacitors. Figure 10 could be normal variations in the capacitor response and no dramatic differences are observed that could be attributed to aging. This was the case for all the 6-W.V. aged capacitors. Again the radiation response is plotted as a function of time in Figure 11 and slight differences were noted in the 50-W.V. capacitors. The difference in magnitude of the peak responses at zero bias is as also within the distribution of normal capacitor responses. Hence, the difference cannot be attributed to aging. A decrease in the decay time, τ_2, over the unaged units was consistently noted at zero bias. The unaged τ_2 for capacitor (S470) was about 950 μsec. In Figure 12, the responses of the same capacitors are shown under 45-volt bias. Note that τ_2 for S470, the aged capacitor, has increased nearly to its unaged value.

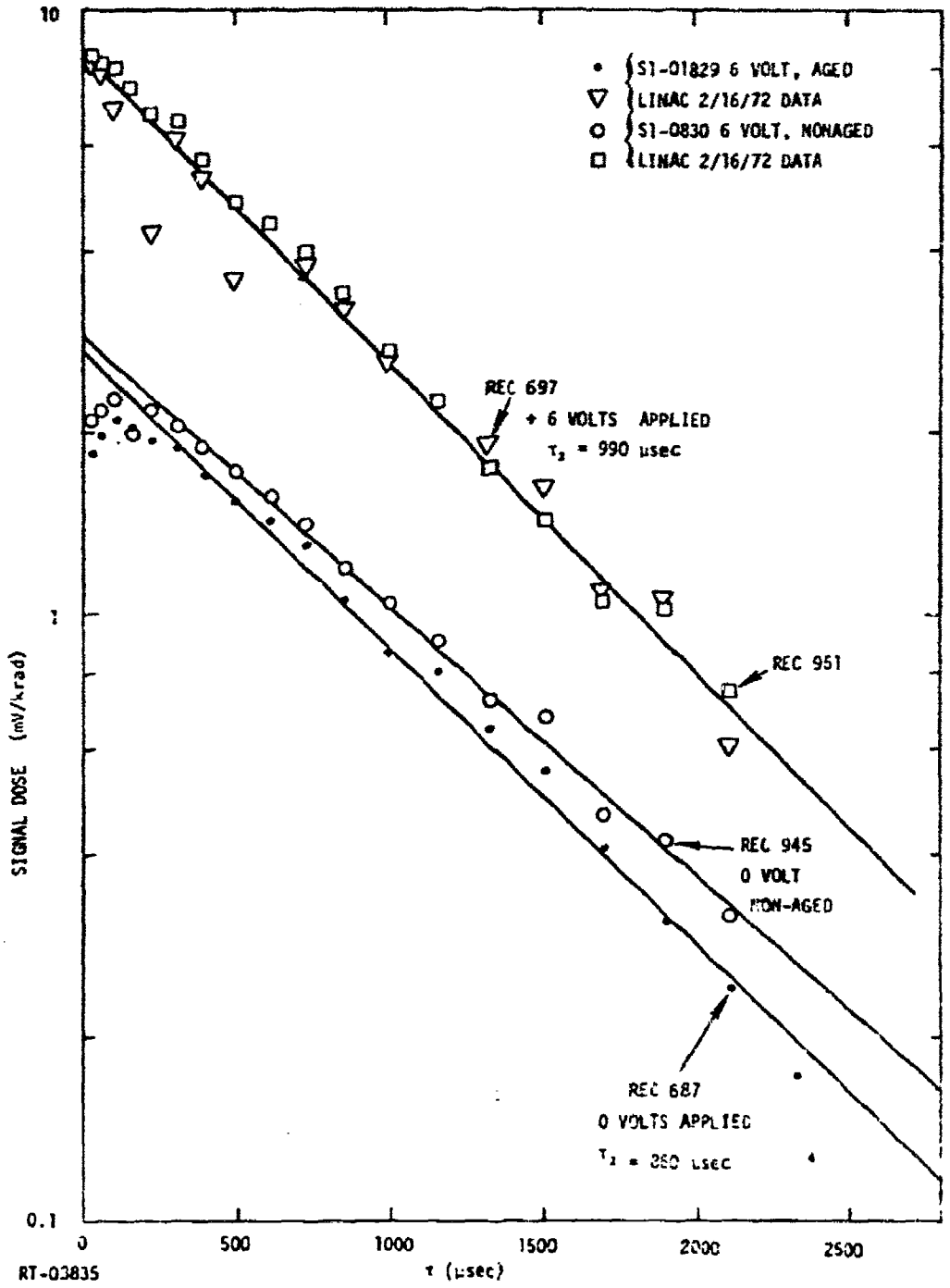

Figure 10. Radiation response of aged and unaged 6-W.V. capacitors

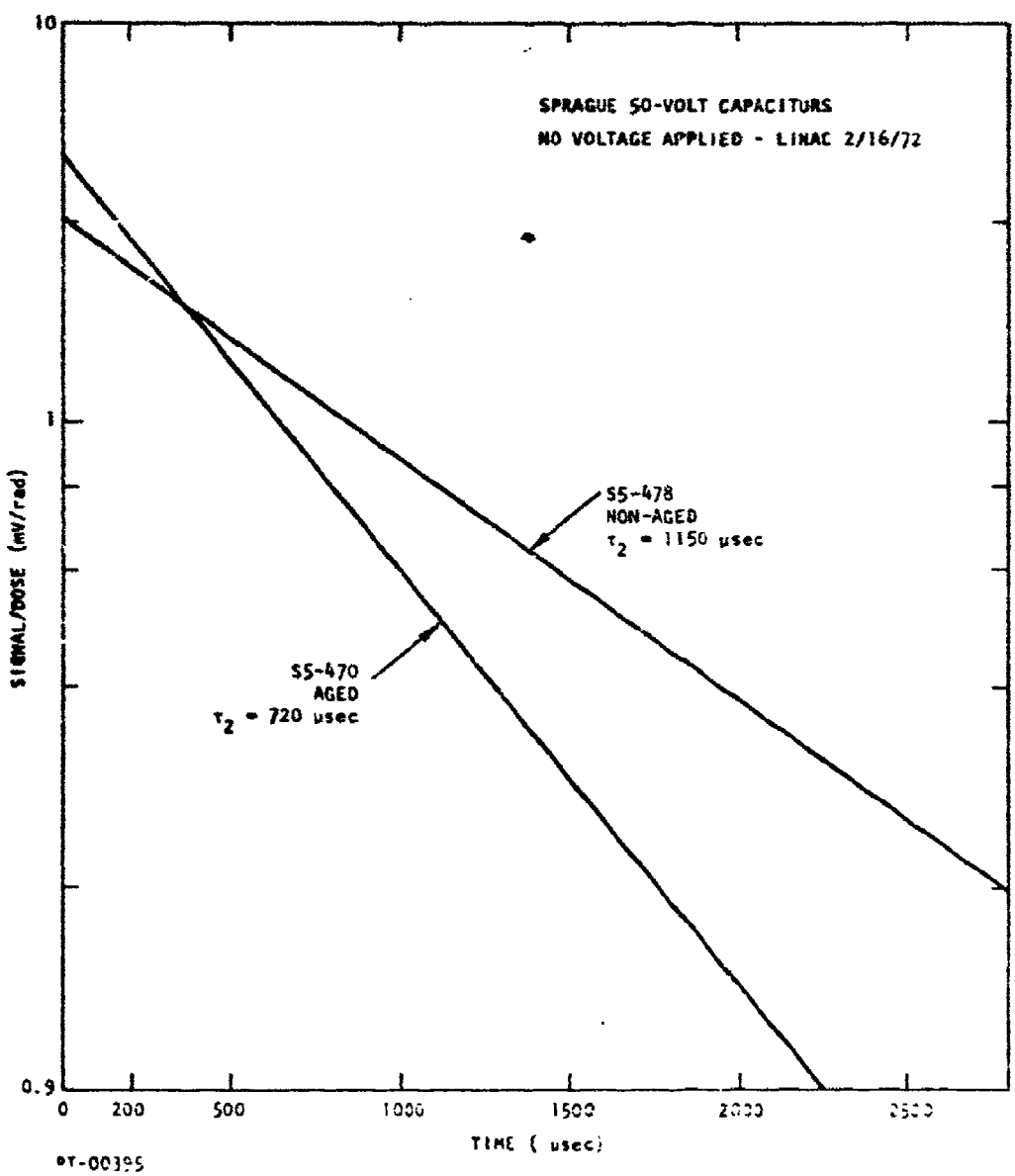

Figure 11. Radiation response of aged and unaged 50-W.V. capacitors, zero bias

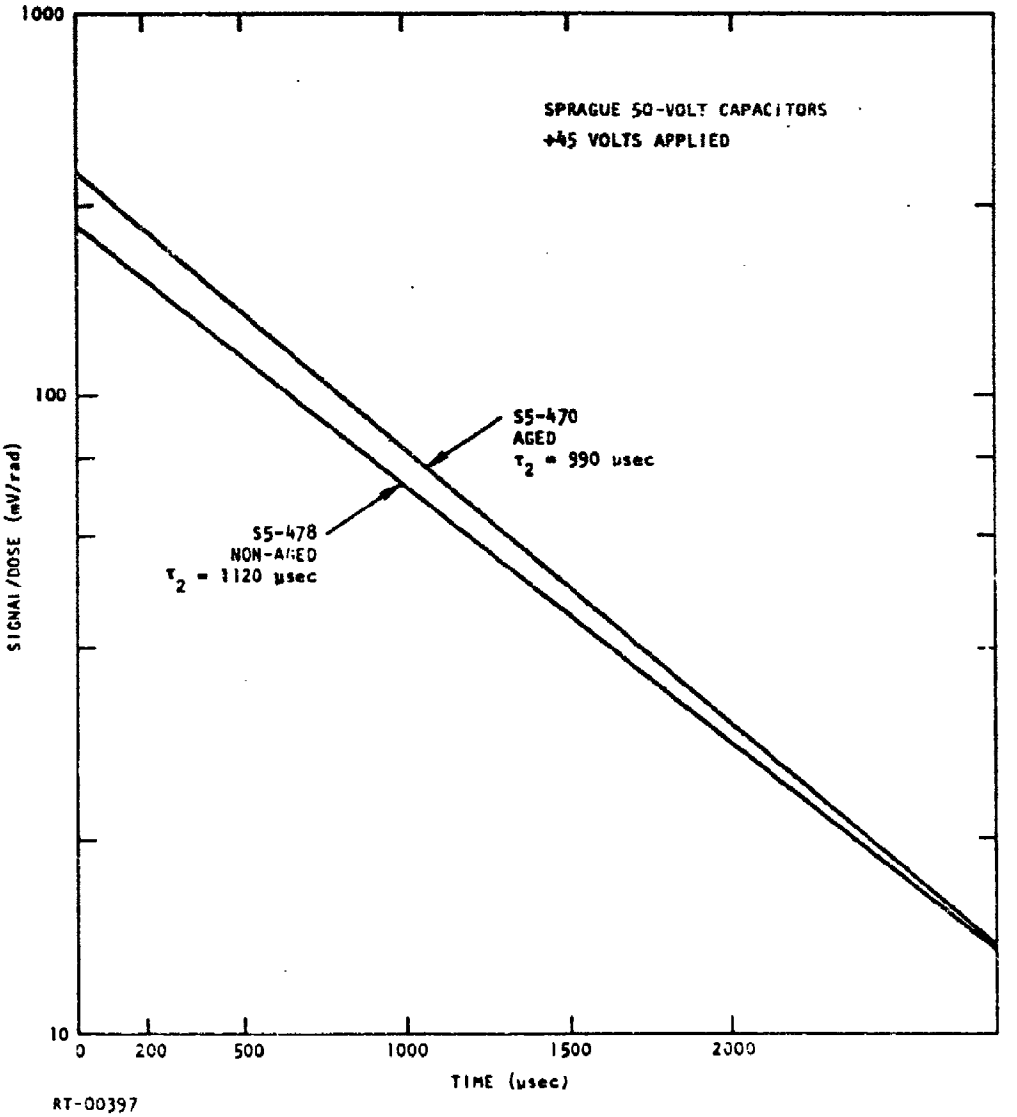

Figure 12. Radiation response of aged and unaged 50-W.V. capacitors, 45 V bias

The aged capacitors show more polarization after irradiating under bias than the unaged units. Figures 7 and 13 show aged and unaged capacitor responses at zero bias after polarization at +45 volts with 200 krad of radiation. Note that the aged capacitor shows more polarization charge release on the first pulse at zero bias. The decay time of the polarization charge release for Record 365 in Figure 8 was about 2000 μsec as mentioned above, while for Record 81 in Figure 13, it is about 2200 μsec. Thus, although more polarization charge release was obtained from the aged unit, relative to the unaged unit, the magnitude of the decay time for most units is still somewhat shorter than had been observed for a maverick capacitor.

One aged capacitor (S472) showed polarization charge release on the first zero-bias pulse, without previous bias and radiation. The zero-bias response of this capacitor for the first nine pulse, 15 krad each, is shown in Figure 14. Note that the decay time constant of Record 407 is about 3600 usec, which is much longer than for polarization in "normal" capacitors. As the capacitor is repeatedly pulsed, the response returns to that of a normal capacitor. The similarity between the response between the response of the (S470) capacitor and the reported mavericks suggests that the aging did indeed produce a maverick capacitor.

The experiments to date on mavericks, which were produced both intentionally and unintentionally, indicate that the hypothesis that the maverick behavior is due to stored charge release is justified and that bias and temperature increase the frequency of incidence of mavericks. Hence, it is desirable to find a way to eliminate mavericks from the population of capacitors.

We have known for some time that one effect of irradiating a tantalum capacitor with ionizing radiation is to leave behind a certain amount of trapped charge within the oxide. This trapped charge is left in the oxide due to the fact that one of the mobile carriers created during the ionization process moves with a higher mobility than the other carrier. For the purposes of modeling, electrons are chosen as more mobile and are swept out of the oxide, leaving behind trapped holes. If the capacitor is shorted after irradiation, electrons distribute between the plates of the capacitor and net charge on capacitor is zero.

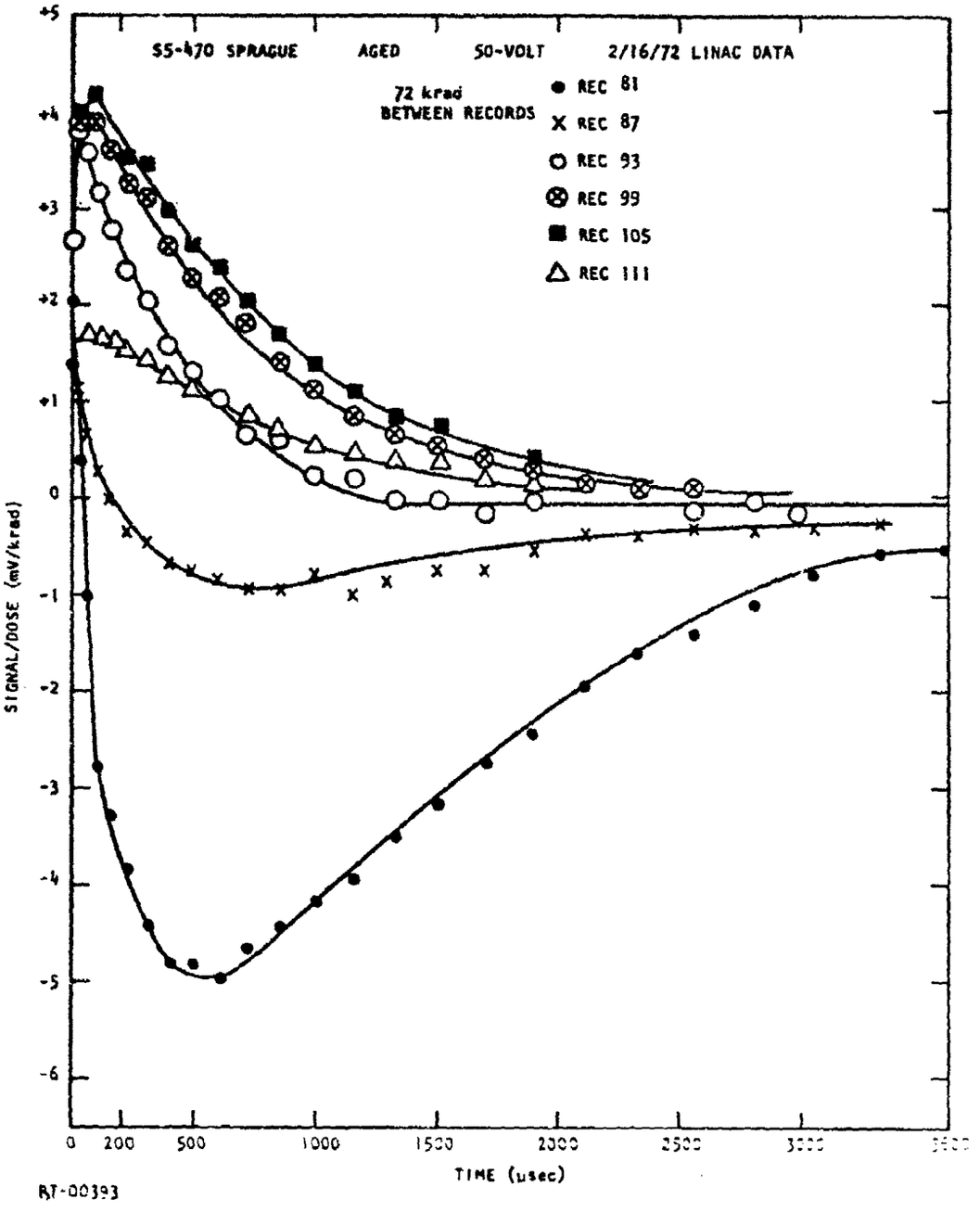

Figure 13. Space-charge polarization relaxation in an aged 50-W.V. capacitor

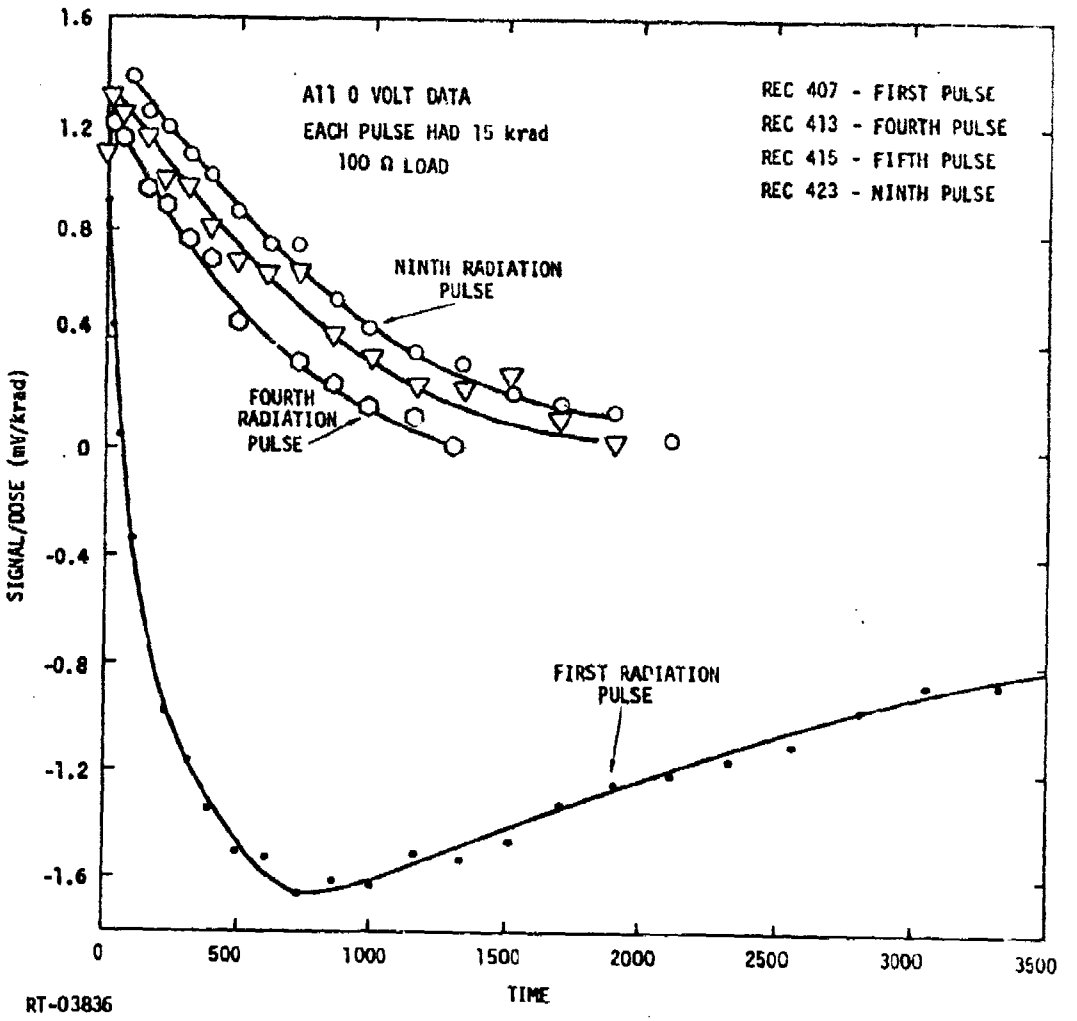

Figure 14. Aged capacitor response which shows maverick behavior

However, electrons and holes are still separated and equilibrate at a rate limited by the injection of carriers from MnO_2. The slow injection of the electrons into the oxide to equilibrate the space charge is observable when an electrometer is connected across the capacitor terminals. A slow voltage buildup is observed and the magnitude of this voltage buildup is related to the amount of stored charge. Hence, this phenomenon should provide a detection method for mavericks.

A maverick capacitor is one which can store charge much more easily than normal members of the population. When a capacitor is charged with a bias for some time and then shorted, the maverick capacitors should have more charge remaining in the oxide than normal capacitors. This should also exhibit itself in the irradiation response. Hence, the following tests were conducted.

1. A capacitor was charged through a 3 ohm/volt resistor to the working voltage for 1 minute.
2. The capacitor was shorted through a 3 ohm/volt resistor for 1 minute.
3. The capacitor was connected across an electrometer immediately after removing the short and the voltage buildup across the capacitor was recorded as a function of time for 5 minutes.

The voltage buildup across the capacitor at the end of 5 minutes is called V_5. The value of V_5 was then correlated with the radiation response of capacitors in the following way. The capacitors were taken to Linac after having been shorted for 24 hours. First, the zero-bias transient was recorded in the usual way. Next, the capacitor was connected across a bias for 15 seconds, then shorted for 15 seconds. A second zero-bias transient was then recorded. The difference between the zero-bias transient before and after charging was plotted as a function of V_5. These experiments were carried out on 125 capacitors: four 10-W.V. Kemet, four 35-W.V. Kemet, 58 6-W.V. capacitors equally divided between Sprague and Kemet, 58 50-W.V. capacitors equally divided between Sprague and Kemet, 15 50-W.V. Mallory capacitors, and 15 6-W.V. Mallory capacitors. The typical

electrometer storage charge results are shown in Figure 15. Note that after 5 minutes most capacitors have built up to about a 200 mV across the plates. The aged capacitors (S470) and S472) have built up to a V_5 of 1 volt for the S470 and 5.1 volts for S472. The capacitor S472 was the maverick capacitor which showed a large stored charge release after aging. The results in the aged capacitors can be compared with Figure 16, which shows the results of the electrometer test applied to two 50-W.V. capacitors which were obtained from the McDonnell Douglas Corporation. These capacitors showed maverick charge releases during subsystem radiation tests.

From the electrometer tests, we can say that most of the capacitors which are regarded as normal show low values of V_5 and low values of dV/dt during the initial portion of the voltage buildup. The maverick capacitors showed enhanced stored-charge capacity in the above test.

The capacitors tested above were shorted and taken to Linac for the radiation correlation. In general, the difference between the zero-bias signal before charging and the zero-bias signal after charging for 15 seconds and shorting for 15 seconds was small compared to the magnitude of the signal itself. In fact, for V_5 of about 150 mV, the change was in the neighborhood of 0.4 mV/krad. This approaches relative measuring error for two readings. The change in the zero-bias response as a result of charging the maverick capacitors 15 seconds and shorting the capacitors for 15 seconds was -8.72 mV/krad for S470, and -35.9 mV/krad for S472. Thus, in every case, a capacitor which exhibits normal behavior in radiation tests also shows low values of voltage buildup during the electrometer tests. In every case where charge storage behavior was observed in the radiation response, large values of V_5 were observed during the electrometer tests.

While the change in the peak voltage was small and subject to considerable error, some interesting differences were revealed by comparing the value of V_5 with the change in the peak zero-bias response as a result of the charge short cycle. These are shown in Figures 17, 18, and 19 respectively, where the value of V_5 is plotted against the change in the peak zero-bias response for different groups of capacitors. The value

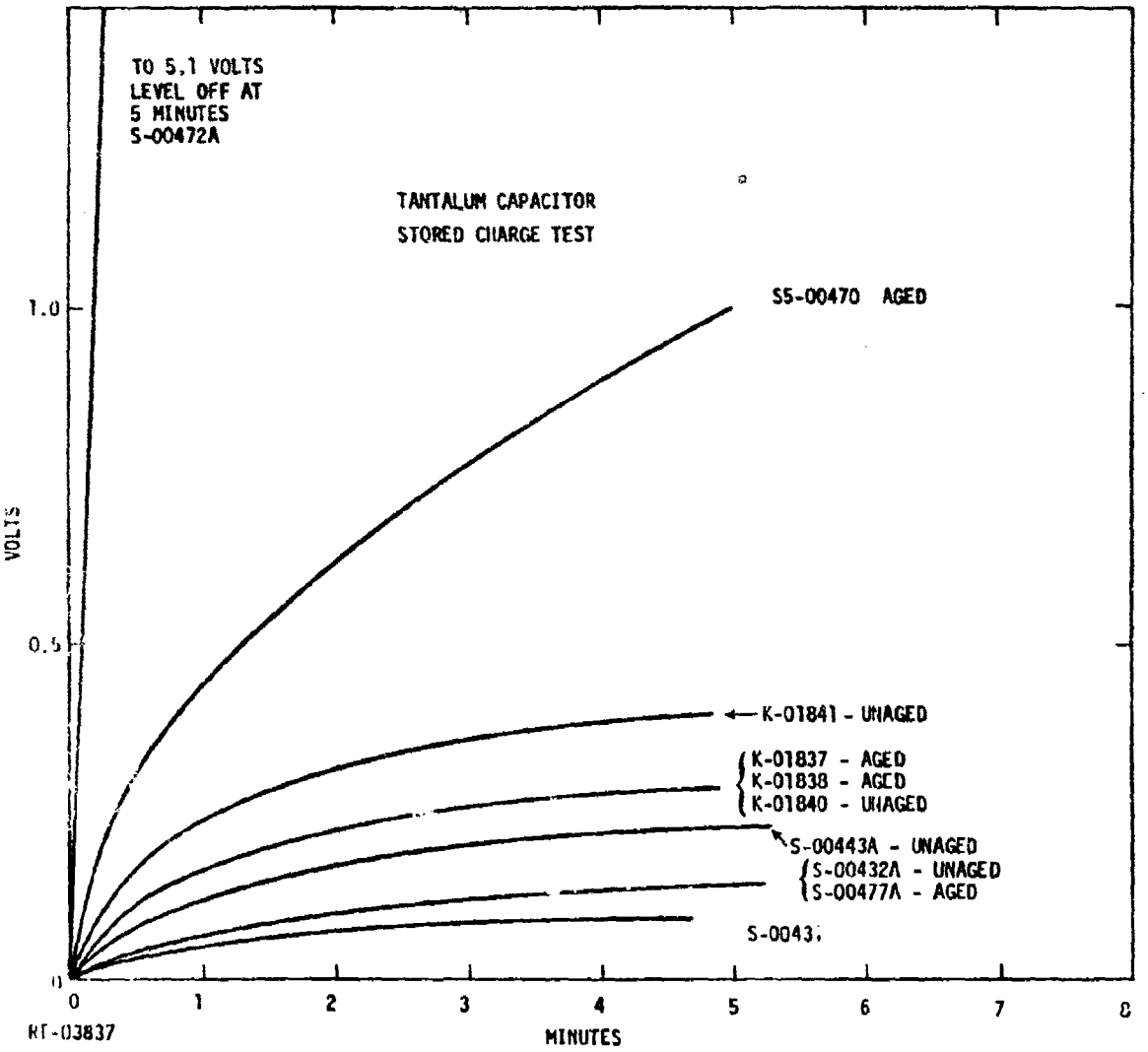

Figure 15. Voltage buildup on capacitors showing stored-charge release

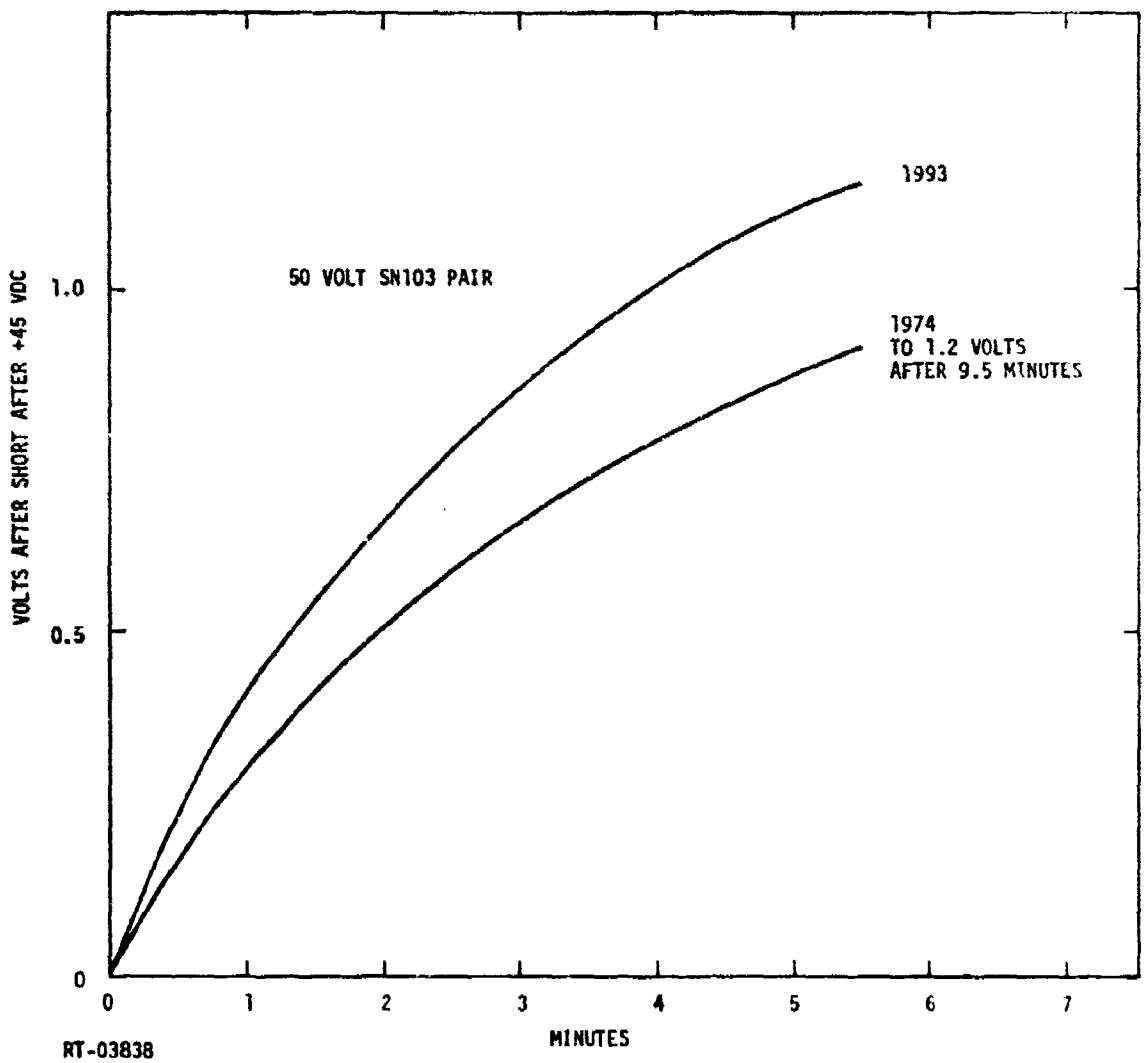

Figure 16. Voltage buildup after charging and shorting for two maverick capacitors

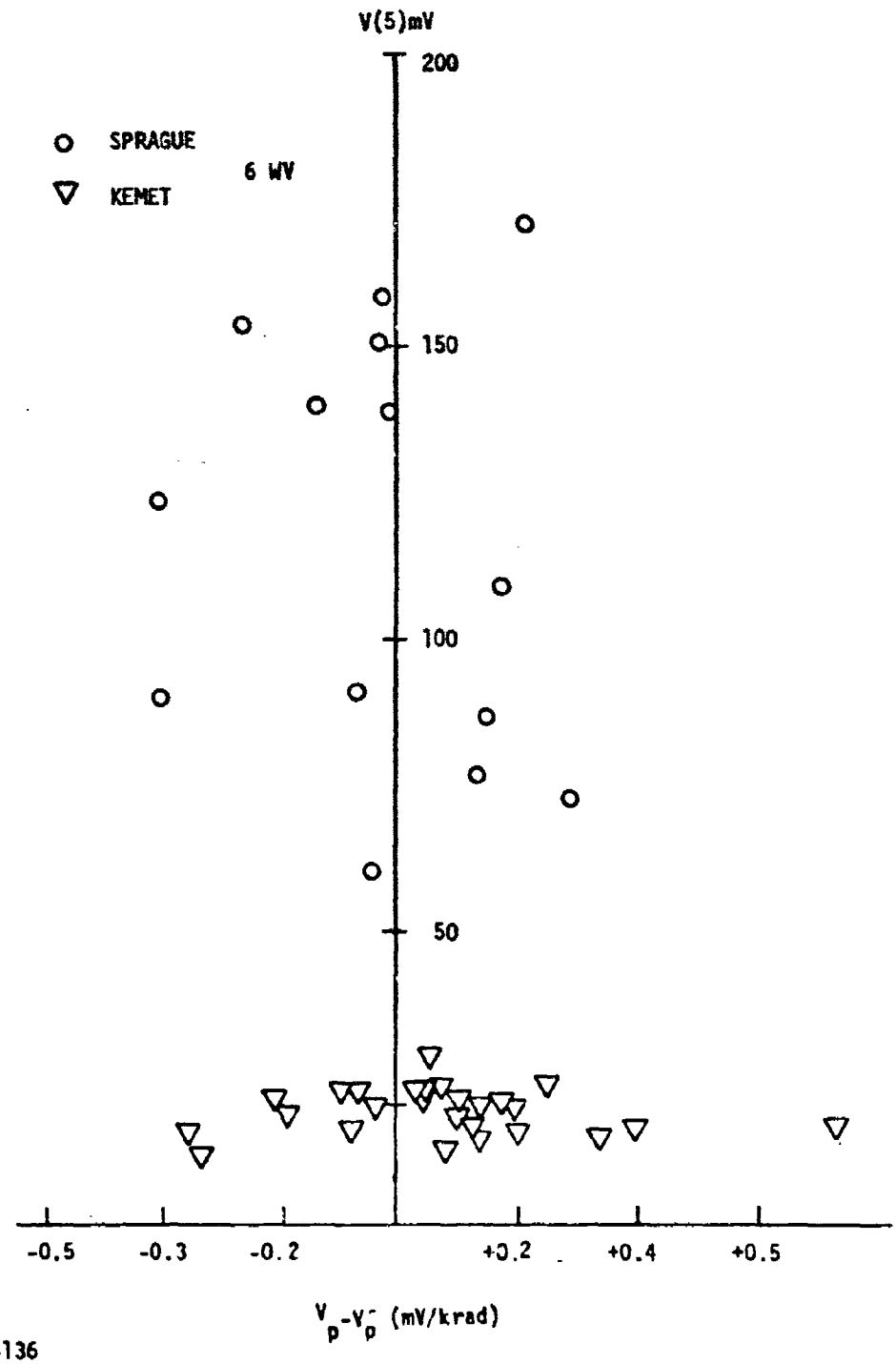

Figure 17. Correlation of radiation response with the stored-charge test for 6-W.V. Sprague and Kemet capacitors

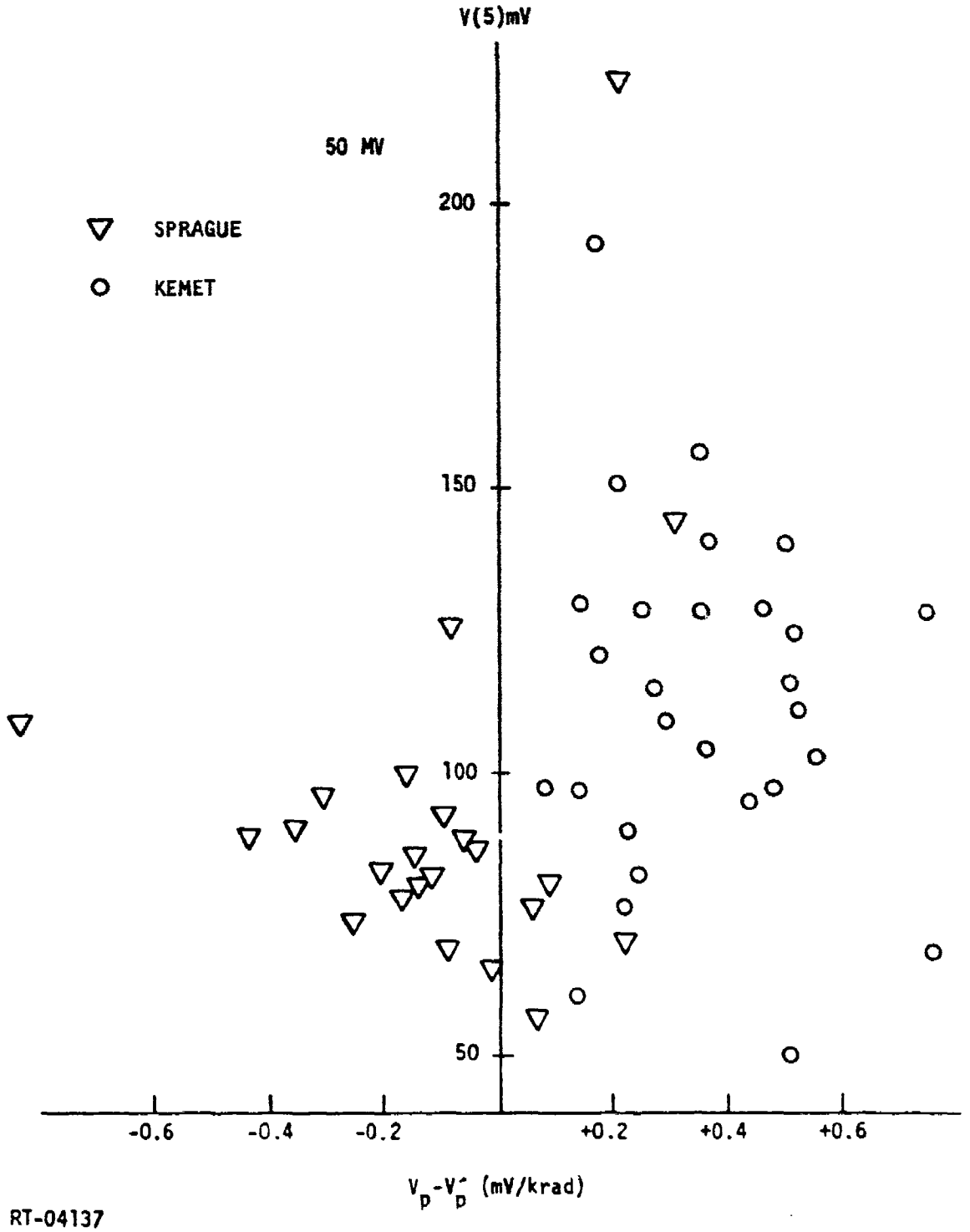

Figure 18. Correlation of radiation response with the stored-charge test for 50-W.V. Sprague and Kemet capacitors

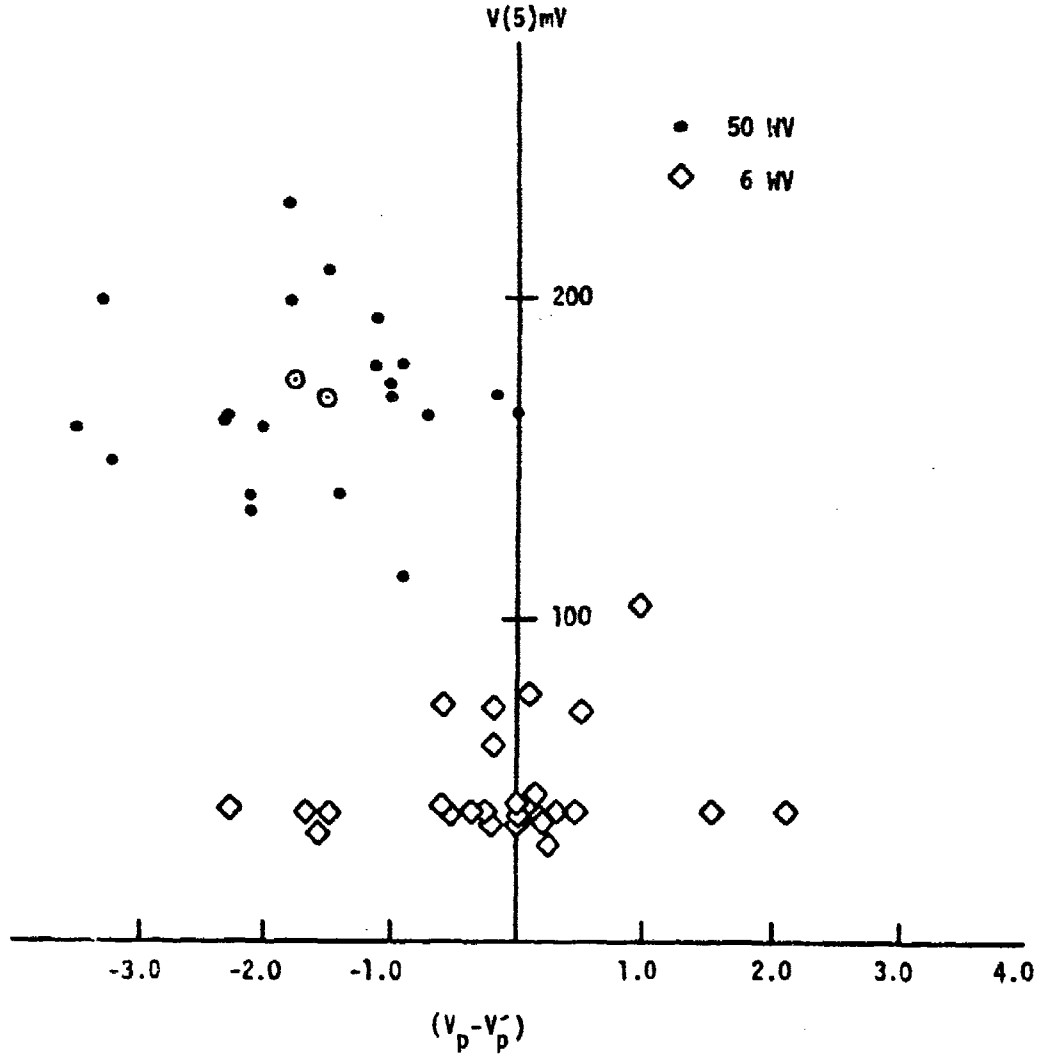

Figure 19. Correlation of radiation response with 6-W.V. and 50-W.V. Mallory capacitors

of V_5 for 6-W.V. capacitors of Sprague and Kemet are plotted in Figure 17. Note that the Sprague V_5 values are all larger than the Kemet V_5 values. The change in the radiation peak is quite randomly distributed about zero, indicating that the change in the peak may well be zero considering the relative measuring error of this system (~5% of peak). Figure 18 shows an interesting division in the responses between the 50-W.V. Sprague and Kemet capacitors. As a result of applying the bias, almost all of the Sprague units show an increase in the zero-bias response, whereas all of the Kemet units show a decrease in the zero-bias response. Figure 19 shows the results for the Mallory capacitors; and as before, the 50-W.V. units show a higher capacity for stored charge and larger changes in peak voltage as a result of the charge-short cycle. The 6-volt capacitors are spread somewhat more uniformly about the zero point, indicating that the change in the peak voltage could be near zero. The fact that the Mallory capacitors were spread somewhat more horizontally than the Kemet or Sprague units indicates that the electrical screen may not apply to Mallory capacitors as well as it does to the others. However, a Mallory maverick capacitor has never been observed. Note that the Mallory units behave about like the Sprague 50-volt capacitors, except that the change in the peak voltage is rather large for the Mallory capacitors for the same buildup on the electrometer. This indicates that the Mallory units store charge more easily than either the Kemet or the Sprague capacitor. This is true for both the 6-W.V. and the 50-W.V. capacitors.

The significance of the division of the points by manufacturer is not understood.

3.2 SUMMARY

The hypothesis that maverick behavior is due to stored charge appears to explain the features of the maverick capacitors which have been observed to date. Mavericks can be produced by an aging process and it is possible to eliminate capacitors with high charge-storage ability from a population by means of an electrical screen. The electrical screen may eliminate a

few normally responding capacitors, but the percentage which fail the electrical screen and still respond normally is negligible.

From the rate of introduction of mavericks under temperature and voltage stress, we infer that once a population is screened, mavericks occur at about the rate at which failures due to leakage current occur.

4. BACK-TO-BACK RESPONSE

4.1 PAIR RESPONSE AS A FUNCTION OF DOSE

As had been mentioned in the earlier report (Ref. 1), connecting two capacitors in a series back-to-back configuration produces considerable cancellation of the photovoltaic response. To examine the response further, the dose dependence and some bias dependence of pairs were studied.

As the pair is irradiated, the charge removed from the dielectric causes the common connection of the capacitors, called the center point, to become charged. As the center point becomes charged, the driving voltage for the photovoltaic effect decreases and, thus, the pair's total response decreases. The capacitors in a back-to-back pair behave as a single capacitor but with an effective bias, V + a, which decreases with dose. Thus, a model for the back-to-back pair must account for the decreasing bias as the dose in a given pulse accumulates. Since each capacitor looks into an open circuit in the back-to-back pair, the $dV/d\gamma$ curve versus dose is similar to the steady-state measurement curve for each capacitor. The curves are not exactly alike, because only the charge which is emitted prior to the peak contributes to the response; but the nonlinearity that arises due to the approach of saturation may be important in the back-to-back application. The approach to saturation produces two effects: (1) a decrease in the bias applied across the capacitor, and (2) a slight decrease in the charge collection probability. To examine the dependence of the photovoltaic response of the back-to-back pair as a function of the center-point voltage, several back-to-back pairs were arranged in the test chamber according to the circuit shown in Figure 20. The irradiation pulse width was again 4.5 μsec, the load resistor was 1 kΩ, and the temperature was 25°C. During and immediately after the radiation pulse, the transient response of the pair was noted. One second after the pulse, the electrometer was automatically connected to the center point and the center-point voltage noted. The results are shown in Figures 21 and 22, where the capacitor

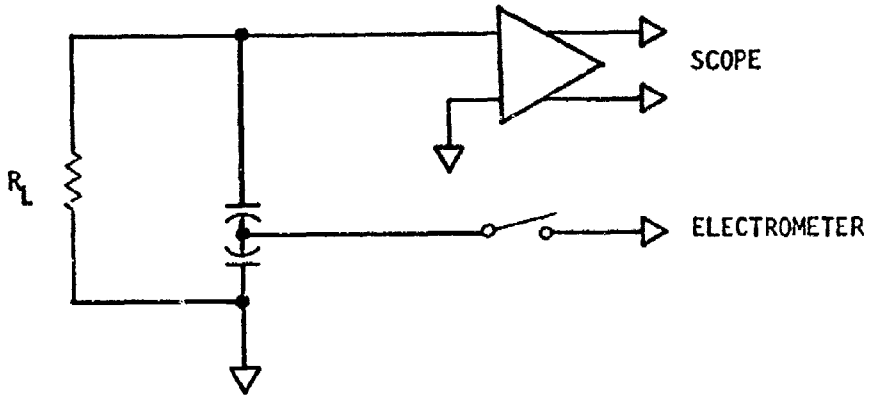

RT-03896

Figure 20. Back-to-back pair test circuit

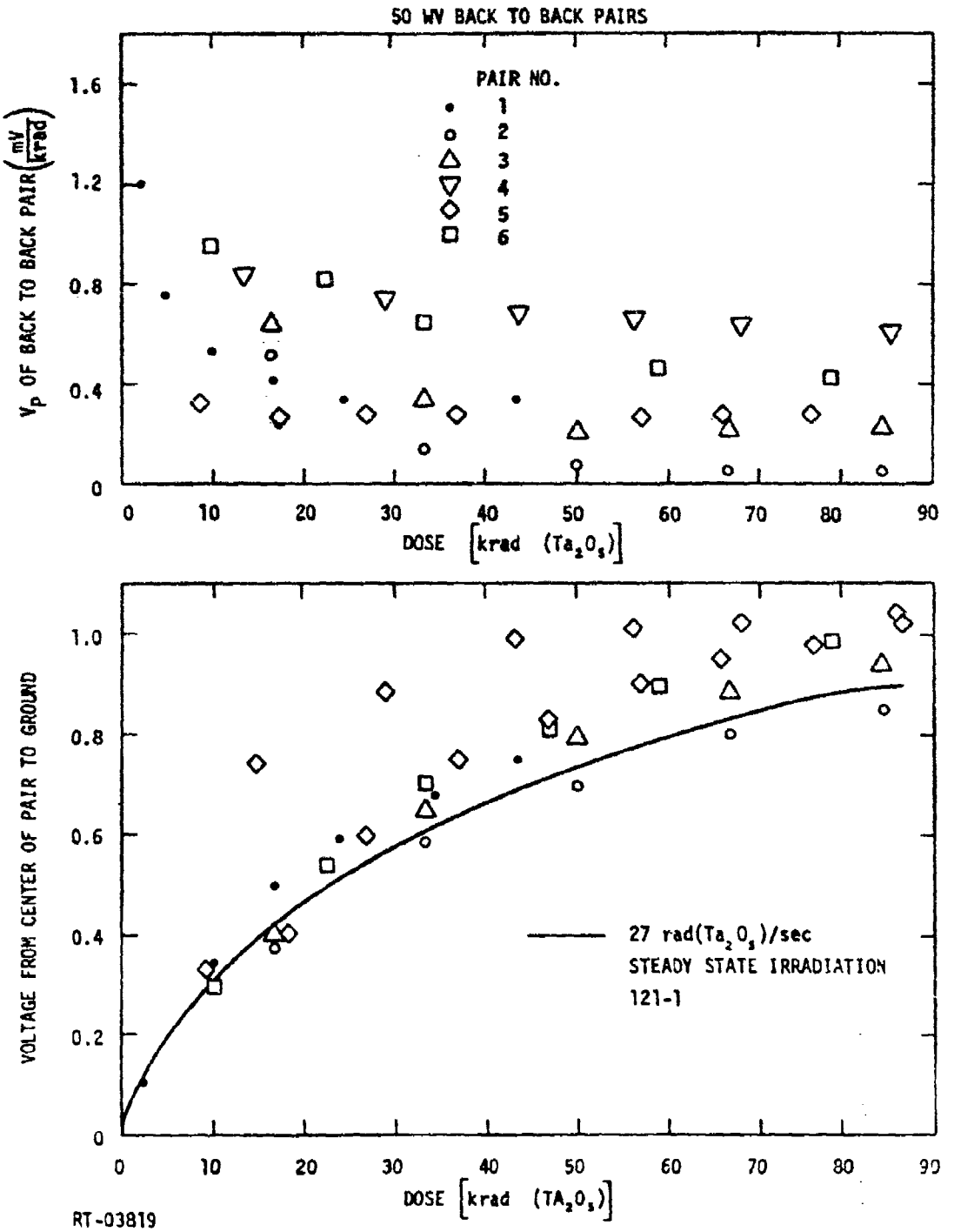

Figure 21. 50-W.V. back-to-back pair results showing correlation of peak response with center-point voltage

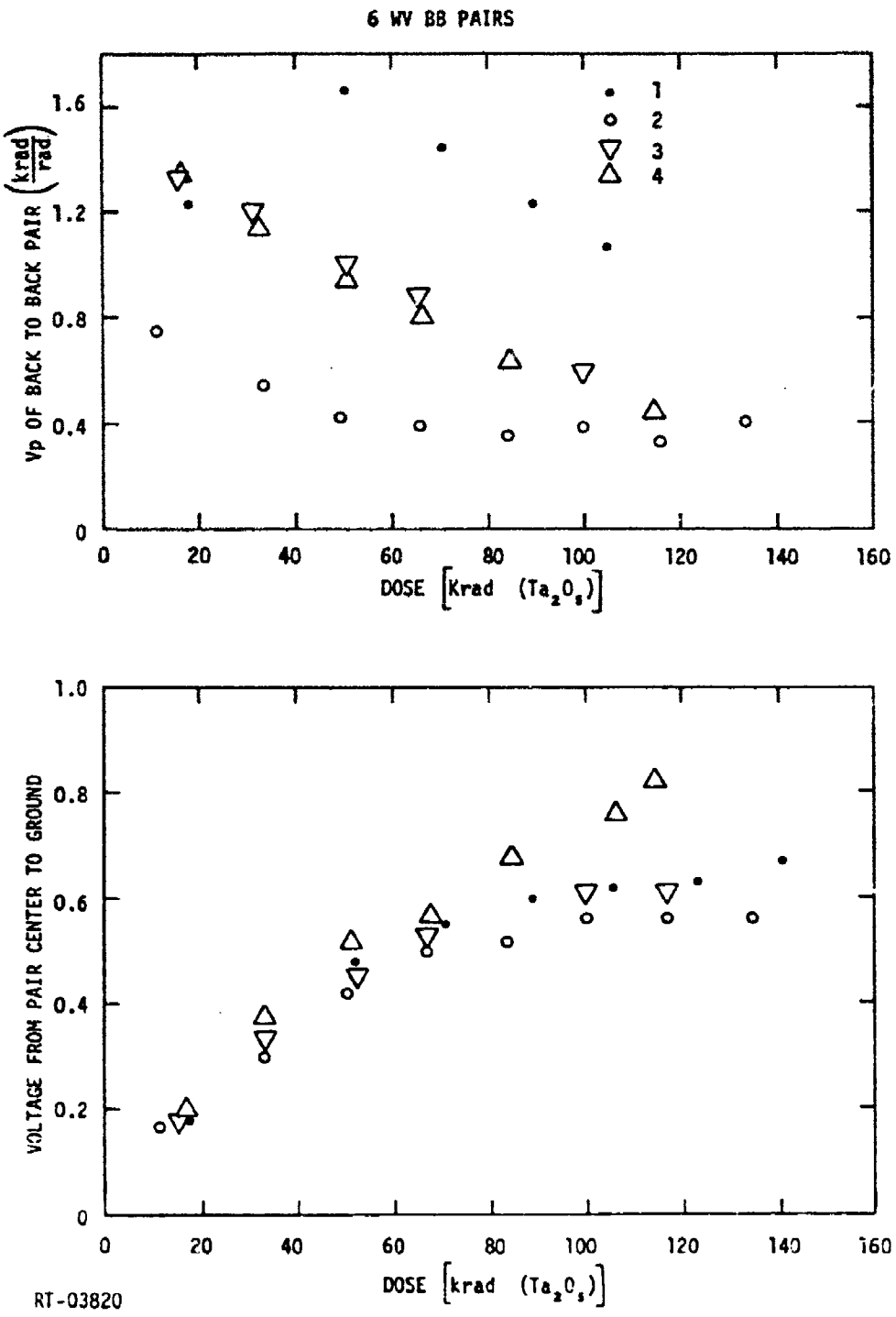

Figure 22. 6-W.V. back-to-back pair results showing correlation of peak response with center-point voltage

identifications which correlate the capacitor serial numbers with the data points in the figure are given in Table 1.

Table 1

BACK-TO-BACK PAIR IDENTIFICATIONS

Pair No.	Capacitor Serial Numbers	W.V.
1	S-1772/1773	6
2	S-1774/1775	6
3	S-1776/1777	6
4	S-1778/1779	6
1	S-421/422	50
2	S-424/425	50
3	S-427/428	50
4	K-1829/1830	50
5	K-1831/1832	50
6	K-1833/1834	50

The upper portion of the figures show the photovoltaic response. It is seen that the photovoltaic response decreases with successive pulsing. The lower curve shows the buildup of the center-point voltage with dose. Since each capacitor looks into the leakage resistance of the other capacitor, the buildup of the center-point voltage should resemble the voltage buildup of an open-circuit capacitor. This is the case as seen in Figure 21, in which the voltage buildup on a capacitor similar to that used in the back-to-back pair is plotted for comparison. The solid curve shown in Figure 21 was taken with a capacitor looking into an electrometer and a steady-state cobalt-60 source. Note that, in general, there is enough distribution in the open-circuit voltage buildup curves at low dose rates to encompass the points seen in the back-to-back tests (see Section 6). The 6-W.V. units are qualitatively similar to the 50-W.V. units, but no direct comparison with the cobalt-60 irradiations can be made since no similar data are currently available

on 6-W.V. units. If the capacitors in the back-to-back pairs are behaving as single capacitors whose photovoltaic effects cancel to some extent, the photovoltaic signal should be approximately linear in the driving voltage, $(a - V_{cp})$. Taking a as the saturation value of V_{cp}, V_p is plotted versus the driving voltage, $(a - V_{cp})$, in Figures 23 and 24 for the 6- and 50-W.V. back-to-back pairs, respectively. Note that linear plots are obtained for most of the capacitors. As V_{cp} increases, V_p for the back-to-back pair decreases and eventually saturates. Saturation occurs at $V_p = 0$ if the built-in voltages are equal. Saturation is perhaps indicated by pair 2 of the 50-W.V. units, although secondary electron emission or collection effects make low values difficult to interpret quantitatively. V_p for pair 2 may have actually changed sign, since the magnitude of the contribution due to secondary electron emission or collection is about 0.2 to 0.5 mV/krad. The onset of secondary emission may also mask other nonlinearities.

The back-to-back pair response is particularly difficult to model due to the fact that the response is nonlinear in the time and in the dose, since each capacitor is looking into a very large load. The dose dependence has been discussed above, and the time dependence arises from the delayed conductivity which causes the voltage of the center node to continue to rise following the pulse. Thus, V_{cp} at the peak response depends on the time at which the peak response occurs. The actual dose dependence of a back-to-back pair can be bounded by two assumptions: (1) that the K is a constant, and (2) the K has the dose dependence of the steady-state case. We have found empirically that the curve in Figure 21 can be approximately fit by the function

$$V_p = a \left\{1 - \exp[(-K'\gamma - K''\gamma_c)\ (1 - \exp(-\gamma/\gamma_c)]\right\} \qquad (1)$$

where a is the built-in voltage, γ = dose, and K', K'', and γ_c are empirical constants. For $\gamma \ll \gamma_c$, this becomes

$$V_p = [1 - \exp(-K' + K'')] \qquad (2)$$

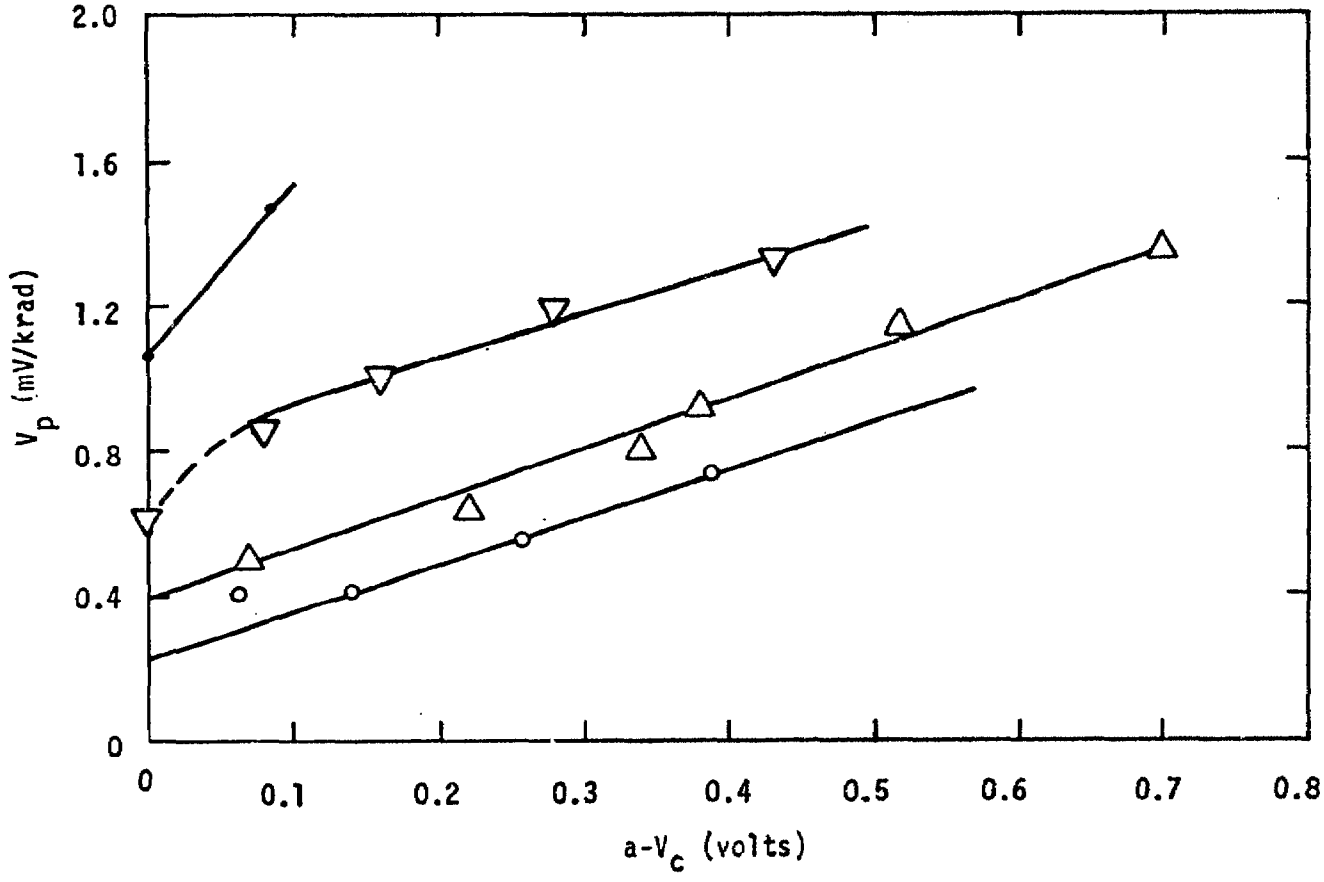

Figure 23. Peak response versus center-point voltage for 6-W.V. back-to-back pairs

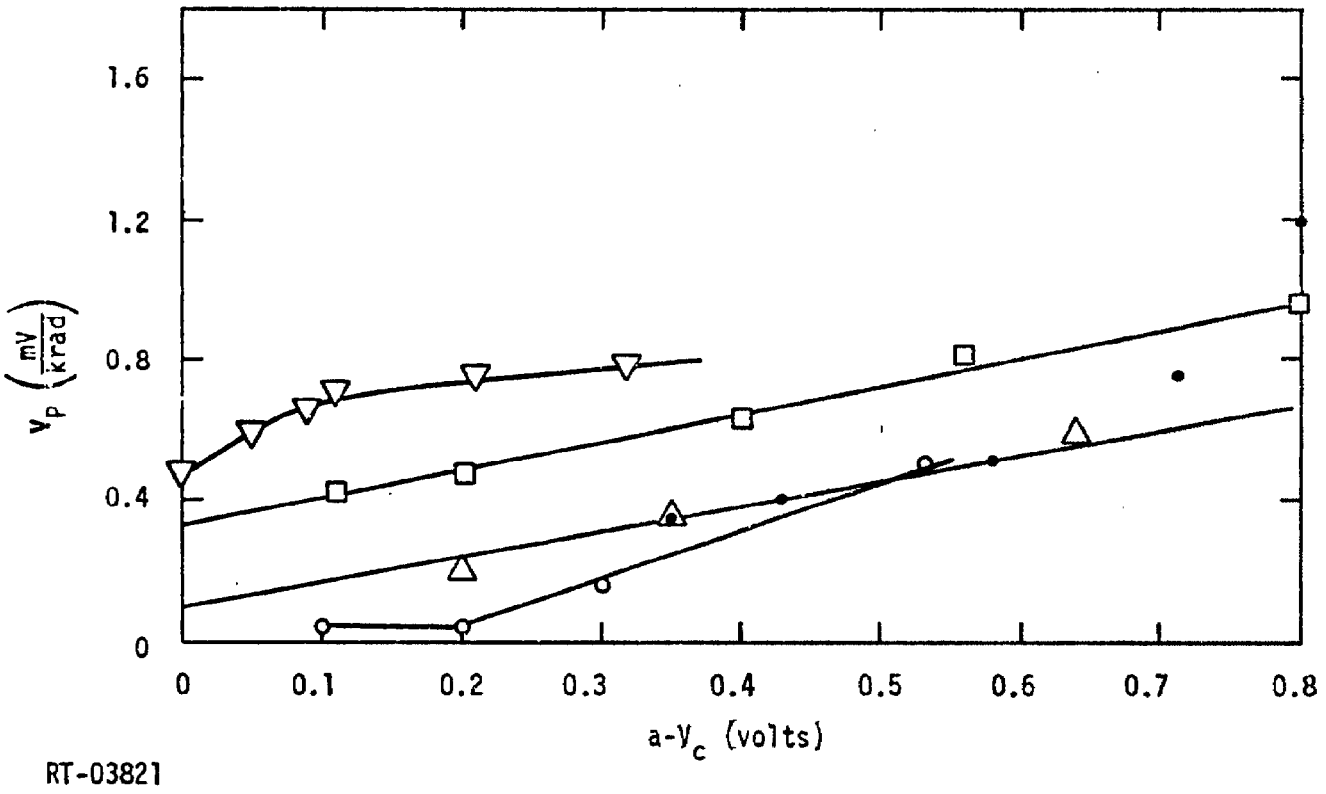

Figure 24. Peak response versus center-point voltage for 50-W.V. back-to-back pairs

which can also be regarded as the constant K assumption. For 50-W.V. capacitor 1 in Figure 21, a = 0.9 volt for $K' = 0.029$ krad^{-1}, $K'' = 0.012$ krad^{-1}, $\gamma_c = 13.16$ krad, and 50-W.V. capacitor 6 in Figure 21 can be fit by a 1.0 volt, $K' = 0.026$ krad^{-1}, $K'' = 0.020$ krad^{-1}, and $\gamma_c = 12.50$ krad. These two curves are plotted in Figure 25. By designating the voltage predicted by the first set of parameters above V_{p_1} and the second set of parameters V_{p_2}, we can construct Table 2, which gives the results from a hypothetical back-to-back pair. The table lists the values of a hypothetical back-to-back pair as a function of dose, both under the K = constant assumption and assuming the empirical curve given above. As can be seen, the K = constant assumption predicts an increasing response with dose, while the K variable technique predicts a decrease in response. This has been found with a few other trial cases as well. Since the decreasing response is experimentally observed, we concluded that it is necessary to include the variation of K with dose in a back-to-back scaling and that taking the second case, the variable K case, is a closer approximation to reality. While this and several other trial cases indicate that a low response at the 5 to 10 krad of the back-to-back pair results in even lower response per krad at higher dose, the complex nature of the process precludes general statements at this time, and some further testing is probably necessary. Such testing should be aimed at an accurate determination of the variation of back-to-back pairs with dose. Such tests were attempted on the Linac, but the results were clouded by inhomogeneous dose across the surface of the back-to-back pair, and large scatter in the data was observed. Hence, further testing will have to be done at a source in which better uniformity can be achieved over the sample area of a back-to-back pair.

4.2 BIAS AND BACK-TO-BACK PAIR RESPONSE

When a bias is applied across a back-to-back pair for times of the order of seconds, a significant reverse bias builds up across one of the capacitors. Workers at HDL have found that the application of

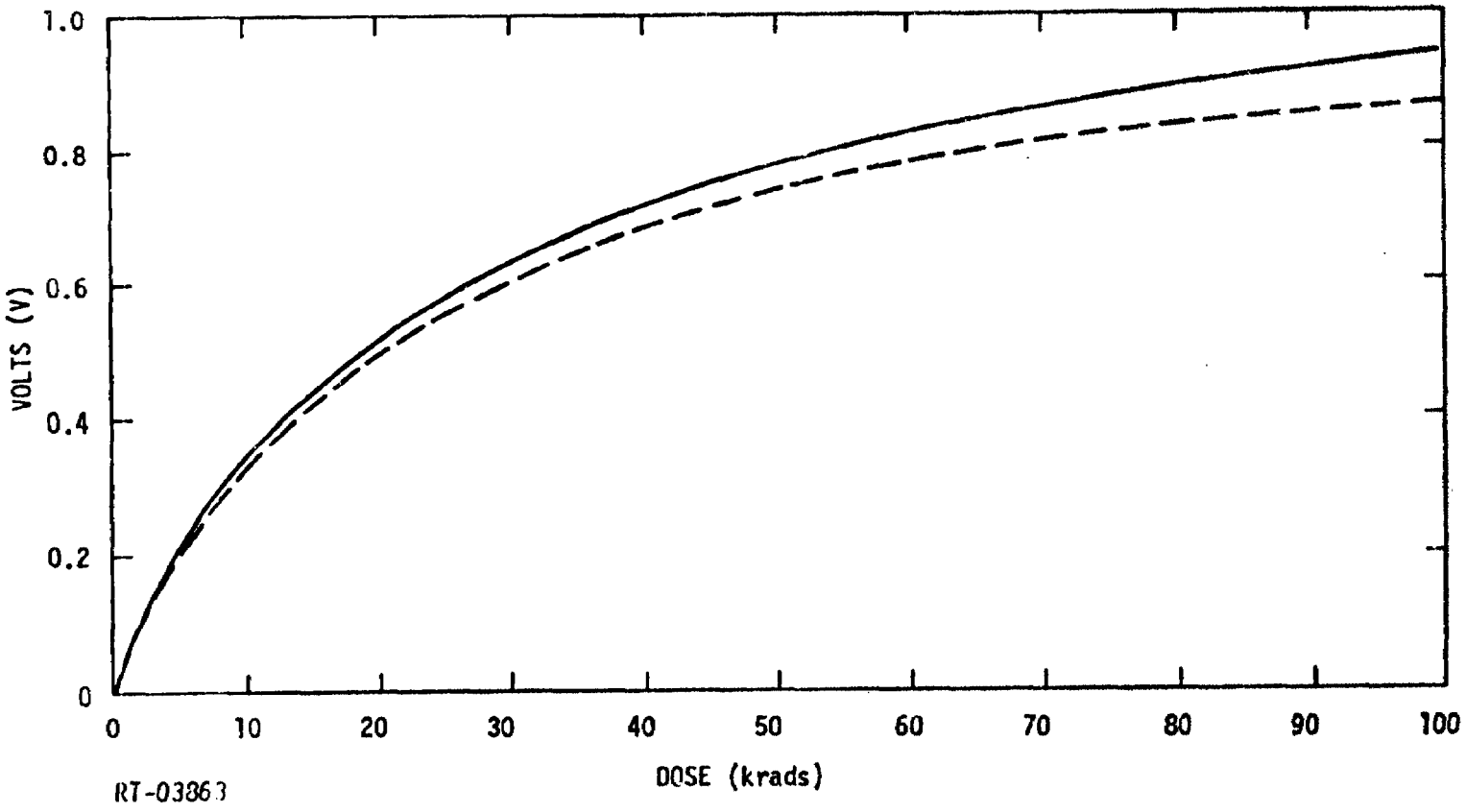

Figure 25. Open-circuit radiation response model for two capacitors

Table 2

COMPARISON OF TWO METHODS FOR CALCULATING BACK-TO-BACK RESPONSE

Dose (krad)	K = constant			K = F(γ)		
	$V_{P_1}\left(\frac{mV}{krad}\right)$	$V_{P_2}\left(\frac{mV}{krad}\right)$	$V_{BB}\left(\frac{mV}{krad}\right)$	$V_{P_1}\left(\frac{mV}{krad}\right)$	$V_{P_2}\left(\frac{mV}{krad}\right)$	$V_{BB}\left(\frac{mV}{krad}\right)$
1	43.9	45.0	1.1	43.0	44.2	1.2
10	35.4	36.8	1.4	31.8	32.8	1.0
20	28.4	30.0	1.6	24.7	25.7	1.0
40	19.5	21.1	1.6	17.1	18.0	0.9

of this reverse bias to a tantalum capacitor induces maverick behavior (Ref. 10). Hence, the biasing of back-to-back pairs could cause response to change significantly. To examine this experimentally, back-to-back pairs were made up of 6- and 50-W.V. Kemet and Sprague capacitors (manufacturers were not mixed in the pairs). The pair response was measured at the Linac on August 2, 1972. Each pair was then biased with 30% of the rated voltage of the capacitors in the pair for 30 seconds. The capacitors were then shorted until September 20, 1972, when their response was again measured at the Linac. The results are shown in Table 3. Although in most cases the response of the pair decreases as a result of the treatment, in a few cases the response increased significantly. Hence, since the cause of the effect is not understood at the present time, the biasing of back-to-back pairs is to be avoided, to avoid possible changes in the response.

Table 3

THE EFFECTS OF BIAS AND PAIR RESPONSE

Manufacturer	Serial No.	W.V.	Peak Response (mV/krad) 8/2/72	9/20/72
Sprague	447/448	50	-1.0	-0.3
Sprague	449/450	50	0.82	-0.2
Sprague	452/451	50	2.5	0.4
Sprague	456/453	50	1.4	0.2
Kemet	1878/1877	50	2.1	1.6
Kemet	1872/1871	50	2.5	0.9
Kemet	1870/1869	50	-2.2	0.2
Kemet	1868/1867	50	0.92	1.2
Kemet	2560/2587	6	<0.1	0.4
Kemet	2557/2558	6	1.62	0.9
Kemet	2555/2556	6	-0.6	+0.2
Kemet	2553/2575	6	2.2	1.1
Kemet	2551/2552	6	-0.9	-0.2
Sprague	1772/1771	6	-0.9	-0.4
Sprague	1773/1774	6	-2.5	1.8
Sprague	1815/1813	6	-0.2	-1.2

5. PARAMETRIC STUDIES

While the model that has been developed for tantalum capacitors explains most of the features of the radiation response, the quantitative prediction of the capacitor response depends upon the parametric values for the model, which vary from capacitor to capacitor. The range of variation of these parameters must be determined empirically. In addition, the qualitative variations predicted by the model should be examined in a variety of circumstances to obtain further confidence in the physical picture presented by the model.

One feature of the model is a prediction that the dose in the Ta_2O_5 determines the response and that the response is independent of the particle type or spectrum which is responsible for the dose deposition. This point was examined to some extent in the previous study (Ref. 1), and the results obtained at that time supported the model. A number of assumptions went into the verification reported in the previous study and further study seemed warranted. Since the Aurora Facility is used for verification tests of electronic assemblies, a comparison of the results obtained at the Rad Tech Linear Accelerator and at the Aurora Facility is of considerable interest. In addition, the Aurora Facility spectrum is of a higher energy than the spectrum used in the previous study, and some of the assumptions made in the previous study are not necessary to make the comparison between Linac and the Aurora Facility.

Six (three Sprague and three Kemet) 6.8-μF, 50-W.V. capacitors were exposed at the Aurora Facility. The zero-bias responses at various levels were measured with a 10-kΩ load. Dosimeters (tantalum compensated TLDs) were placed in front and back of the capacitors in the test cassette, except for one shot where the TLDs were placed side by side by mistake. The results are given in Table 4. The peak signals for each capacitor are given for the three shots at Aurora for which

Table 4

COMPARISON OF ZERO-BIAS RESPONSE
AT LINAC AND AURORA

Cap. Ser.	Manufacturer	Aurora Results mV/krad(Ta_2O_5) V_{P_1}	V_{P_2}	V_{P_3}	$\overline{V}_P$	Linac Results mV/krad(Ta_2O_5) V_P
473	Sprague	6.1	6.9	7.6	6.9	8.8
474	Sprague	10.0	11.3	11.9	11.1	13.4
475	Sprague	7.8	9.4	10.8	9.3	10.4
1864	Kemet	14.7	15.0	16.8	15.5	18.8
1865	Kemet	12.1	14.4	15.6	14.0	18.0
1866	Kemet	13.0	13.8	14.6	13.8	17.4
Front Dose (krad(Ta_2O_5))		6.1	17.1	9.6		
Back Dose (krad(Ta_2O_5))		5.4	14.7	8.9*		

* Side dose

good data were obtained. (Experimental errors caused the data to be lost on the one shot.) The dose reading of the TLD located in front of and behind the capacitor is also listed for each shot. These readings were used to compute the volumetric average of the dose which produces the response. Since the attenuation of the beam is small, let us assume one absorption coefficient for the entire capacitor:

$$\gamma_x = \gamma_0 e^{-\frac{\mu}{\rho} x}, \qquad (3)$$

where γ_0 is the incident radiation, γ_x is the gamma flux at any point, $\frac{\mu}{\rho}$ is the attenuation coefficient, and x is the distance into the capacitor.

Now

$$\bar{\gamma} = \frac{\gamma_0}{\ell} \int_0^{\ell} \exp(-\mu/\rho)\, x\, dX$$

$$= \frac{\gamma_0}{\frac{\mu\ell}{\rho}} [1-\exp(-\mu\ell/\rho)] = \frac{\gamma_0 - \gamma_\ell}{\frac{\mu\ell}{\rho}} \tag{4}$$

where ℓ is the thickness of the capacitor and γ_ℓ is the flux at the exit side of the capacitor from which

$$\frac{\mu\ell}{\rho} = \ell n \frac{\gamma_0}{\gamma_\ell} \tag{5}$$

For the two shots where the TLDs were placed in front of and behind the capacitors, the values of this quantity were 0.122 and 0.151, respectively, confirming that the attenuation was small. The side dosimeters were within the standard deviation of a pair of TLD readings. The values of the doses obtained in the above manner were used to obtain the response in mV/krad of the capacitors tested at Aurora. The last column in Table 4 shows the Linac results on the same capacitors. The ratio of responses of capacitors is the same in the Aurora shots and the Linac shots, but the Linac responses are higher than the Aurora values by about 20%. This systematic error is probably due to a systematic dosimetric error but does bear some investigation.

5.1 BIAS TEMPERATURE AND DOSE/PULSE VARIATIONS

To examine the bias, temperature, and dose/pulse variations, the parametric matrix given in Table 5 was derived for characterizing the capacitor response. In addition to the measurements indicated in the table, the response of each capacitor type at 65°C was measured for R_L at load resistance values of 100 ohms, 1 kohm, 2.6 kΩ , 2.6 kΩ, 10 KΩ, and 50 kΩ at a fixed dose but as a function of bias. The capacitors

Table 5

PARAMETRIC VARIATIONS

W.V.	V_o =	0	2	4	6	8	10	15	20	25	30	35	45
6		X	X	X	X								
10		X	X	X	X		X						
20		X	X			X		X	X				
35		X	X			X		X		X		X	
50		X	X			X				X		X	X

Measurements performed at 25°C, 45°C, 65°C, 85°C

were also measured as a function of dose per pulse to doses in excess of 40 krad (Ta_2O_5).

It would have been ideal to carry out the complete parametric variation for each capacitor, but two radiation damage mechanisms prevent such complete experimentation on a given capacitor. The first mechanism is an enhancement of the deep recombination center density and some space charge induced energy band warping. When the carriers are ionized, electrons* are far more mobile than holes and produce most of the conductivity. The trapped holes produce a small internal space charge field and an incremental number of deep recombination centers for subsequently generated electrons. Thus, even at zero bias, an accumulation of dose causes the time signature and the magnitude of the radiation response to change as dose is accumulated. Secondly, irradiation with bia applied injects charge, creating significant space charge fields and nges in response as described previously. One can release the space ch. ge polarization with radiation at zero bias but enough radiation at zero bias changes the capacitor response, at least for the time of experiment. Thus,

* An arbitrary choice

damage is always built into the capacitor. Although polarization probems haunt all experiments of this type, such problems were avoided as much as possible in the experiments by following a certain set of procedures.

1. Most tests were performed with small dose/pulse [0.2 to 0.5 krad (Ta_2O_5)].

2. After each pulse with the bias applied, the capacitor was depolarized with 10 pulses at zero bias.

3. The data were taken on a given capacitor in the order of increasing bias.

4. Several capacitors of the same type were used for a given test. No one capacitor was used for all of the tests and obviously damaged capacitors were not used for further data taking.

Even with the above precautions, an occasional data point appears which is strongly inconsistent and is likely to be influenced by polarization which is built into the capacitor.

The response as a function of working voltage and temperature and bias is shown in Figures 26 through 42. When the data were fairly well separated for a given capacitor for two temperature readings, or virtually identical for two temperatures, the points are plotted on the same graph for reasons of economy. The Mallory capacitor data were taken late in the program so the Mallory capacitor data are plotted separately. The capacitor numbers shown in the figures correlate with individual capacitors listed in Table 6. In general, the data are consistent with the model showing a linear increase in $dV/d\gamma$ with applied voltage until saturation begins to set in at higher biases. The saturation effect is due to the fact that the charge liberated by the ionization pulse is being depleted at the higher biases. Hence, for a given dose of irradiation there is a limit to the amount of charge that can be removed.

Figure 43 shows a comparison of the temperature dependence of the response in the linear portion of the curve of response versus bias averaged over several capacitors. Even though the test covered limited

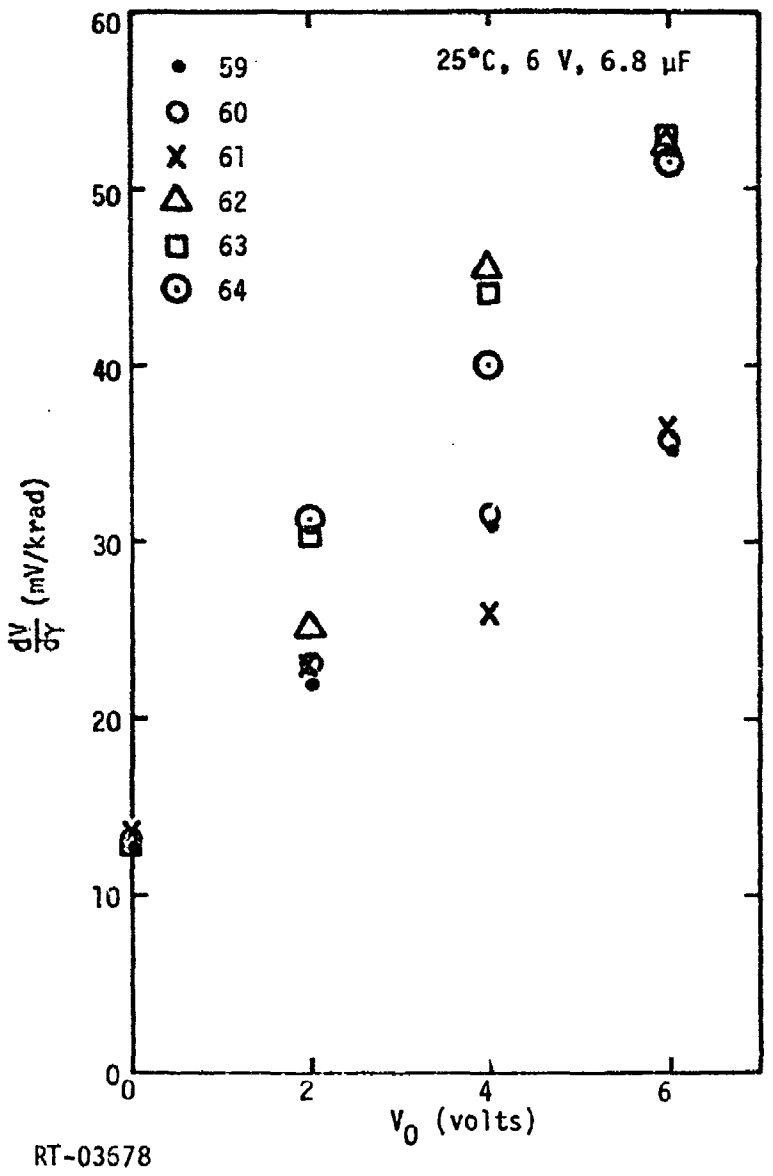

Figure 26. Peak radiation response for 6-W.V. capacitors at 25°C versus bias

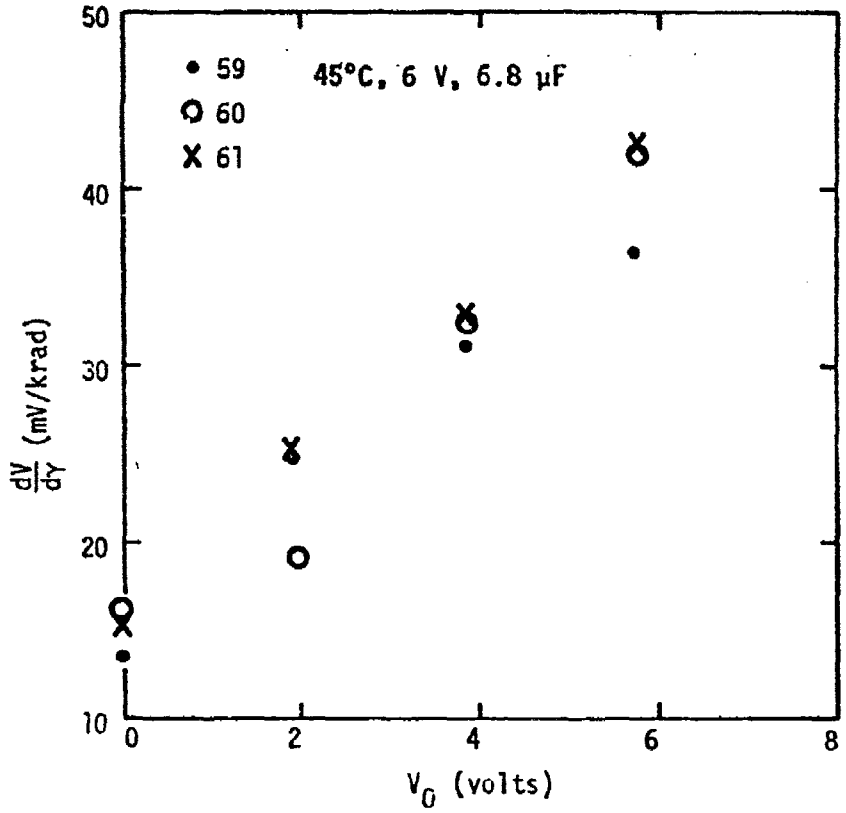

Figure 27. Peak radiation response for 6-W.V. capacitors at 45°C versus bias

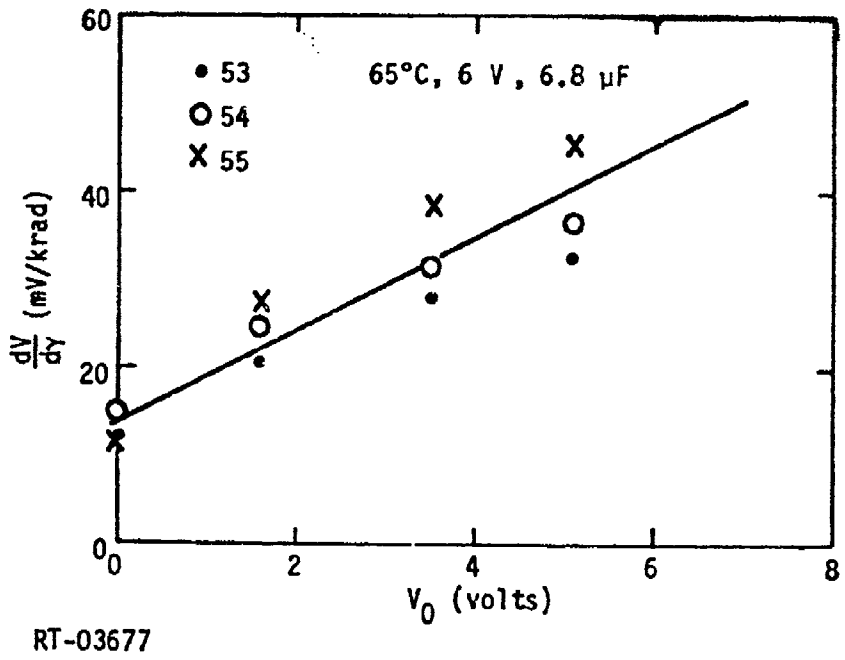

Figure 28. Peak radiation response for 6-W.V. capacitors at 65°C versus bias

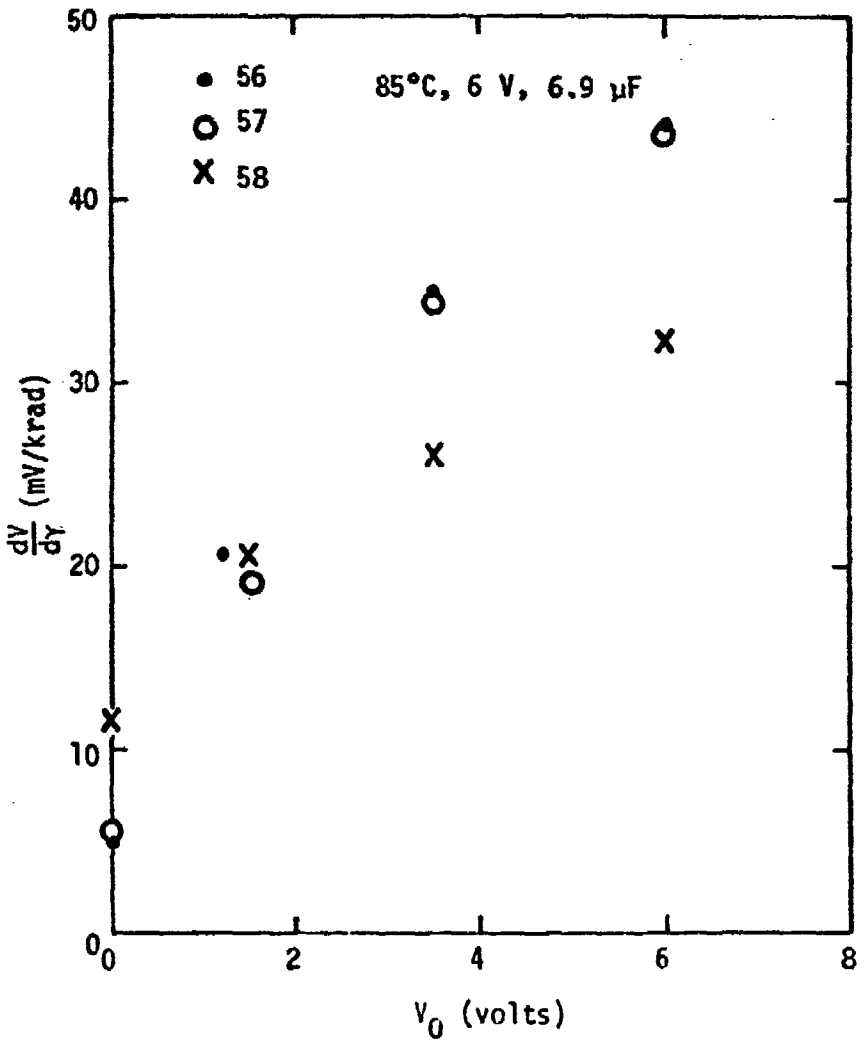

Figure 29. Peak radiation response for 6-W.V. capacitors at 85°C versus bias

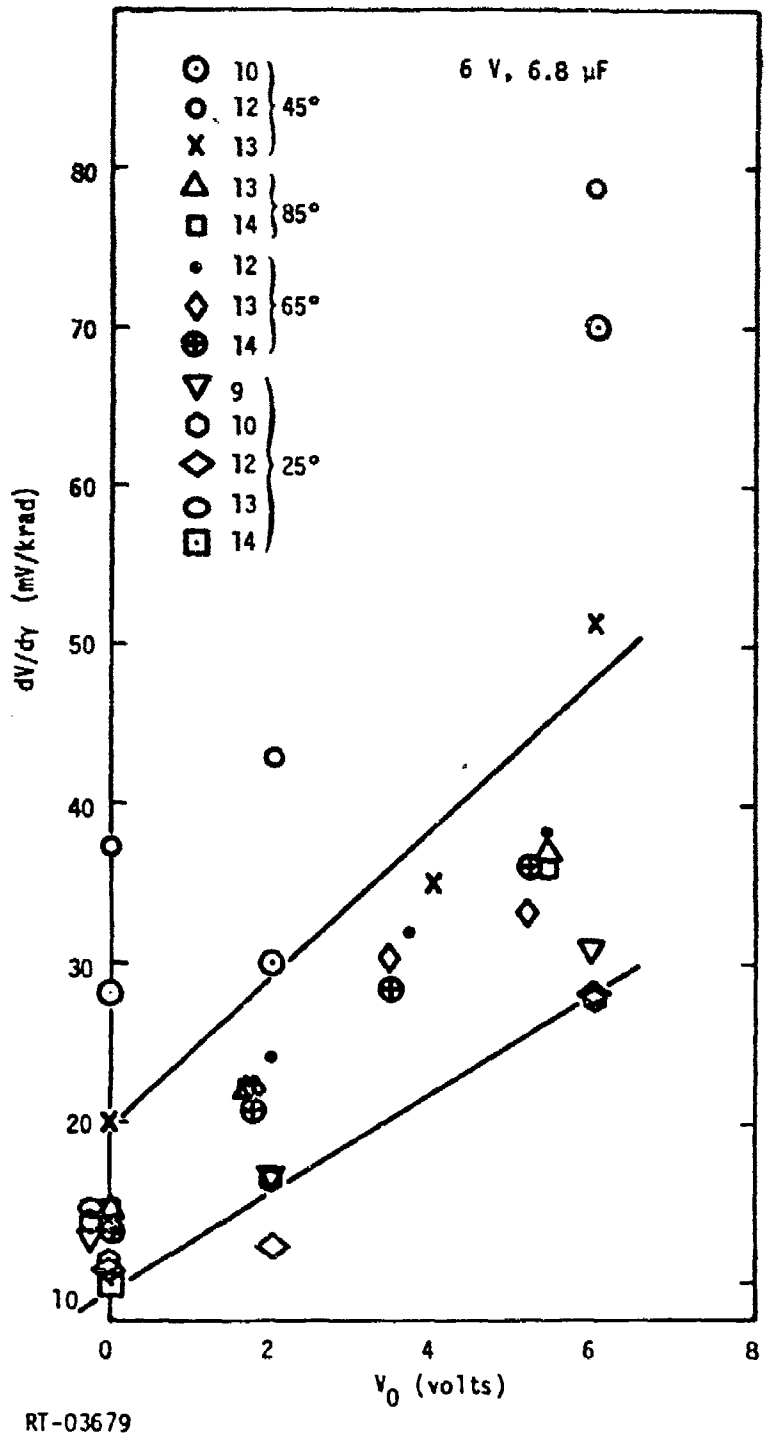

Figure 30. Peak radiation response for 6-W.V. Mallory capacitors at 25, 45, 65, and 85°C versus bias

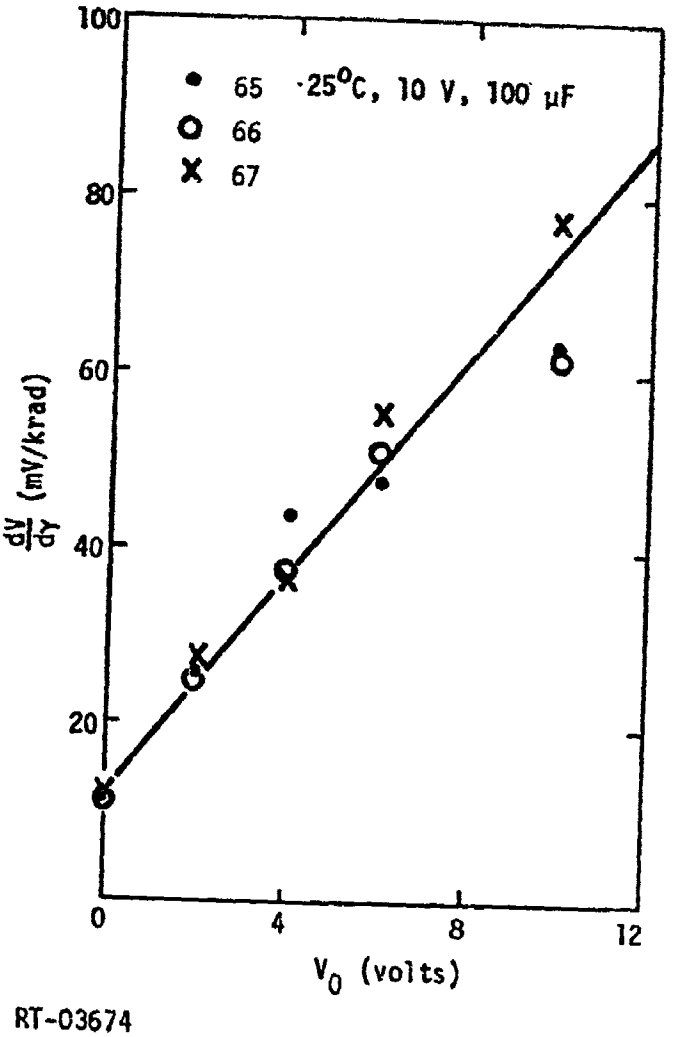

Figure 31. Peak radiation response for 10-W.V. capacitors at 25°C versus bias

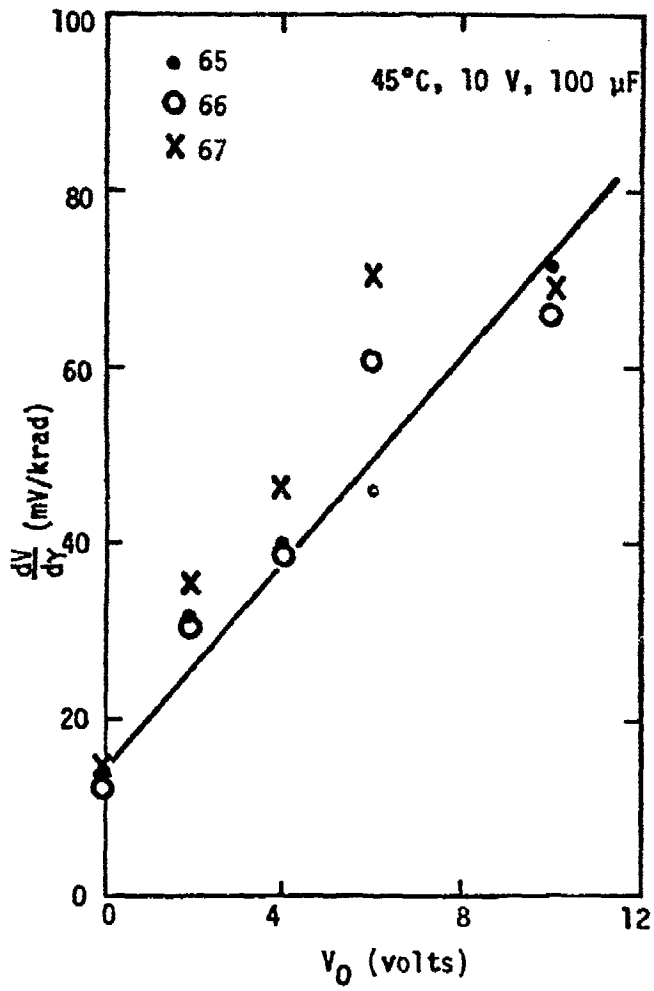

Figure 32. Peak radiation response for 10-W.V. capacitors at 45°C versus bias

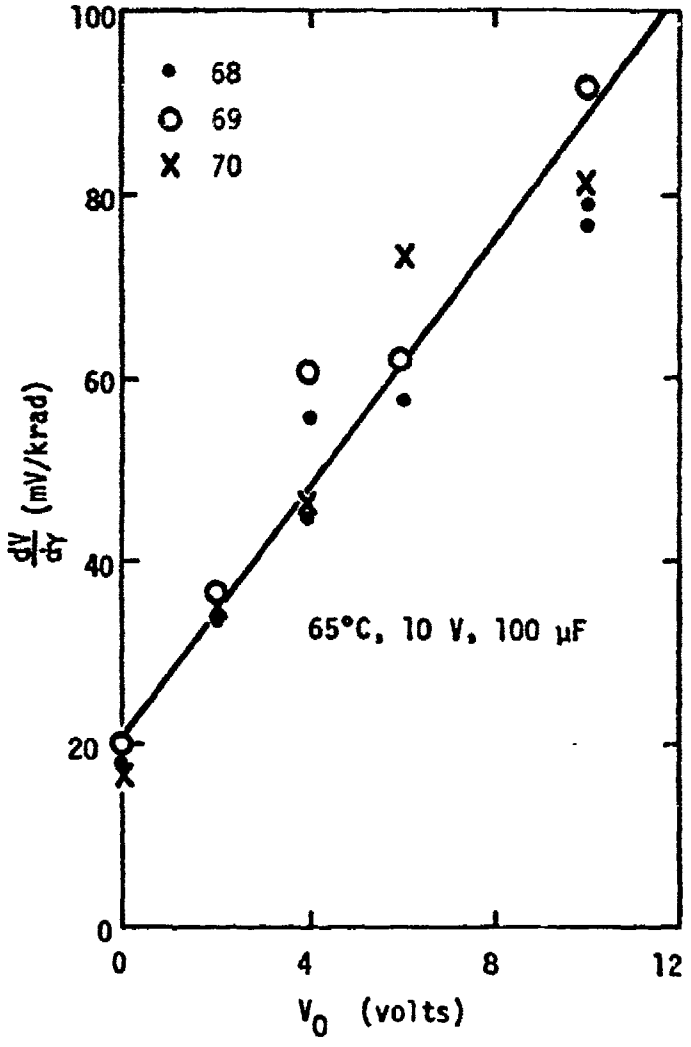

Figure 33. Peak radiation response for 10-W.V. capacitors at 65°C

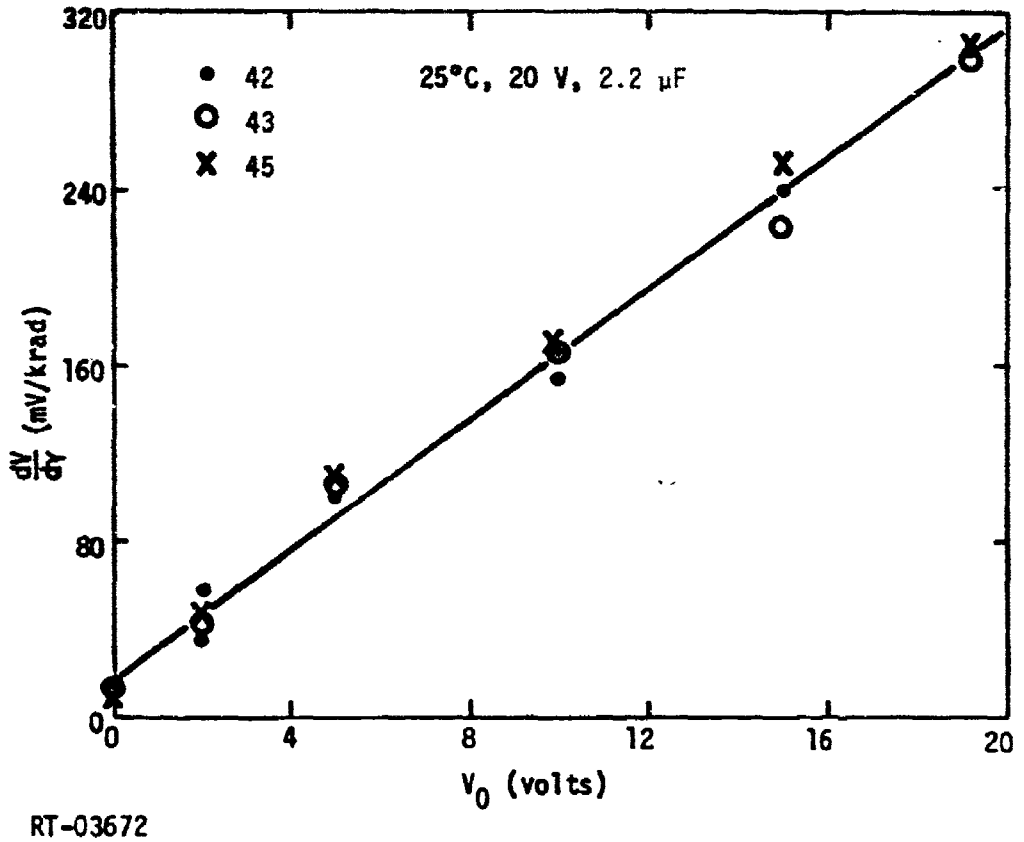

Figure 34. Peak radiation response for 20-W.V. capacitors at 25°C versus bias

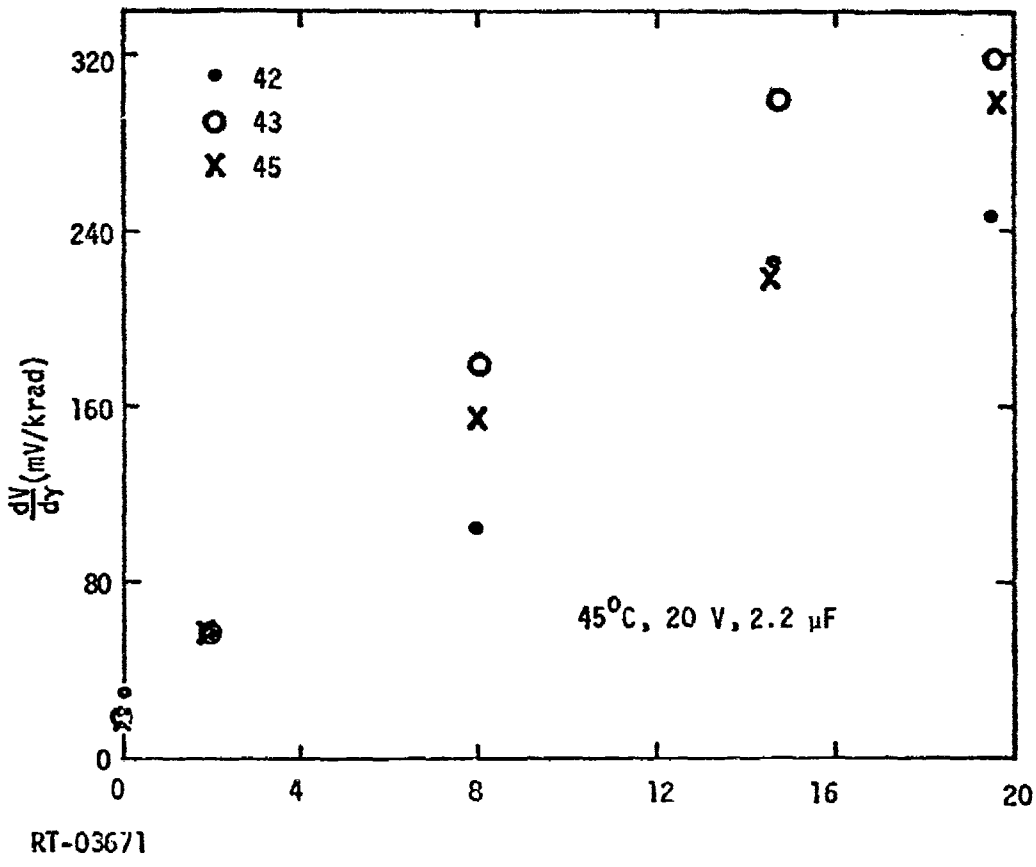

Figure 35. Peak radiation response for 20-W.V. capacitors at 45°C versus bias

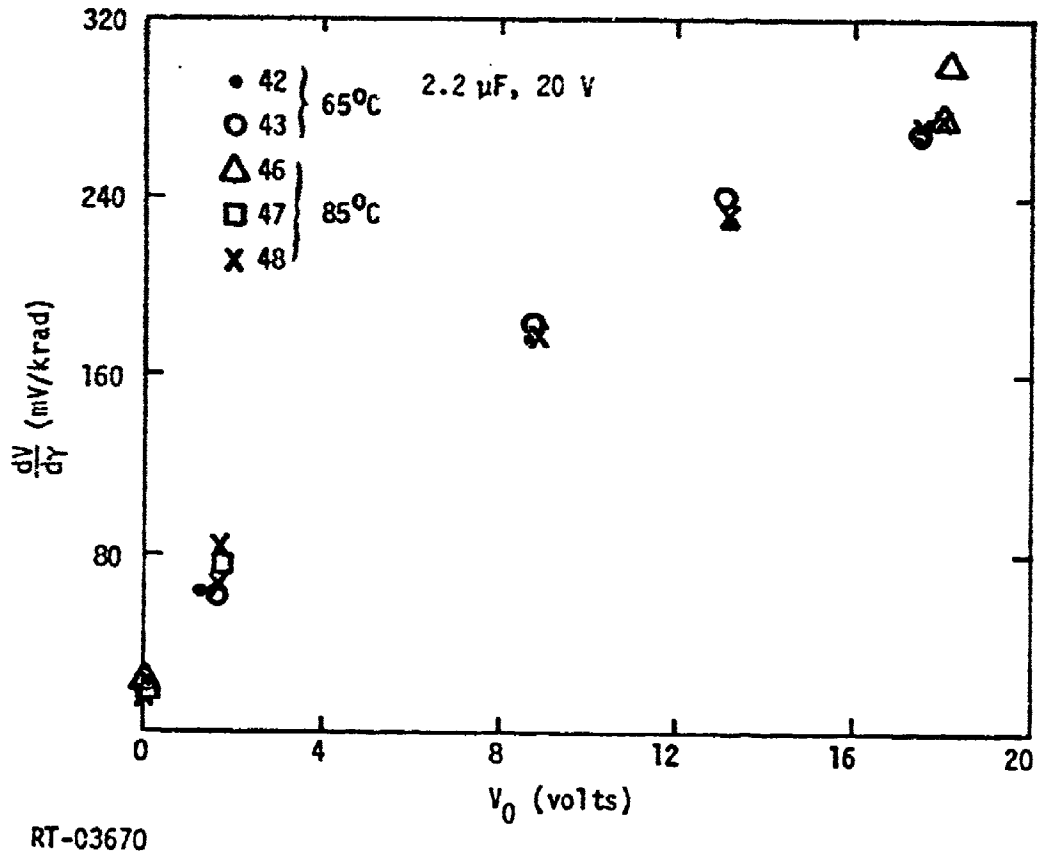

Figure 36. Peak radiation response for 20-W.V. capacitors at 65°C and 85°C

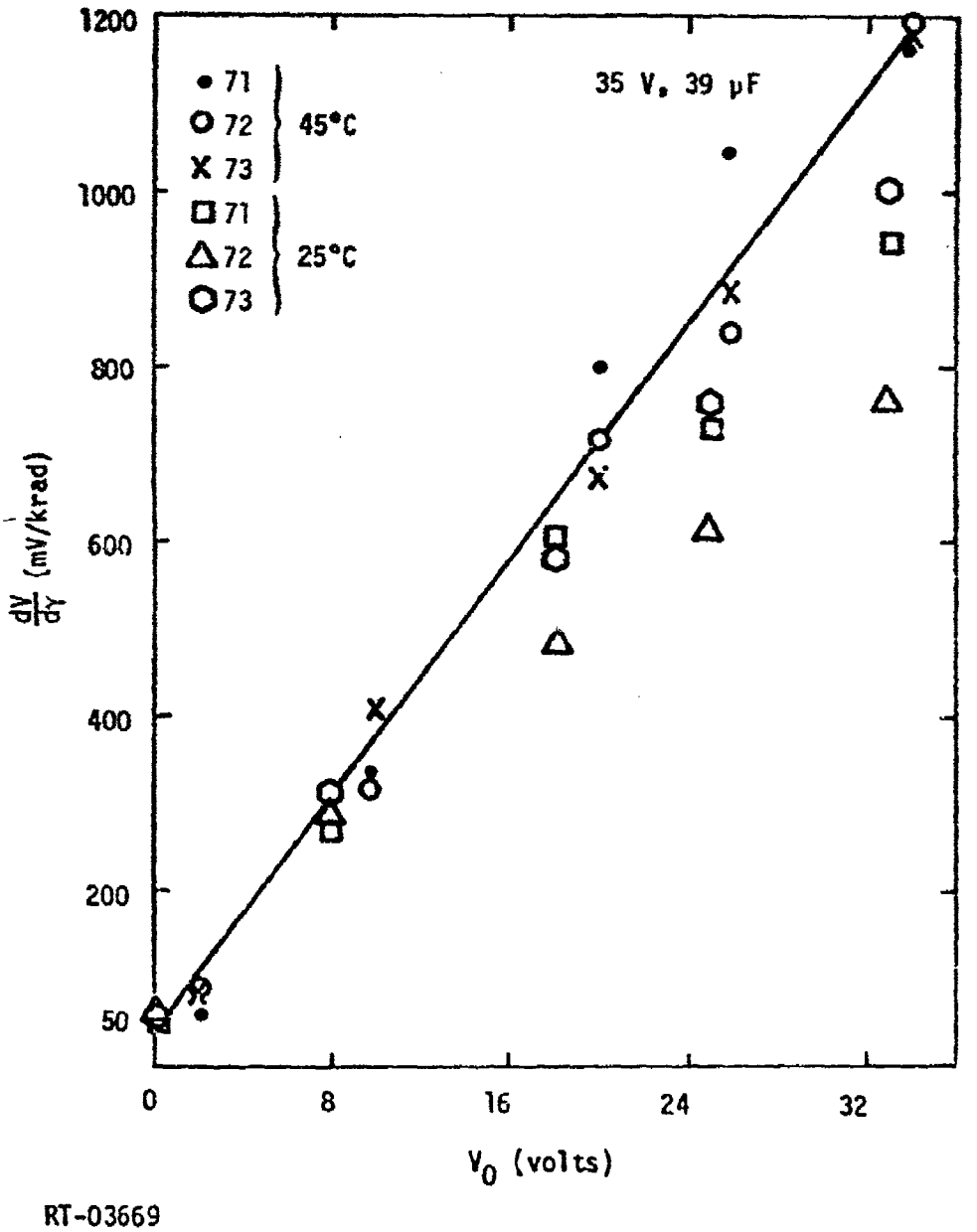

Figure 37. Peak radiation response for 35-W.V. capacitors at 25°C and 45°C versus bias

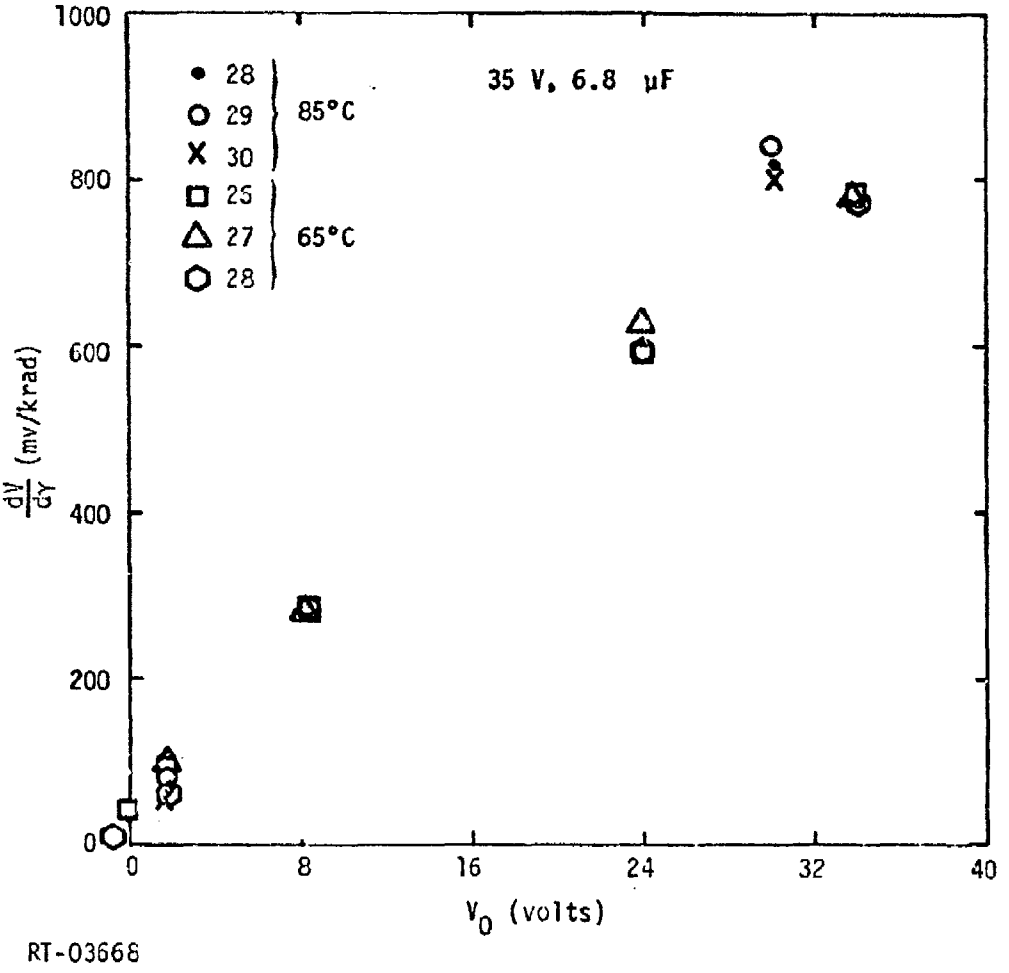

Figure 38. Peak radiation response for 35-W.V. capacitors at 65°C and 85°C versus bias

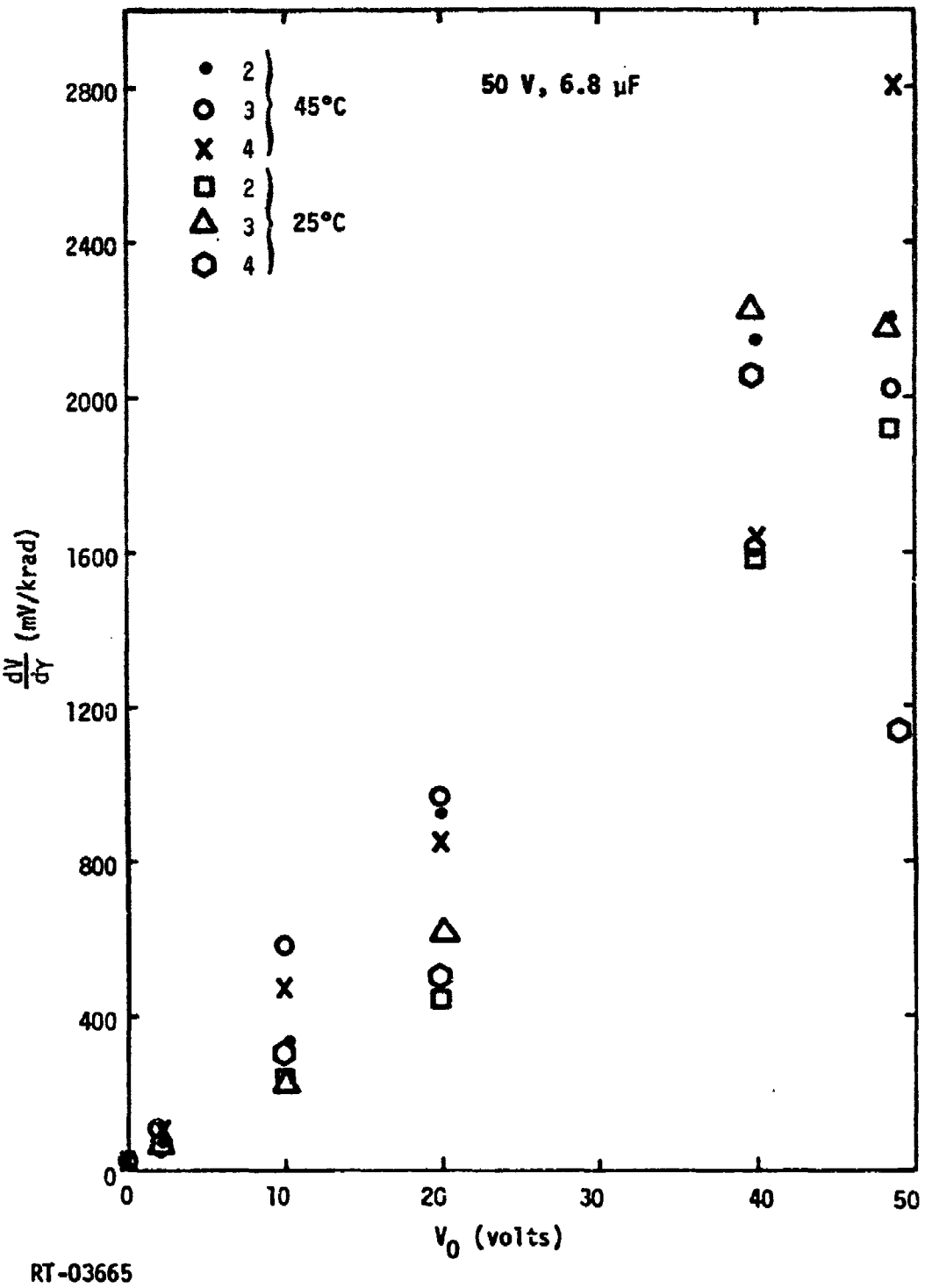

Figure 39. Peak radiation response for 50-W.V. capacitors at 25°C and 45°C versus bias

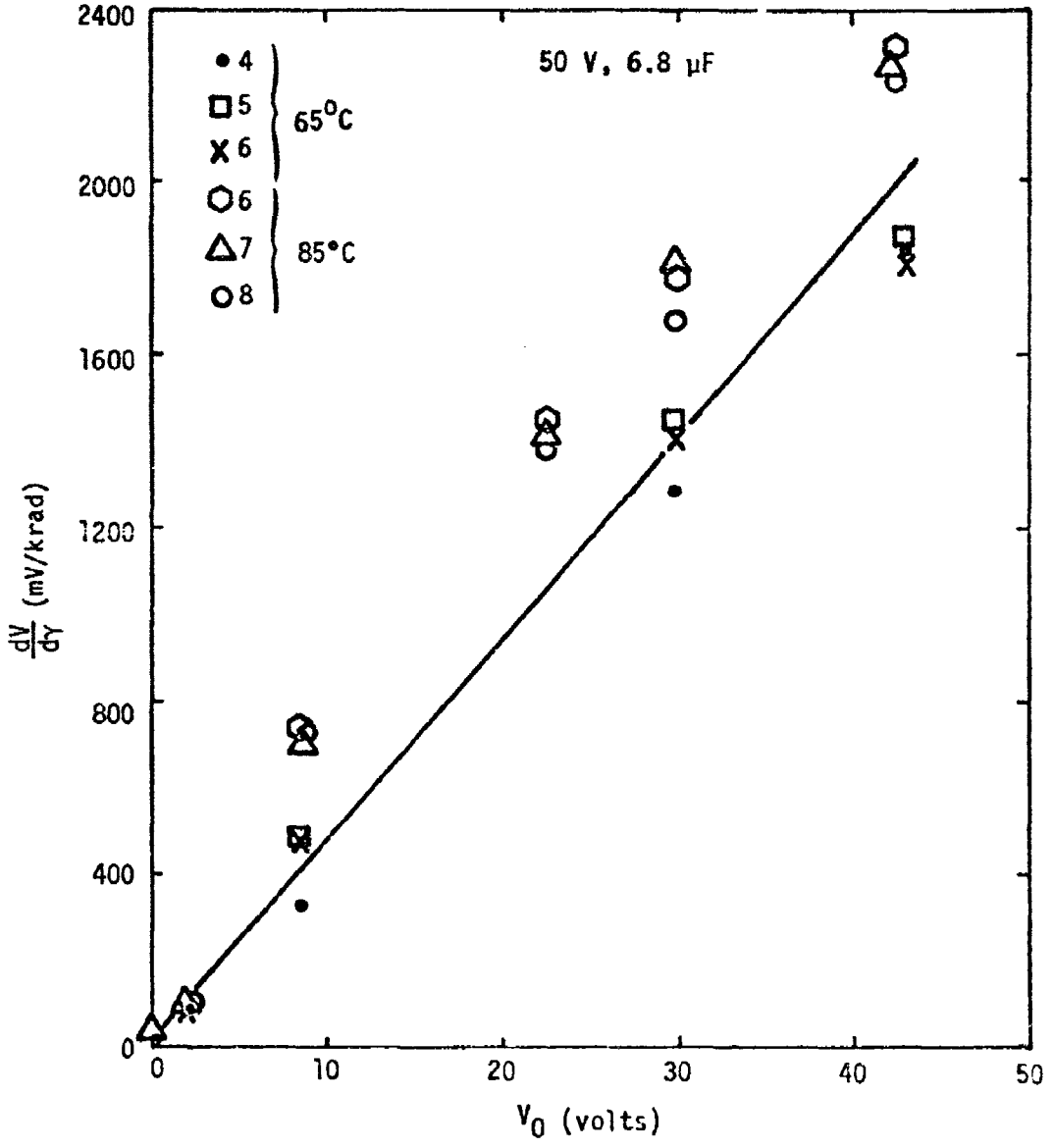

Figure 40. Peak radiation response for 50-W.V. capacitors at 65°C and 85°C versus bias

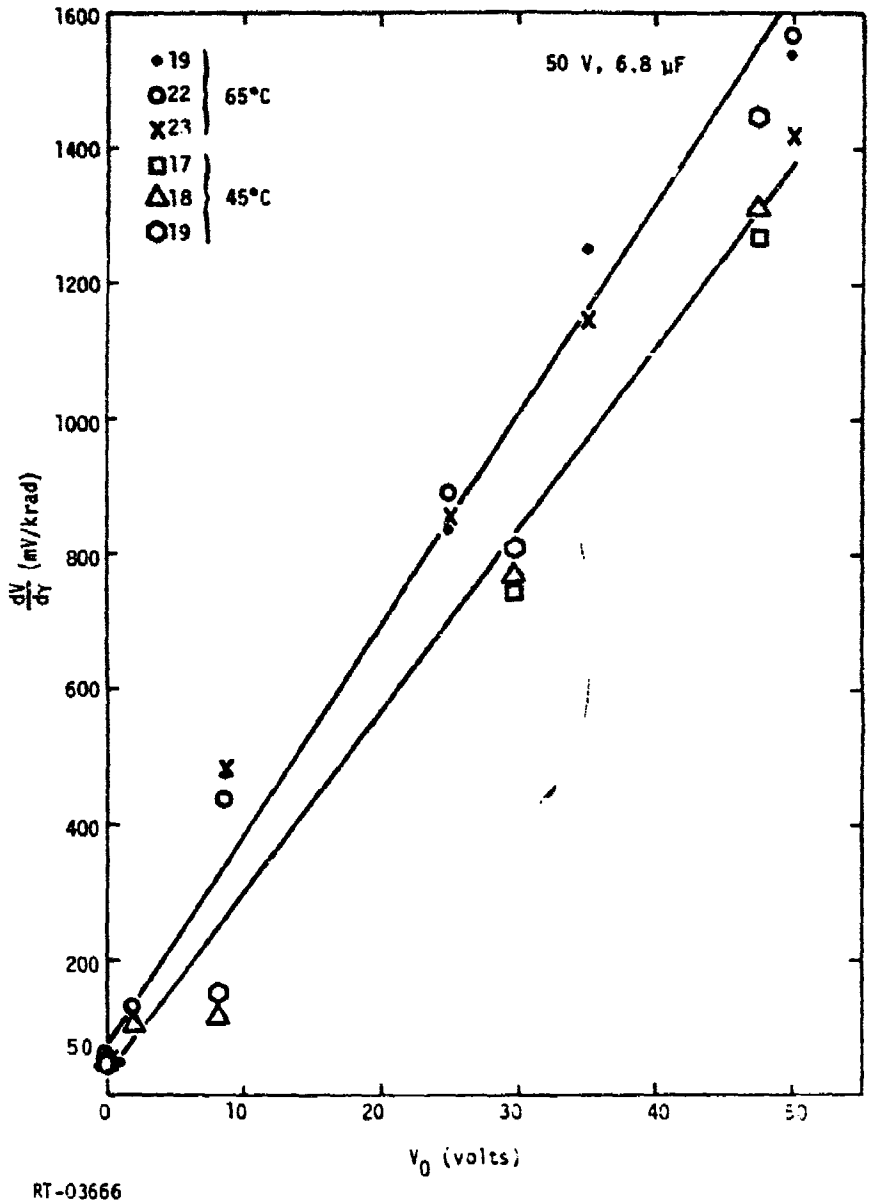

Figure 41. Peak radiation response for 50-W.V. Mallory capacitors at 45°C and 65°C versus bias

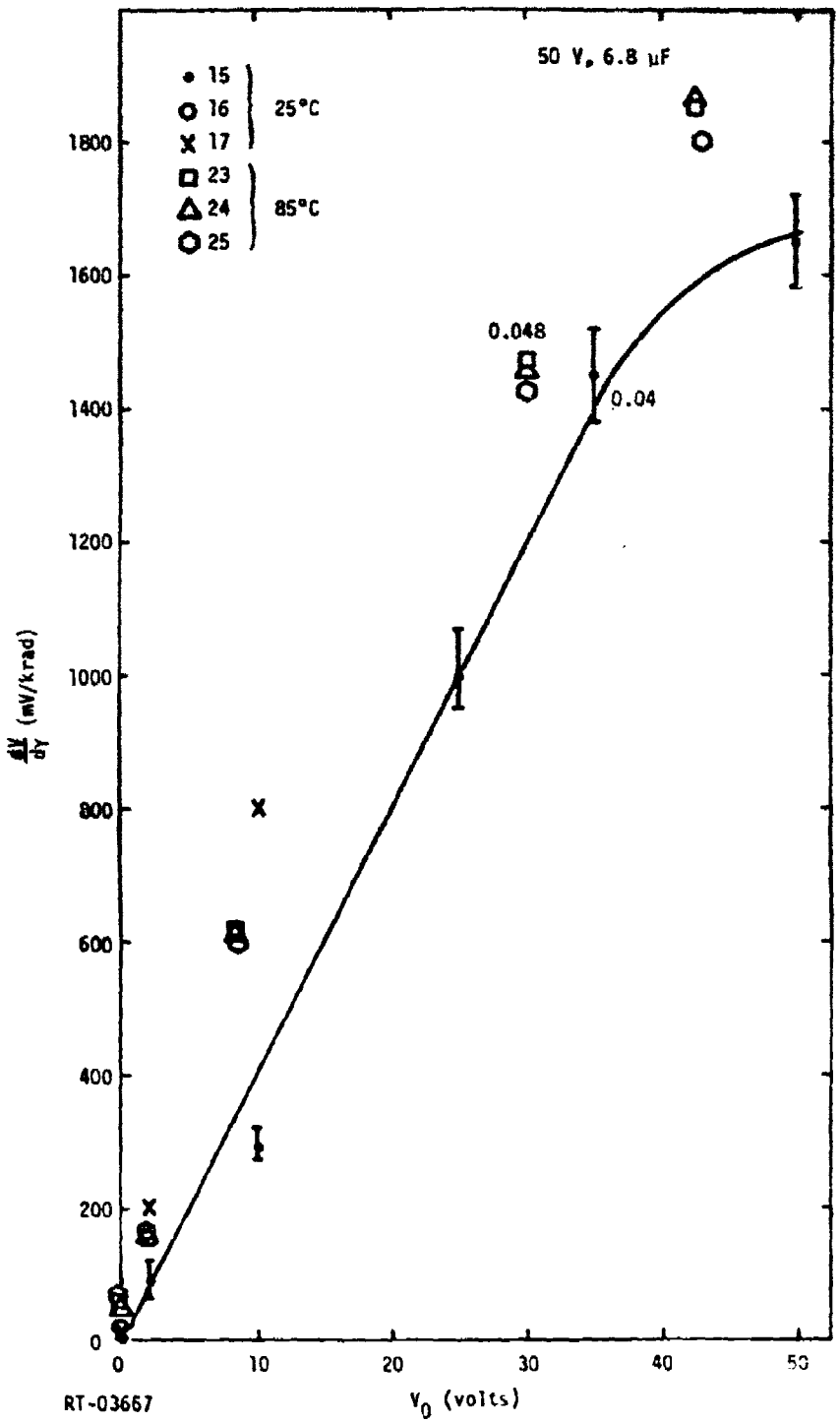

Figure 42. Peak radiation response for 50-W.V. Mallory capacitors at 25 and 85°C versus bias

Table 6

IDENTIFICATION OF CAPACITORS USED FOR PARAMETRIC STUDIES

No.	C (μF)	W.V.	Mfr.	Serial No.	No.	C (μF)	W.V.	Mfr.	Serial No.
2	6.8	50	Kemet	1840	30	6.8	35	Sprague	225
3				1839	31				277
4				1838	32				224
5			Sprague	430	33	3.3	15	Sprague	115
6				428	34				114
7				429	35				116
8				427	36				077
9	6.8	6	Mallory	No Mall. Ser.No.	37				117
10					38				118
11					39				119
12					40				120
13					41				121
14					42	2.2	20	Sprague	945
15	6.8	50	Mallory		43				952
16					45				955
17					46				954
18					47				950
19					48				942
20					49				946
21					50				944
22					51				951
23					52	6.8	6	Sprague	1772
24					53				1782
25					54				1787
26	6.8	35	Kemet	27422	55			Kemet	2550
27				27423	56				2588
28			Sprague	228	57				2549
29				143	58			Sprague	1820

Table 6 (Cont'd)

No.	C (μF)	W.V.	Mfr.	Serial No.	No.	C (μF)	W.V.	Mfr.	Serial No.
59	6.8	6	Sprague	1785	66	100	10	Kemet	1325
60				1783	67			Sprague	451
61				1822	68				450
62				2584	69				453
63				2561	70				452
64				2670	71	39	35		6013
65	100	10	Kemet	1324	72				6022
					73				352

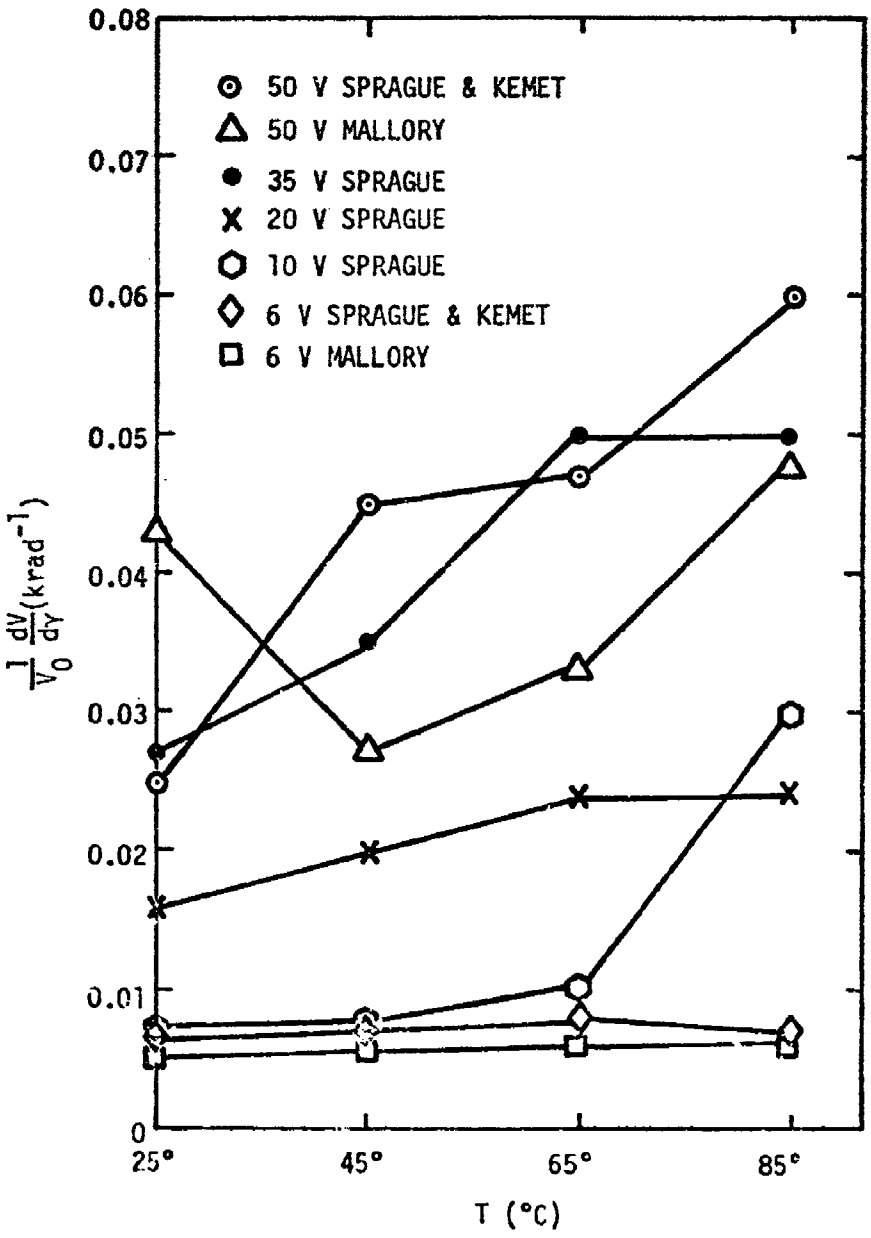

Figure 43. Peak radiation response versus temperature for various capacitors

numbers of capacitors, the results show definite consistent trends. Low-working-voltage capacitors respond less and have less temperature dependence. Larger working-voltage capacitors all behave about the same way, and the variation among capacitors is almost as large as the variation among manufacturers. There is a strange data point for the 50-W.V. Mallory at 25°C, but that is probably due to polarization inadvertently left in the capacitors. The 10-volt Sprague also stands out as being suspect at the 85°C point.

5.2 CHANGE IN RESPONSE WITH DOSE/PULSE AT 65°C

The voltage change of a given capacitor charged to a bias V_0 stimulated by an irradiation dose γ in the absence of a recharging source can be written

$$V = (V_0 + a) \exp(-K\gamma), \tag{6}$$

where V_0 = applied voltage,

a = built-in voltage,

and γ = charge loss factor,

which is the familiar exponential decay law for capacitors (Ref. 5).

To examine the accuracy of the exponential decay law for tantalum capacitors, capacitors were tested in the circuit shown in Figure 44 for total charge loss using 4.5 μsec pulses and doses from 0.5 krad to an excess of 40 krad at 1.4-volt bias and at 9.4-volt bias. Due to an experimental error, the data at 0.5 krad were lost, but data were obtained at 2, 5, 9, 25, and 45 krad (Ta_2O_5). The measurement taken was the total change in voltage, ΔV, resulting from a pulse of radiation

$$\Delta V = V_0 - V + a$$

where

V_0 is the applied bias,

V = voltage at end of radiation pulse,

and a = the built-in voltage.

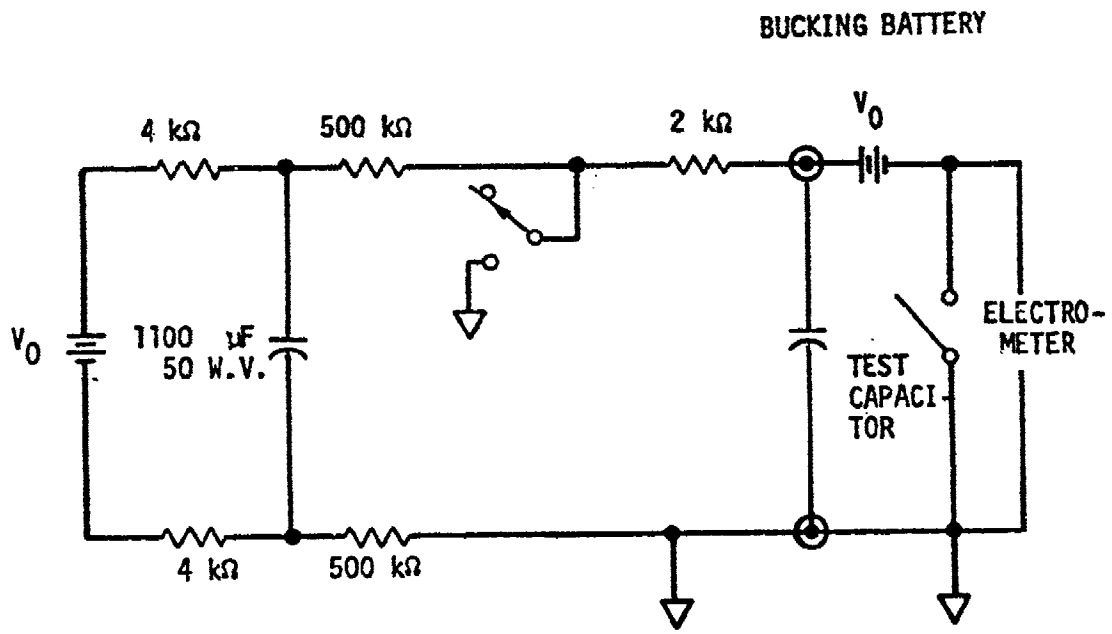

Figure 44. Total charge loss test circuit

Now

$$\frac{\Delta V}{V_0 + a} = 1 - \exp(-K\gamma) \tag{7}$$

and

$$K = \frac{1}{\gamma} \ln \frac{V_0 - a}{V_0 + a - \Delta V} .$$

The problem in analyzing the data is in selecting a value of a. Based on Linac tests and cobalt 60 tests using similar types of capacitors, the above data were analyzed with a = 1.2 V for Mallory capacitors and a = 1.0 volt for the remaining capacitors. These assumptions can introduce sizable errors where V_0 is small or where ΔV is large. However, since radiation damage problems prevent a measurement of the value of a on the same capacitors, some assumptions must be made about the value of a. The assumption, which was made here, is not unreasonable and is expected to introduce a small error, usually.

Another problem is that the response of the capacitor changes with bias applied as dose is accumulated. If a unit is susceptible to space-charge effects, the higher dose data will fall below the prediction of the exponential decay law due to the buildup of space charge polarization during the pulse. As is seen, this will introduce a spread in the data, and some capacitors appear to have a low response at high dose.

The data are listed in Table 7 in order of increasing working volts on the capacitors. The total charge loss constant K is given in Table 7. This total charge-loss constant is related to the peak response in %/krad, $K = (\tau_2/RC)V_p(\%/krad)$, if the response decays with a single time constant τ_2 with a load resistor R. K is actually greater than the expression on the right above due to the fact that a number of time constants are longer than τ_2. The data showed increasing charge-loss factors with increasing working voltage and showed that the exponential law is either correct or conservative. Those cases where the response is below that predicted by the exponential decay law are probably due to the build-up of space-charge polarization during the pulses at the higher doses. The very large values of charge loss observed at low doses in some capacitors may also be due to errors in a. While qualitatively we attribute

Table 7

CHARGE LOSS VERSUS DOSE: NO RECHARGE

			DOSE [krad (Ta_2O_5)]									
			2		5		9		25		45	
			Voltage (V)									
C (μF)	W.V. (V)	Mfr.	1.4	9.4	1.4	9.4	1.4	9.4	1.4	9.4	1.4	9.4
6.8	6	Sprague	1.4	0.5	1.7	0.9	1.0	0.9	1.2	0.6	1.2	0.6
6.8	6	Sprague	1.6		1.6	0.9	1.6	0.9	1.1	0.6	1.2	0.6
6.8	6	Kemet	1.3		1.4	0.9	1.5	0.8	1.1	0.6	1.2	0.5
6.8	6	Kemet	1.3	0.4	0.8	0.4	0.8	0.3	0.7	0.3	0.9	0.3
		Mallory	1.7	0.9	1.8	1.0	2.0	1.0	1.4	0.7	1.7	0.8
			1.7	0.9	1.7	0.84	2.2	1.0	1.5	0.7	1.8	0.8
100	10	Sprague	2.8		2.6		2.5		2.7		2.6	
3.3	15	Sprague		4.3		5.0		3.4		3.9		3.0
	15	Sprague		2.0		1.5		1.6		1.4		1.5
	15	Sprague		2.5		2.5		2.5		2.4		2.6
	15	Sprague		2.7		2.6		2.5		2.4		2.6
	15	Sprague	4.2		3.6		3.8		3.6		3.3	
	15	Sprague	4.5		4.7		4.1		4.1		4.1	
	15	Sprague	5.8		5.1		5.5		5.3		5.1	

The numbers in the columns are K_τ in %/krad (or in units of $x10^5$ rad^{-1})

Table 7 (Cont'd)

C (μF)	W.V. (V)	Mfr.	DOSE [krad (Ta_2O_5)] 2 VOLTAGE (V) 1.4	9.4	3 1.4	9.4	9 1.4	9.4	25 1.4	9.4	45 1.4	9.4
	20	Sprague	7.7		6.7		6.1		6.3		5.4	
			8.1		7.9		7.1		7.1		5.5	
			8.1		8.1		7.0		6.4		5.9	
				3.5		3.2		3.4		3.3		3.3
				2.8		2.5		2.5		2.9		2.8
	35	Sprague	2.7	5.6	2.8	4.7	2.6	4.2	1.7	3.0	0.93	2.0
			13	9.2	12	8.5	6.7	7.5	4.3	5.2	4.2	4.0
			11	9.4	9.1	8.1	8.5	7.6	4.8	5.6	5.0	3.6
6.8	50	Sprague	5.8	11	5.4	7.4	5.1	6.2	3.6	3.6	2.6	2.1
6.8	50	Sprague	9.0	11.5	7.9	7.8	7.2	—	4.7	3.4	3.0	2.2
6.8	50	Kemet	7.8	9.3	9.7	7.4	7.4	5.8	4.6	3.8	5.0	2.8
6.8	50	Kemet	8.8	11.1	14	7.8	9.4	6.8	5.3	3.6	3.9	2.4
6.8	50	Mallory	11	12	8.6	9.7	9.2	10	5.9	6.8	--	7.4
6.8	50	Mallory	16	12	16	11	14	7.4	6.0	7.0	--	6.3

the lower value of K at high doses to space-charge polarization, unfortunately the amount of decrease is not constant for all capacitors. Some capacitors do not show any significant deviations from the exponential decay law predictions. Hence, we conclude the exponential decay law is a valid one, and for more precise data on individual units, we need (1) a better value for a, and (2) a reasonable accounting for polarization effects. The second condition may require a change in manufacturing process or an additional screen. However, a screen based on our current understanding of space-charge polarization effects cannot be regarded as providing a high confidence since the details of the injection and trapping are not well understood.

5.3 LOAD DEPENDENCE AT CONSTANT DOSE: T = 65°C

The usual way of modeling the charge release with radiation from a capacitor is with a current generator:

$$I \alpha K_\rho \dot{\gamma} + F_{di} \int_{-\infty}^{t} \exp\left[-(t-t')/\tau_{di}\right] \sum \dot{\gamma}(t')dt' , \qquad (8)$$

where

K_ρ is the prompt charge loss constant,
$\dot{\gamma}$ is the dose rate,
F_{di} is the delayed conductivity coefficient for the ith component,

and τ_{di} is the decay time constant for the i^{th} conductivity component. In this expression, the linear term in $\dot{\gamma}$ describes the prompt current while the sum extends over each trapped-charge-release time constant, τ_{di}, which gives rise to a delayed current. Such a formulation is attractive because it describes the physical processes which are occurring and it is useful in a usual case where only a few trapping levels are significant. Unfortunately, for tantalum capacitors large numbers of traps are distributed in energy throughout the bandgap in the dielectric.

Thus, to obtain the F_{di} and the τ_{di}, a fit would have to be made of the decay of the current from times of the order of microseconds to seconds. The fit would involve many exponentials and would not only be cumbersome but also would not be unique since (1) the point at which one exponential took over from another would have to be arbitrarily chosen since there are so many exponentials, and (2) when the trapping levels interact (as they do in such trap distributions) the deceay is not exponential anyway. Additionally, the trap distribution may vary from capacitor to capacitor, and a fit for one capacitor is unlikely to be applicable for all.

There is a way around such a problem. For most circuit applications, the entire decay does not have to be characterized. What is important is the charge loss which occurs in a time comparable to the circuit recharge time. Hence, if a semi-empirical model can be found which describes the magnitude of the charge release in terms of the load resistor, the problem is somewhat simplified. The decay time in a given circuit configuration, τ_2 , must always be greater than RC. The trapped charges being evolved at times comparable to RC continue to charge the capacitor in competition with the RC recombination process occurring in the external circuit. Figure 45 shows a plot of τ_2 for a typical tantalum capacitor at both 25 and 65°C as a function of the load resistor. The dashed line has a unity slope and, as is seen, τ_2 has a slight sublinear dependence on the load. The fact that there is virtually no difference between τ_2 at 25 and 65°C indicates that there is a very smooth distribution and high density of electron traps which are emitting during these times. τ_1 and τ_2 have the same load dependence as is shown in Figure 46, where again a typical capacitor is plotted. The transient response of the capacitor can be expressed approximately as

$$V = -A \exp(-t/\tau_1 + B \exp(-t/\tau_2) ,$$

as discussed in the previous report (Ref. 1) where both τ_1 and τ_2 and A and B are fitting constants. Taking dV/dt = 0, and solving for the peak value of V, we obtain

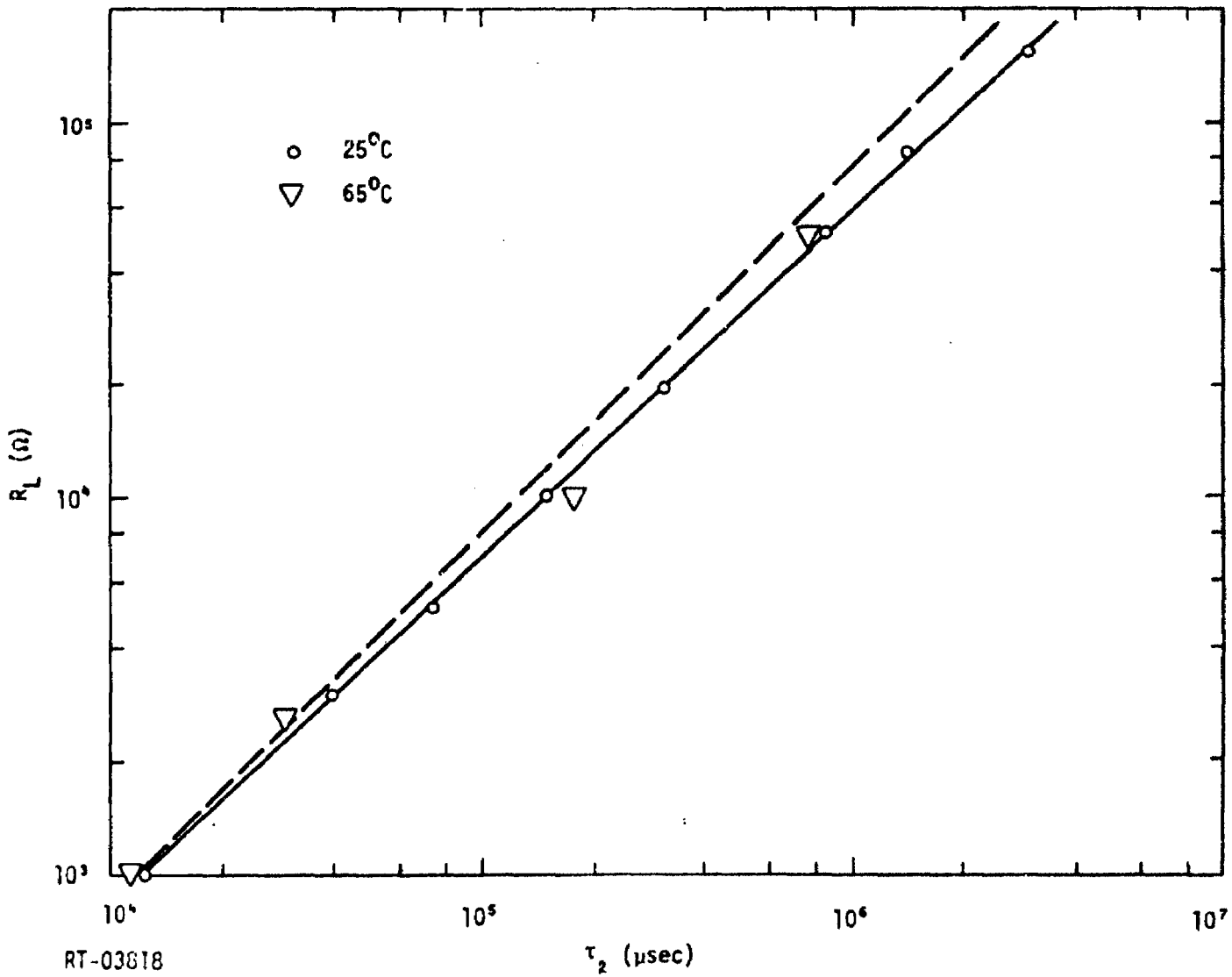

Figure 45. Decay time of the radiation response as a function of load resistor for 25 and 65°C

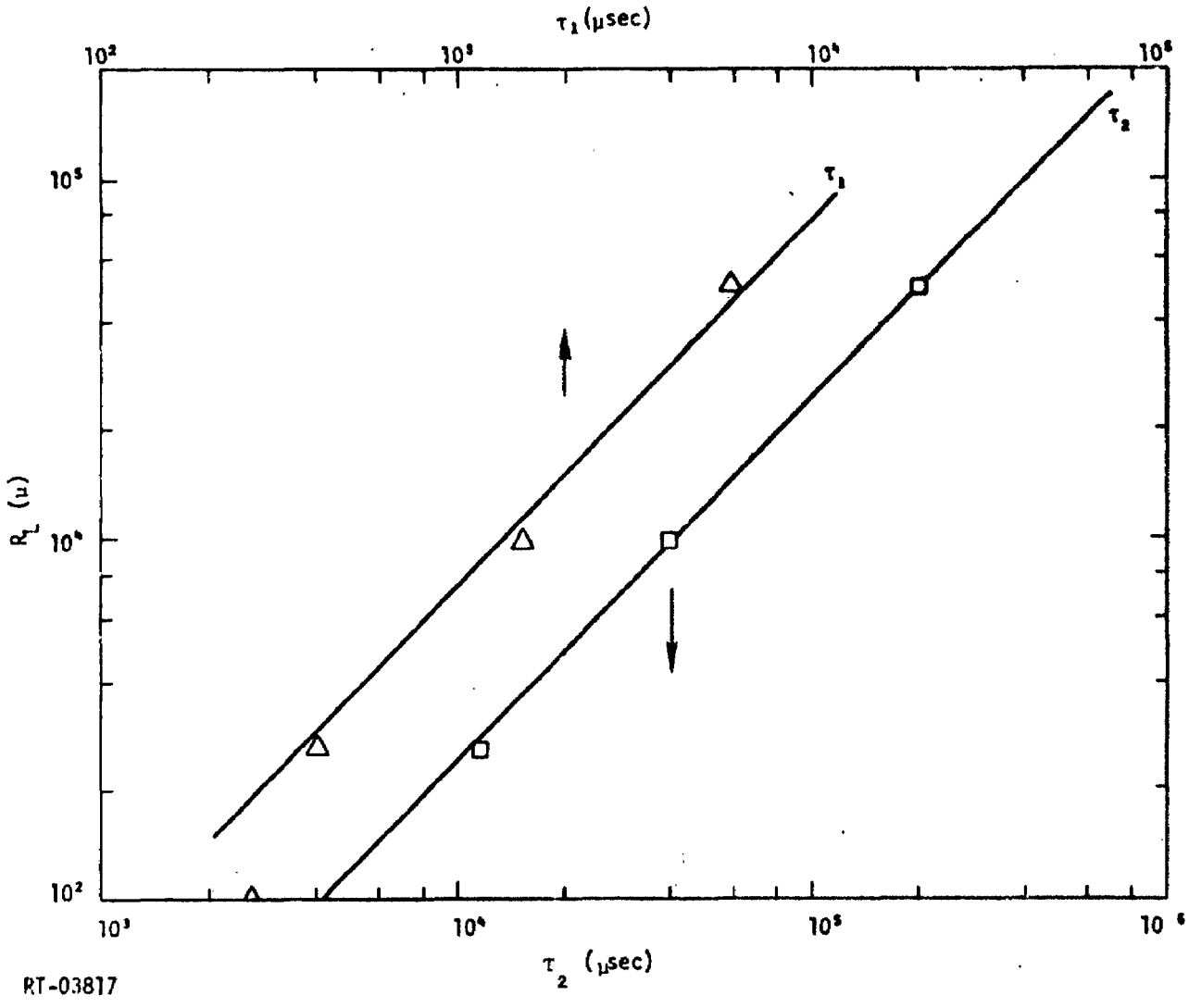

Figure 46. τ_1 and τ_2 as a function of load resistor

$$V_p = A \exp -\left[\frac{\tau_2}{\tau_2-\tau_1} \ln \frac{A\tau_2}{B\tau_1}\right]$$

$$B \exp -\left[\frac{\tau_1}{\tau_2\ \tau_1} \ln \frac{A\tau_2}{B\tau_1}\right] \qquad (9)$$

The peak of the transient response depends on the ratios of τ_2 and τ_1 and on A and B. Since τ_1 and τ_2 have the same load dependence, all of the load dependence of V_p comes from the load dependence of A and B. As seen in Figure 47, this is true where A and B are plotted for various loads for the same capacitor as shown in Figure 46. The load dependence is however, somewhat dependent on bias. Figures 48 through 54 show the load dependence of the peak response at 65°C for various capacitors and bias. Again, the inherent variability of the capacitor limits the conclusions to be drawn from such plots, but a few general observations can be made. The high-working-voltage capacitors have a stronger dependence on the load resistor, and a higher applied bias also produces a larger load resistor dependence. The dependence varies from less than $R^{0.1}$ for a 6-W.V. capacitor to $R^{0.25}$ for a 50-W.V. capacitor. From all of these plots, it can be assumed that V_p is proportional to $R^{1/6}$ for capacitors with less than a 20-W.V. rating and that V_p is proportional to $R^{1/4}$ for capacitors having rated voltage between 20 and 40 volts. This will be about 20 to 30% conservative in scaling upward over the range of most circuit loads when measurements are made in the 1-kΩ range. Because of the inherent variability of the capacitors, when greater confidence is required the units should be tested at the appropriate circuit load.

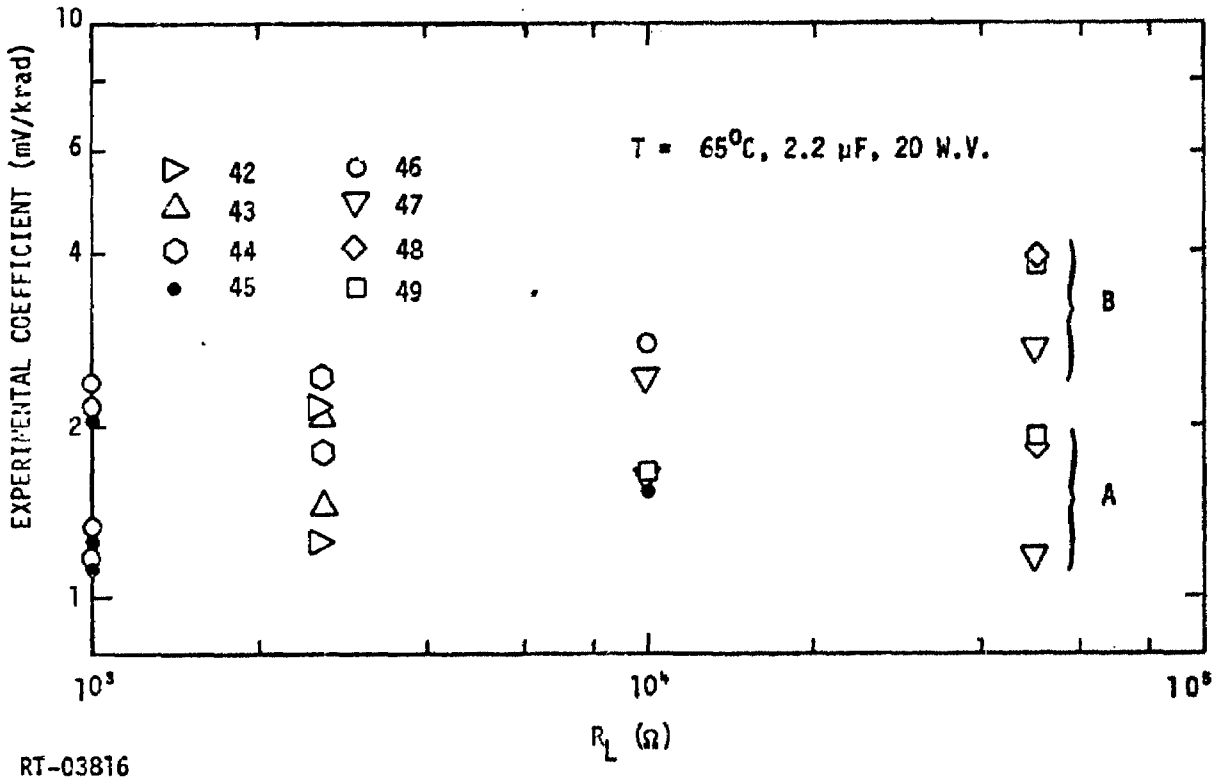

Figure 47. Fitting parameters as a function of load resistor

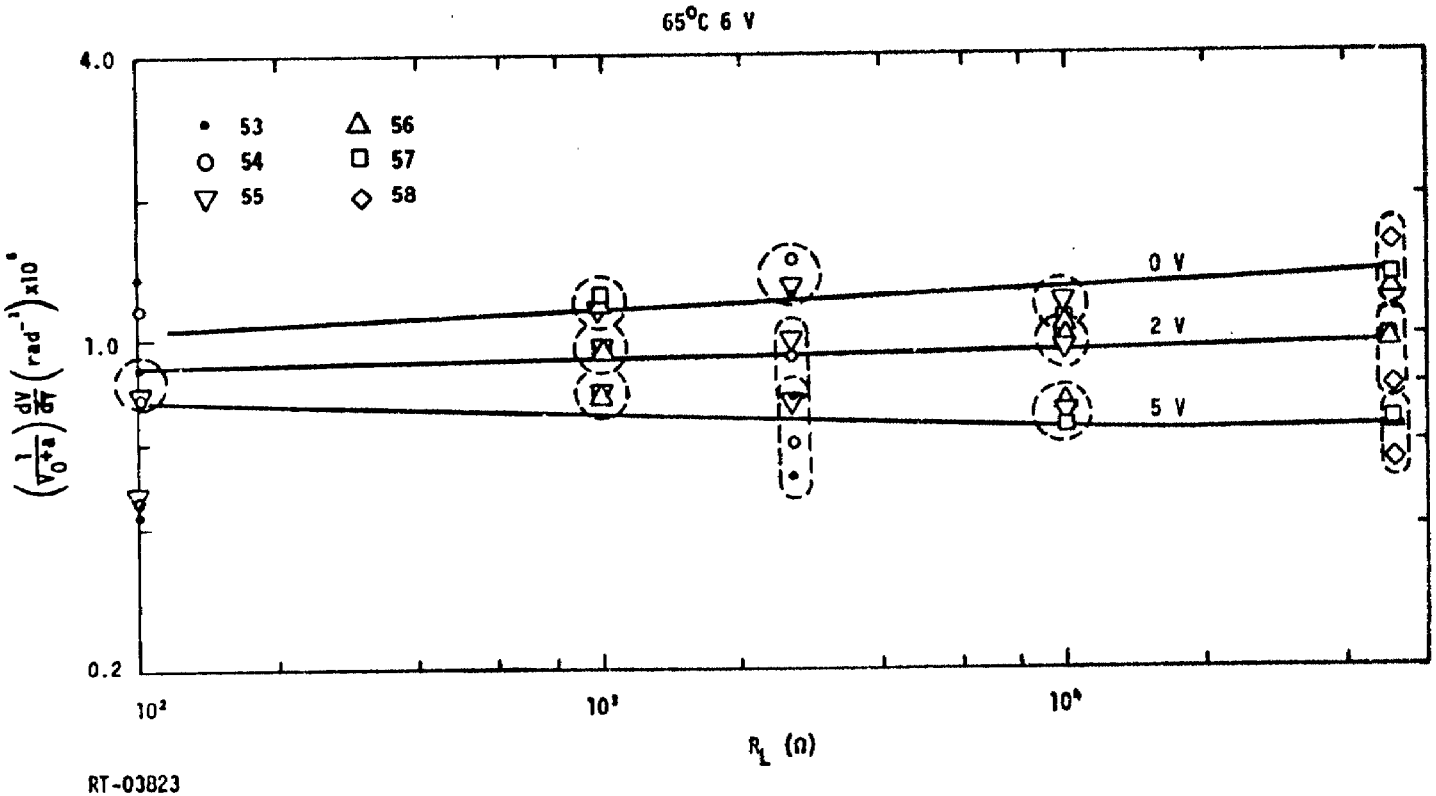

Figure 48. Load dependence of peak radiation response versus bias for 6-W.V. Sprague and Kemet capacitors at 65°C

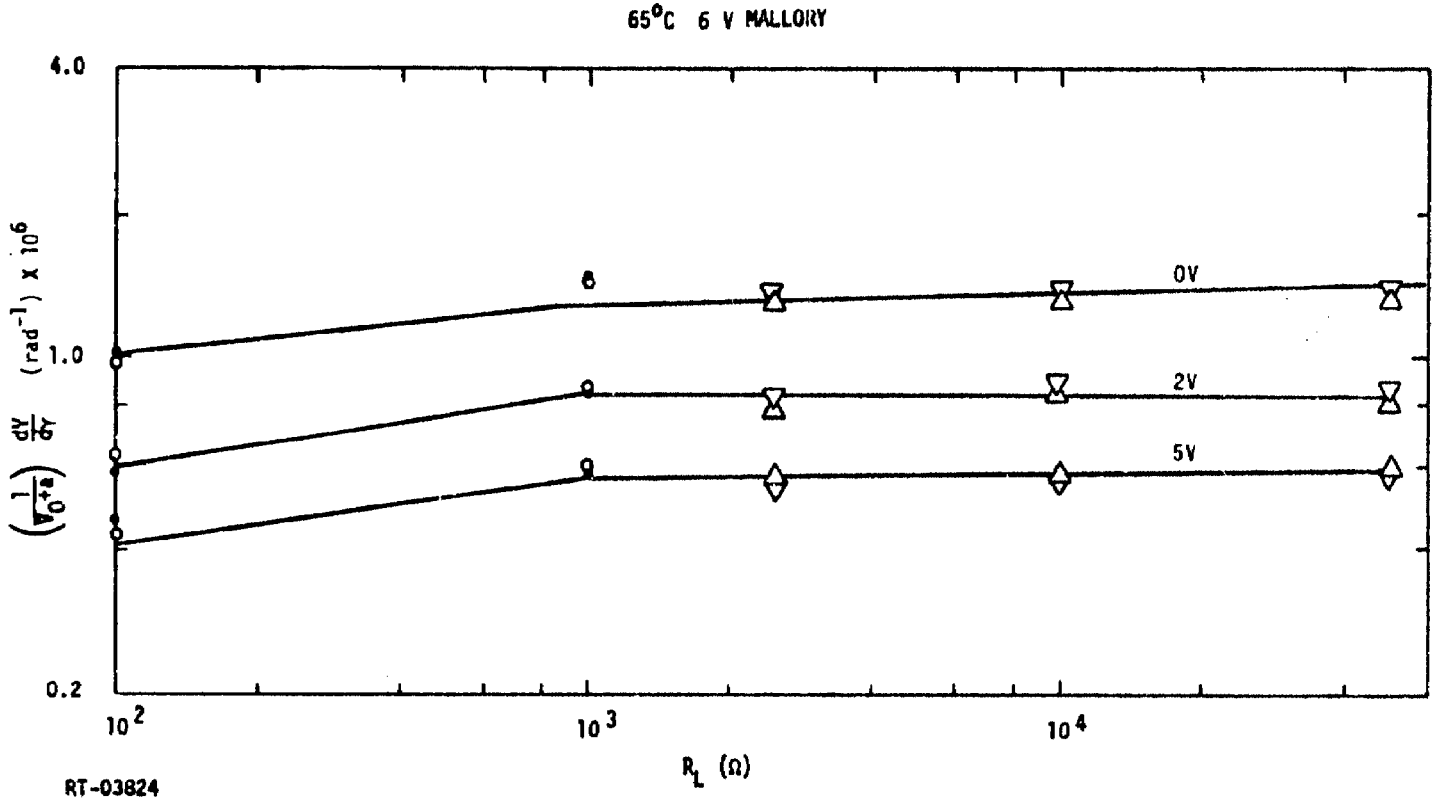

Figure 49. Load dependence of peak radiation response versus bias for 6-W.V. Mallory capacitors at 65°C

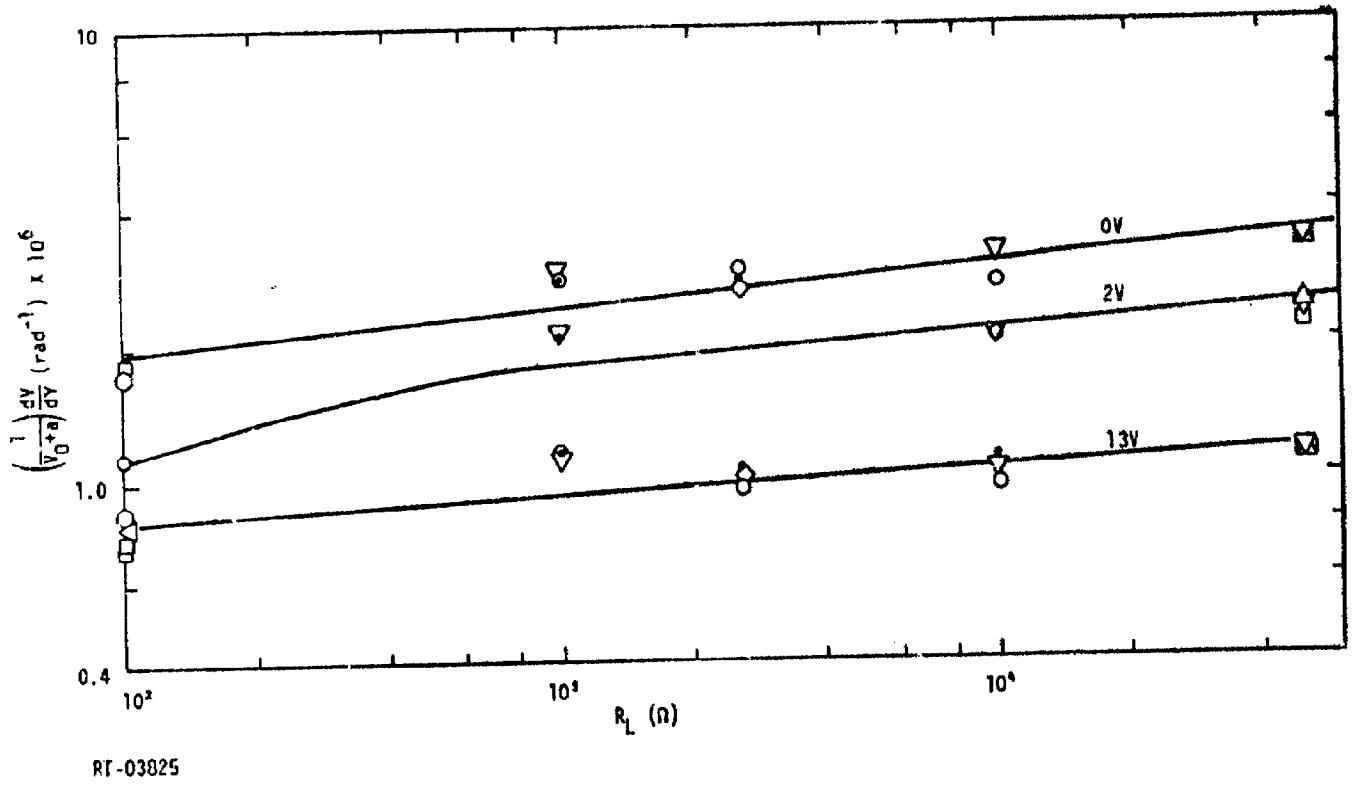

Figure 50. Load dependence of peak radiation response versus bias for 15-W.V. Sprague capacitors at 65°C

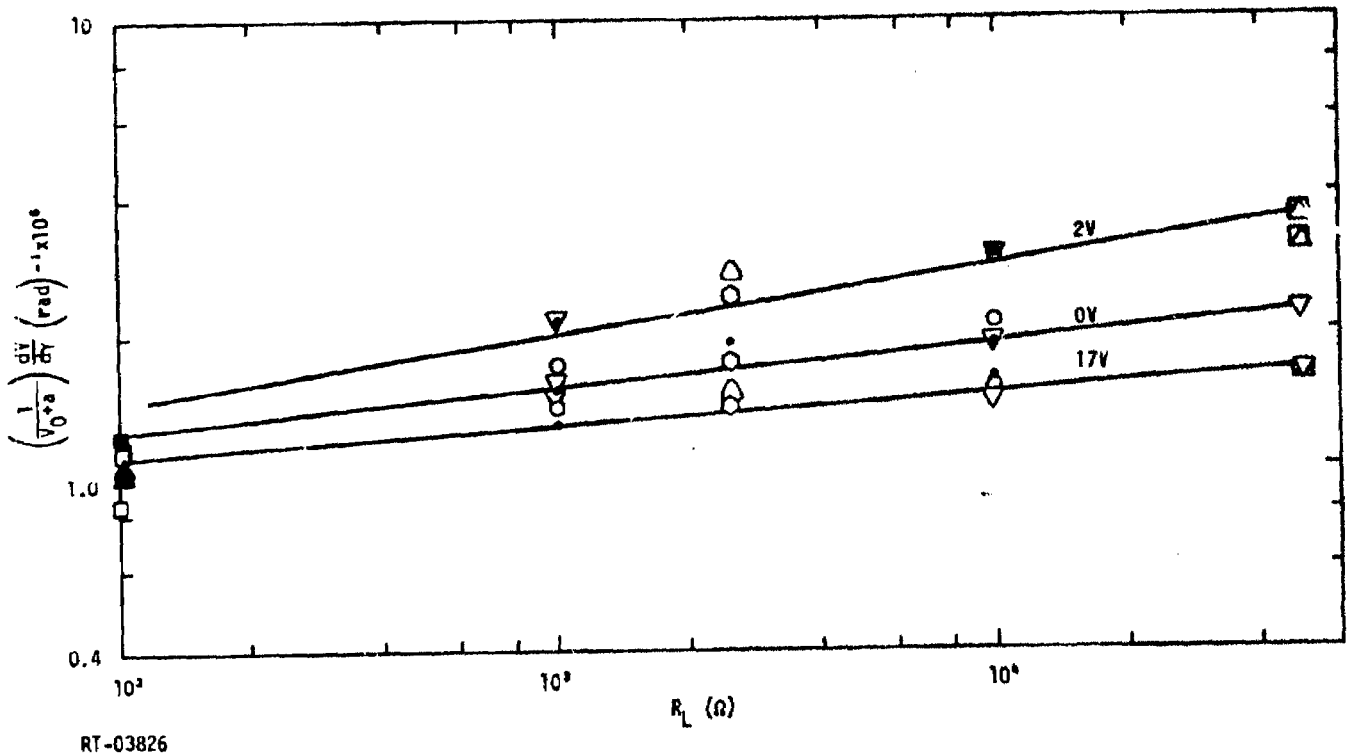

Figure 51. Load dependence of peak radiation response versus bias for 20 W.V. Sprague capacitors

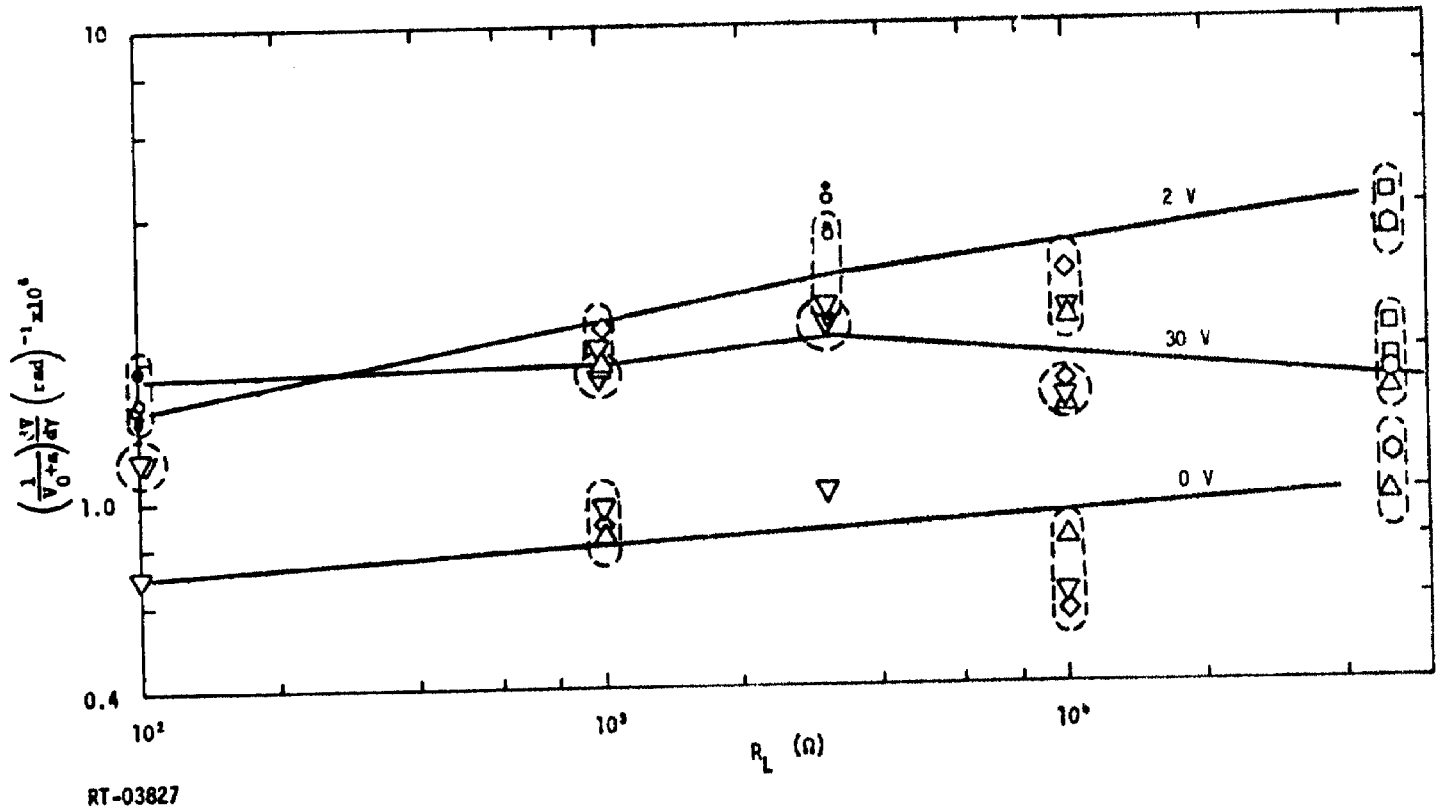

Figure 52. Load dependence of peak radiation response versus bias for 35-W.V. Sprague capacitors at 65°C

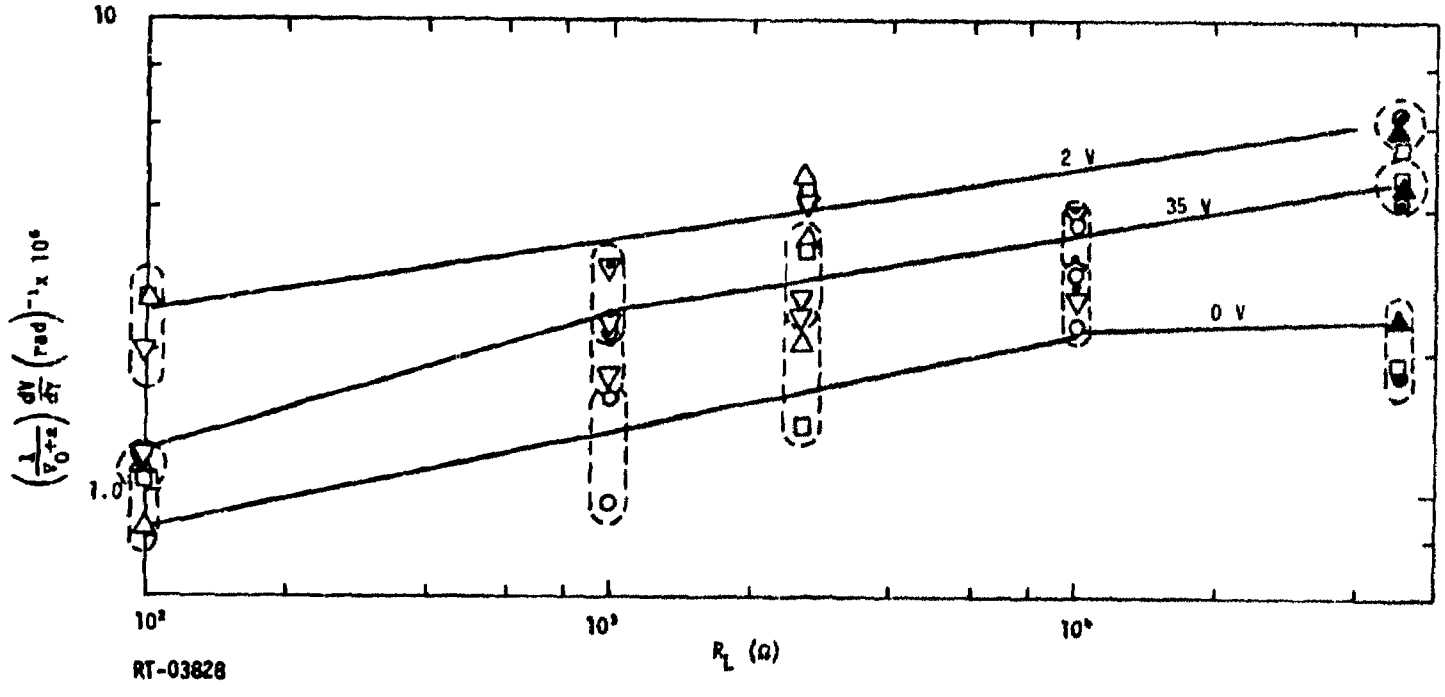

Figure 53. Load dependence of peak radiation response versus bias for 50-W.V. Sprague and Kemet capacitors

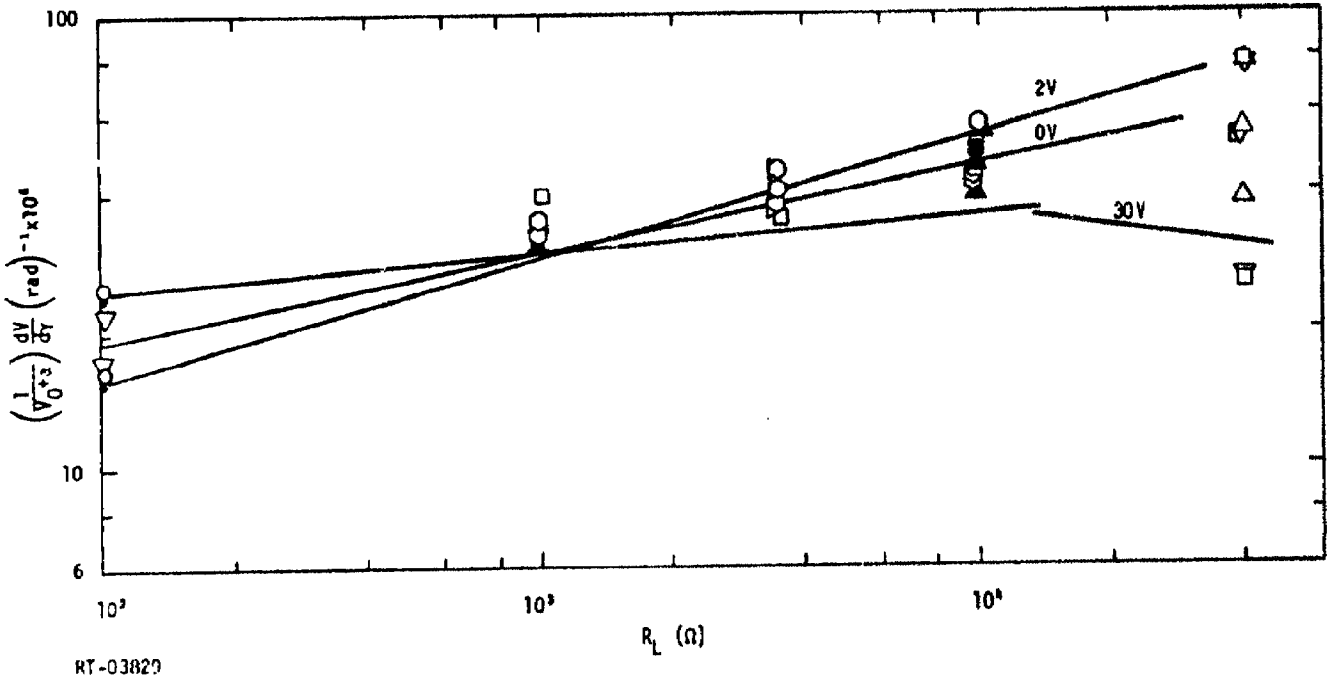

Figure 54. Load dependence of peak radiation response versus bias for 50-W.V. Mallory capacitors

6. MEASUREMENTS OF a, THE BUILT-IN VOLTAGE

Since the value of built-in voltage, a, strongly affects the photovoltaic response of the capacitors both in a single and back-to-back configuration, the means of measuring this quantity were examined. The model for the photovoltaic response described in the earlier report (Ref. 1) shows that the ionized carriers in the dielectric drift in an electric field $(V-a)/L$, where a is the built-in voltage, V is the applied voltage, and L is the thickness dielectric. Thus, V is equal to a when V is allowed to build up until no further charge moves. Alternatively, since $dV/d\gamma$ is proportional to $(V-a)$, a measurement of $dV/d\gamma$ as a function of V should yield a value of a when $dV/d\gamma = 0$. Thus, three techniques can be used to measure the quantity a.

1. Measure the saturated open circuit ($R_L = 10^{11}$) voltage on the capacitor produced by irradiation with Linac pulses.
2. Measure $dV/d\gamma$ versus applied voltage (V_0) for applied voltages between +1 and -1 volts. $a = V_0$ when $dV/d\gamma = 0$.
3. Measure the saturated open circuit voltage on the capacitor produced by irradiation with cobalt-60 gamma rays.

The results of measurements of the saturation voltage using 4.5-μsec Linac pulses of about 40 krads each at 65°C are shown in Table 7. These are arranged in order of increasing working voltage. The capacitors measured here had seen considerable irradiation testing previously during the charge-loss versus dose test. The irradiation damage resulting from these tests was expected to affect the dose required to reach saturation but not to affect the saturation voltage. However, an effect was observed which makes the results in Table 7 somewhat uncertain. For some capacitors, a rapid ($\tau \sim = 1$ sec) decay of the voltage across the capacitor was observed. The short-time-constant decay would drop the voltage by 20 to 30% of its value immediately after the pulse. When the same capacitor was charged to an equivalent voltage, the RC decay constant was observed to be in the order

Table 8

MEASUREMENTS OF a WITH PULSED ELECTRONS

C (μF)	W.V.	Mfr.	Number Tested	Volts		
				a	Std. Dev.	Range
6.8	6	Mallory	11	1.01	0.08	0.84-1.11
6.8	6	Sprague	4	0.64	0.06	0.60-0.74
6.8	6	Kemet	3	0.97	0.01	0.96-0.99
100.	10	K-Sprague	4	0.75	0.14	0.59-0.93
3.3	15	Sprague	6	0.81	0.12	0.60-0.84
2.2	20	Sprague	6	0.41	0.10	0.33-0.63
6.8	35	Sprague	5	0.93	0.15	0.72-1.11
6.8	50	Kemet	5	1.06	0.04	1.02-1.11
6.8	50	Sprague	4	0.91	0.16	0.75-1.08
6.8	50	Mallory	4	1.18	0.02	1.16-1.20

of 10^4 sec. Hence, the fast decay must have been associated with radiation-induced leakage which persisted for a few seconds. The leakage was found to be larger for more damaged capacitors. To attempt to get around this problem as much as possible, each capacitor was given three pulses in rapid succession. The maximum voltage at the conclusion of the pulses (γ=120 krad) was taken as the value of a. Still, the voltage could have decayed during the 1 sec or so taken for the three pulses, or the number of pulses may not have been adequate to completely saturate the sample; thus, the numbers given in the table may be slightly low.

The data measuring a with the dV/dγ versus V technique produced low values for related reasons. The capacitors were damaged and the attendant space-charge polarization effects caused the first attempt on 50 capacitors to yield values of a in the 0.2- to 0.5-volt range. Such low values of a are inconsistent with the other results obtained on the program. To spot-check the method, two previously undamaged capacitors were exposed, and the results are shown in Figure 55. Great care was taken to avoid polarization problems in these data and an interesting feature appeared. The 6.8-μF

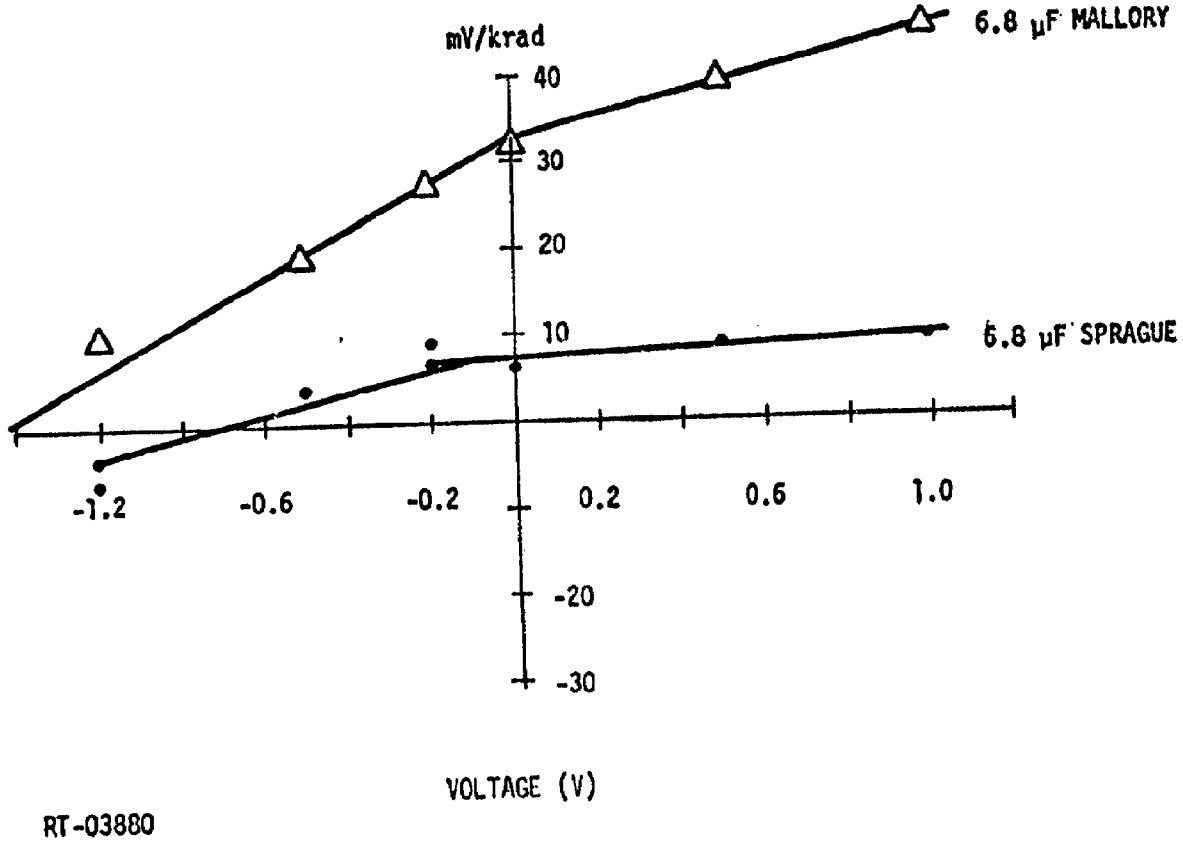

Figure 55. dV/dγ versus applied bias near zero bias

50-W.V. Mallory capacitor indicates an a value of about 1.2 volts and the 6.8-μF 35-W.V. capacitor indicates a value of a of about 1.7 volts. Both are in reasonable agreement with the Linac results mentioned above. Both capacitors show a change in slope of the dV/dγ versus V curve for a reverse bias. At the present time, this change in slope is not included in the model and the slope change is not understood. Little work has been done in this area but the two 50-W.V. capacitors measured previously (Ref. 1) did not show a sharp slope change when the polarity of the voltage was changed.

The numbers obtained for a from the Linac tests were somehwat different from what was expected. Hence, several of the capacitors measured at Linac were also checked at the Salk Institute cobalt-60 source at a dose rate of about 30 rad(Ta_2O_5)/sec. The capacitor leads were potted with silicone rubber to eliminate air-ionization effects. The results for the 50-W.V. capacitors are shown in Figure 56, and for the 20-W.V. capacitors in Figure 57. The value of one of the 20-W.V. capacitors in the cobalt-60 tests was larger than obtained at the Linac, and one of the 20-W.V. units showed a severe increase in leakage current which restricted the saturation voltage in the cobalt-60 cell to 0.3 volt.

The saturation voltage was approached for doses in excess of 200 krad, which may be the reason for the low values obtained at the Linac.

In summary, all three methods appear to be adequate for obtaining value of a in undamaged ionization. To assure consistency, two methods should probably be used on each capacitor. First, the dV/dγ versus V_0 should be measured at low dose. Second, the saturation value of the open-circuit voltage should be measured.

6.1 MEASUREMENTS AND CALCULATIONS OF THE NEUTRON DOSE IN TANTALUM CAPACITORS

A simple experiment was performed to relate the response of a tantalum capacitor in a gamma environment to the response in a neutron environment. The measurement consists of irradiating a tantalum capacitor with leakage neutrons from a bare spherical U-235 nuclear reactor and measuring the voltage on the capacitor after a measured irradiation time. In a separate

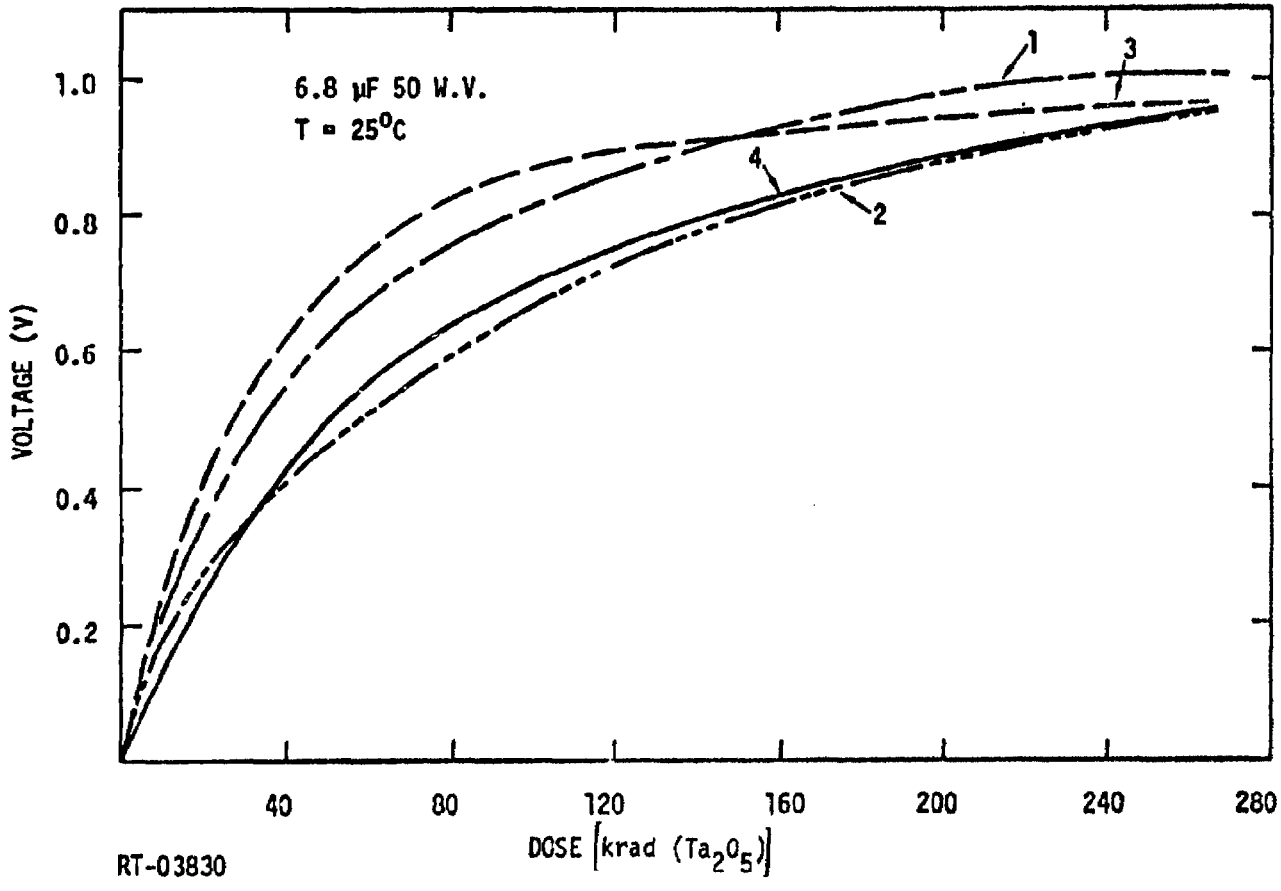

Figure 56. Open-circuit voltage versus dose for 50-W.V. capacitors

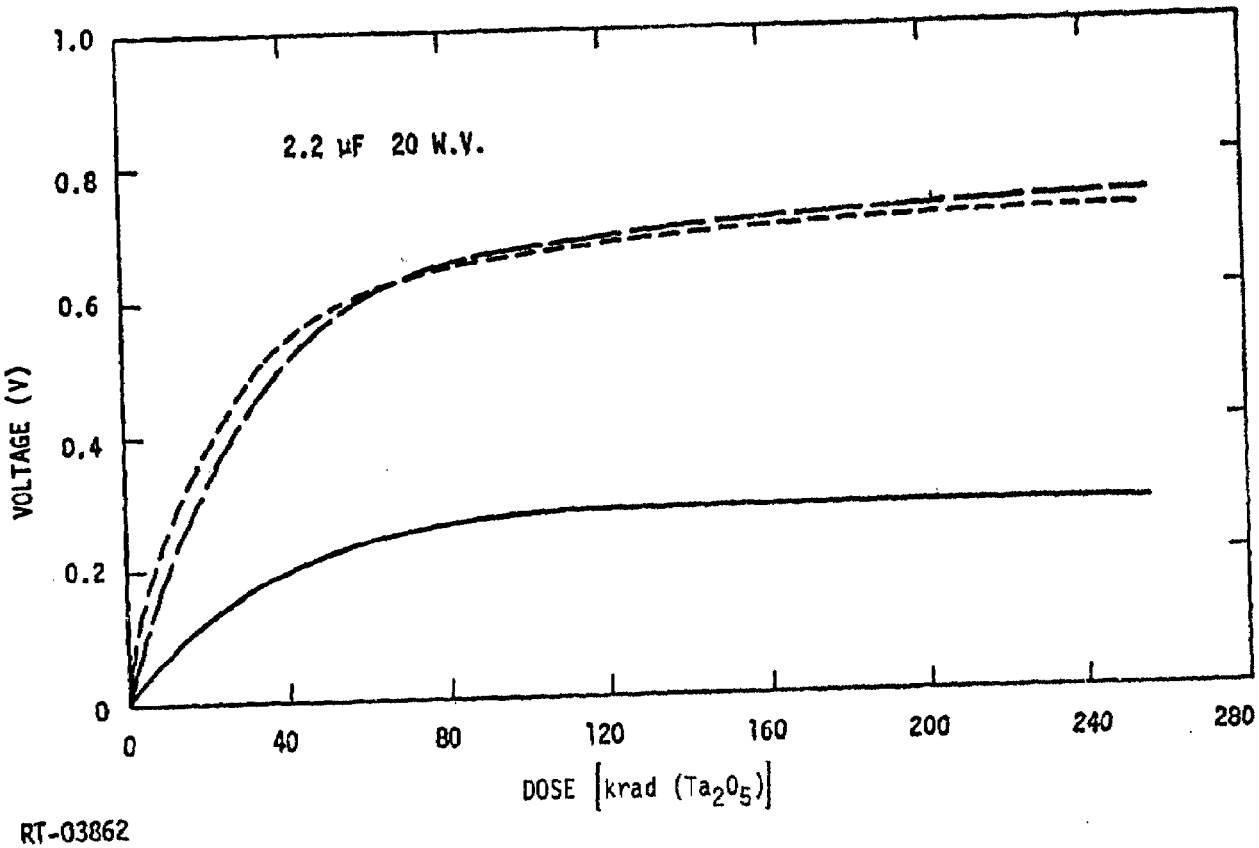

Figure 57. Open-circuit voltage versus dose for 20-W.V. capacitors

measurement performed using a calibrating gamma-ray source, the voltage-to-dose conversion factor for the capacitor was determined. Combining these results can give the total dose received for a given irradiation time. Because of the high neutron-to-gamma ratio at the irradiation position, the total dose at the irradiation position of the capacitor should be dominated by neutrons. Even so, the dose due to the gammas was monitored and then some subtractions were attempted.

A neutron response function for T_a (Ref. 5) was folded into the APFA Reactor spectrum, which is well known (Ref. 6). For 1.5×10^{13} n/cm^2 (E > 10 keV), 47 rad(Ta) are expected in the capacitor. A calculation of the gamma yield gives 2.8×10^{12} γ/cm^2 or about 1400 rad(Ta) from the gamma energy deposition. This gives a predicted fluence-to-dose conversion of 2×10^{-12} rad(Ta)/n/cm^2.

In the experiment, eight capacitors were first irradiated in a spent-fuel gamma source. Tantalum-covered calcium-fluoride TLDs were used for dosimeters, and the open-circuit voltage was observed with an electrometer. The results are shown in Figure 58. Note that the voltage rise is linear in the dose, as is expected, since the dose is under 1 krad. The capacitors were then shorted for several days and then exposed to the mixed-neutron gamma flux from the APFA reactor. Both calcium-fluoride and lithium-fluoride dosimetries were used, and a sulphur-neutron dosimeter was used for the neutron determination. The voltage build-up as a function of irradiation time is shown in Figure 59. Again, a linear rise with exposure is seen. The results are given in Table 9, in which the doses have been left in rad(CaF_2) since relative comparisons are to be made. Unfortunately, due to the relatively equal importance of the neutron and gamma effects on the TLDs, it is difficult to separate neutron and gamma effects in the dosimetry.

In the reactor irradiation, 1.5×10^{13} n/cm^2 (E > 10 keV) was received by the capacitors. The manufacturer of the TLD specifies that the neutron response is about 2×10^{-10} R/n/cm^2 which implies that 2460 rads of the 3100 rad(CaF_2) read by the TLD is due to neutrons. Using these numbers and the gamma response measured in the spent-fuel reactor yields neutron response values in the next to last column in Table 9.

Using the gamma output calculations referred to above, 600 rad(Ta) or 900 rad(CaF_2) come from neutrons in the TLD, with 2200 rad(CaF_2) from gammas.

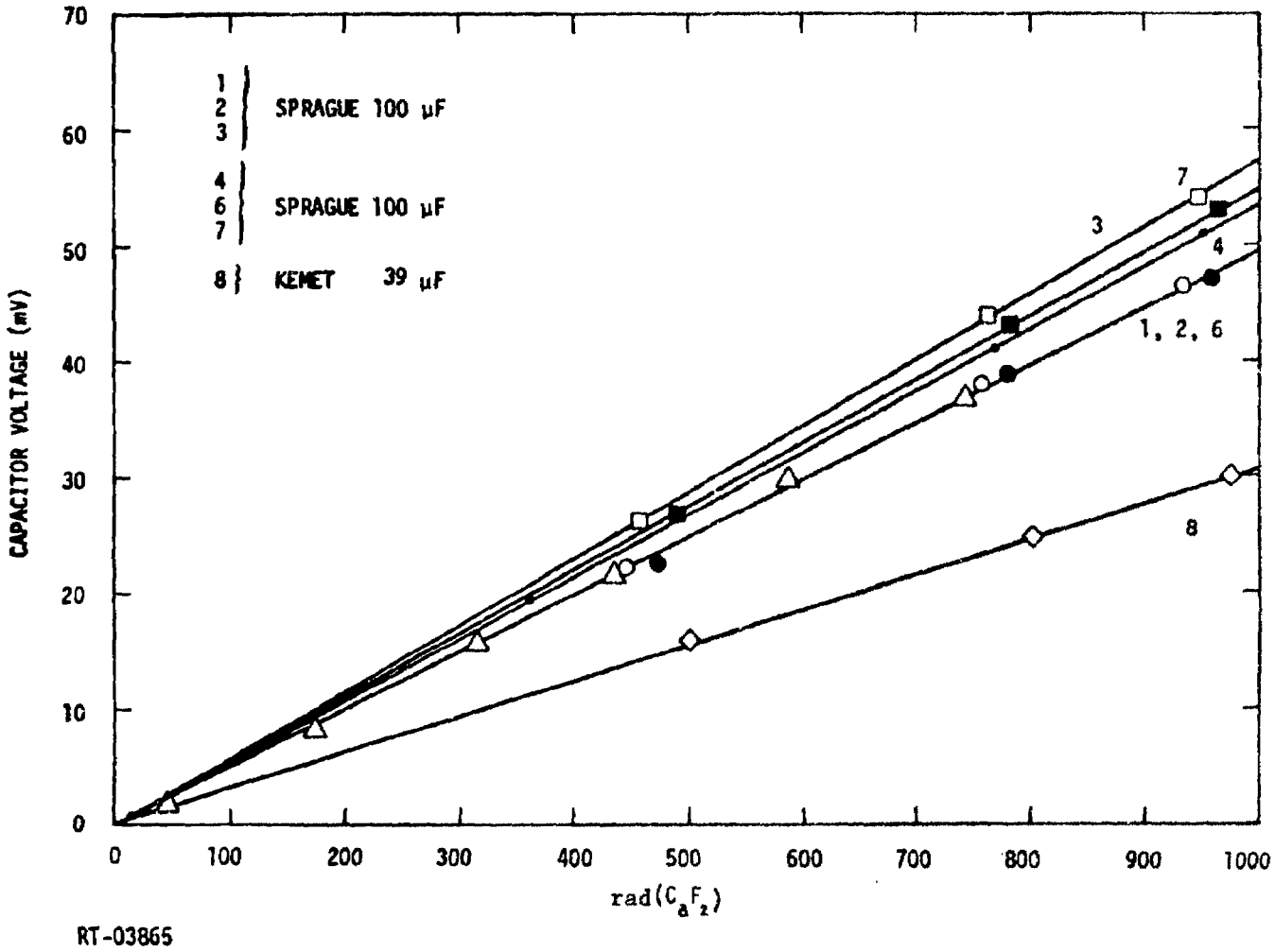

Figure 58. Open-circuit voltage versus dose during gamma exposure

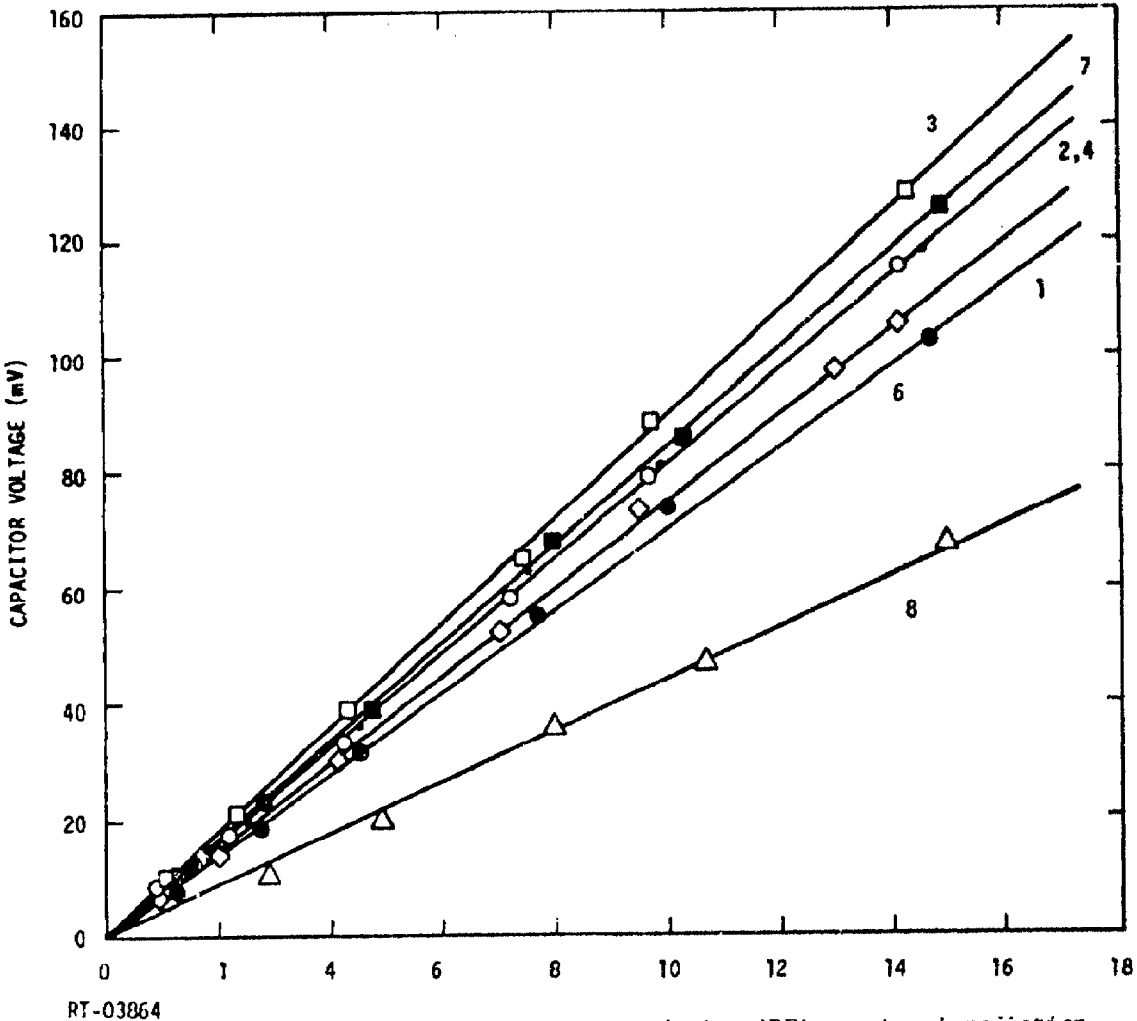

Figure 59. Open-circuit voltage versus time during APFA reactor irradiation

Table 9

NEUTRON RESPONSE EXPERIMENT

Capacitor Positions	Mfr.	C (μF)	W.V. V	$\frac{dV/d\gamma}{\frac{mV}{rad(CaF_2)}}$	$\frac{dV/d\gamma}{\frac{mV}{rad(Ta_2O_5)}}$	$\frac{mV}{n/cm^2}$	$\frac{rad\ (Ta_2O_5)^*}{n/cm^2}$	$\frac{rad(Ta_2O_5)^{**}}{n/cm^2}$
1	Sprague	100	10	0.050	0.032	7.8×10^{-12}	1.8×10^{-10}	5×10^{-13}
2	Sprague	100	10	0.050	0.032	8.5×10^{-12}	2.0×10^{-10}	1×10^{-12}
3	Sprague	100	10	0.037	0.037	9.4×10^{-12}	2.1×10^{-10}	4×10^{-12}
4	Sprague	100	10	0.053	0.034	8.5×10^{-12}	1.9×10^{-10}	7×10^{-13}
6	Sprague	100	10	0.050	0.032	7.4×10^{-12}	1.7×10^{-10}	1×10^{-13}
7	Sprague	100	10	0.055	0.035	8.9×10^{-12}	1.9×10^{-10}	9×10^{-13}
8	Kemet	39	35	0.031	0.020	4.6×10^{-12}	4.6×10^{-12}	1×10^{-13}

* Upper limit

** Based on calculation of γ-dose.

If these numbers are used to calculate the fluence to dose conversion, the numbers in the last column of Table 9 are obtained.

Hence, the value from these experiments based on gamma yield calculations is about 1×10^{-12} rad(Ta)/n/cm^2 for the APFA spectrum. This is not too far from the predicted value. The upper limit (assuming the neutron-to-rad conversion for the TLD) is 2×10^{-10} rad(Ta)/n/cm^2.

6.2 CIRCUIT MODEL FOR TANTALUM CAPACITOR RADIATION RESPONSE

Circuit models have been developed to describe the radiation response of a tantalum capacitor by R. Leadon (Refs. 1,7) and R. Baker (Refs. 7,8). These models represent the capacitor in terms of circuit components which generate currents, store charge, etc., as required, and they represent the observed transient response with considerable accuracy. However, obtaining appropriate parameters for the models from experimental data is not straightforward and thus makes the models somewhat difficult to use. A simpler approach based on results from this program and from Baker's work (Ref. 8) was applied by H. Sugar (Ref. 9). Sugar's model describes the radiation response in terms of a single time-dependent current generator. This latter approach is somewhat easier to use and is an approach which will be pursued here.

In sugar's model, the initial conductivity is represented by an impulse function, followed by a current which decays as $\exp(-t/\tau_2)$. The final current generator expression appears as follows.

$$I(t) = CV_\rho/t_0 + V_\rho C \left(\frac{1}{RC} - \frac{1}{\tau_2}\right)\exp(-t/\tau_2) \qquad (10)$$

where

$$V_\rho = (V_0 + a)\ [1-\exp(-K\gamma)]\ , \qquad (11)$$

I = the current as function of time,

C = the capacitance,

t_0 = a time chosen to be shorter than RC (the precise value is not important),

τ_2 = the decay time,

K = the peak charge loss factor,

V_0 = applied bias,

and γ = dose in krad(Ta_2O_5) .

A similar but less phenomenological model can be derived from a consideration of the processes within the capacitor. From our previous measurements, we know that during the pulse the voltage across the capacitor rises linearly in time:

$$V(t) = \left(\frac{B-A}{t_\rho}\right) \dot{\gamma} t, \tag{12}$$

while after the pulse,

$$V(t) = -A\gamma \exp(-t/\tau_1) + B\gamma \exp(-t/\tau_2) , \tag{13}$$

where A, B, τ_1, and τ_2 are empirical constants, and t_ρ = pulse width. Now, suppose we have a short pulse of ionization during which two traps capture electrons. Suppose the traps emit these electrons at some rates such that their effective densities decay with τ_1 and τ_2:

$$Q_1(t) = Q_1(0) \exp(-t/\tau_1) \tag{14}$$

$$Q_2(t) = Q_2 (0) \exp(-t/\tau_2)$$

where

$Q_i(t)$ = the charge in the ith trap at time K.

Then

$$\frac{dV}{dt} + \frac{V}{RC} = \frac{I(t)}{C} = \frac{1}{C} \left[\frac{Q_1(0)}{\tau_1} \exp(-t/\tau_1) + \frac{Q_2(0)}{\tau_2} \exp(-t/\tau_2)\right] . \tag{15}$$

But since Q_1 and Q_2 are not known, lump these together and write

$$\frac{dV}{dt} + \frac{V}{RC} = \frac{I}{C} = \left[\frac{I_1(0)}{C} \exp(-t/\tau_1) + \frac{I_2(0)}{C} \exp(-t/\tau_2)\right] , \tag{16}$$

and using Eqs. 12 and 13 and equating coefficients,

$$\frac{I(t)}{C} = (B-A)\,\dot{\gamma}\,(t) + A\gamma\left(\frac{1}{\tau_1} - \frac{1}{RC}\right)\exp(-t/\tau_1)$$

$$+ B\gamma\left(\frac{1}{RC} - \frac{1}{\tau_2}\right)\exp(-t/\tau_2) \quad . \tag{17}$$

Hence, adding the currents, both during the pulse and from the traps, we find that there is an initial prompt current during the pulse and then a fast- and slow-decaying component in the current generator. Taking Eq. 10 and modifying it for low doses, we have

$$\frac{I(t)}{C} + \frac{(V_0 + a)}{t_0} K\gamma + (V_0 + a)\,K\gamma\left(\frac{1}{RC} - \frac{1}{\tau_2}\right)\exp(-t/\tau_2) \tag{18}$$

Clearly, the last two terms of Eqs. 17 and 18, which represent the two models, correspond if

$$B = (V_0 + a)\,K \quad . \tag{19}$$

The first term in Eq. 18 was obtained by requiring that the capacitor lose enough charge to produce V_p in a time comparable to the time to reach the maximum voltage change. Call the time to reach the maximum t_m. Empirically, t_m is of the order of $R_C/4$. If we force all the current in the first two terms of Eq. 17 to flow in a time less than t_m, Eqs. 17 and 10 can be made to correspond. Now, the average of the current per unit C per unit dose from t = 0 to t = t_m is

$$\frac{1}{t_m}\left\{\int_0^{t_p} \frac{B-A}{t_p}\,\dot{\gamma}dt + \int_0^{t_m} A\gamma\left(\frac{1}{\tau_1} - \frac{1}{RC}\right)\exp(-t/\tau_1)\,dt\right\} \quad . \tag{20}$$

Since τ_1 is approximately $R_C/10$ and t_m approximately $R_C/4$, the above is closely approximated by

$$\frac{1}{t_m}\left[\int_0^{t_\rho} \dot{\gamma}\,\frac{B-A}{t_\rho}\,dt + \frac{\gamma A}{\tau_1}\int_0^{\infty} \exp(-t/\tau_1)\,dt\right], \tag{21}$$

since the error in neglecting 1/RC compared to $1/\tau_1$ is compensated to a great extent by extending the integral to infinity. This can be reduced to

$$\frac{B-A}{t_m} + \frac{A}{t_m} = \frac{(V+a)\,K}{t_0} = \frac{B}{t_0} \tag{22}$$

by combining Eqs. 21 and 19. Thus, Eqs. 10 and 17 correspond if $t_0 = t_m$ and τ_1 is very much less than RC and t_m is greater than $2\tau_1$. Since the variation of the response with load is accounted for by changes in A and B, the load dependence can be explicitly incorporated into K by the function $(R/R_o)^{1/n}$. To account for a finite pulse lengths, we should write

$$\frac{I(t)}{C} = (B-A)\,\dot{\gamma}\,(t) + A\gamma\left(\frac{1}{\tau_1} - \frac{1}{RC}\right)[1-\exp(-t_\rho/\tau_1)][\exp-(t-t_\rho)/\tau_1] + B\gamma\left(\frac{1}{RC} - \frac{1}{\tau_2}\right)[1-\exp(-t_\rho/\tau_2)][\exp-(t-t_\rho)/\tau_1] \tag{23}$$

to account for the buildup of trapped charge.

6.3 SUMMARY OF CURRENT GENERATOR REPRESENTATION

1. When the pulse is short ($t_p < 0.01$ RC) and only the peak voltage change and the recovery of the capacitor to its normal state are significant,

$$\frac{I(t)}{C} = (V_0+a)\,[1-\exp(-\gamma\gamma)]\left[\frac{1}{t_0} + \left(\frac{1}{RC} - \frac{1}{\tau_2}\right)\exp(-t/\tau_2)\right]$$

where $t_0 < 0.2$ RC and K and τ_2 have their usual meaning.

2. When the radiation pulse is short ($t_p < 0.01$ RC) and the rising time constant is important,

$$\frac{I(t)}{C} = (B-A)\dot{\gamma}(t) + A\left(\frac{1}{\tau_1} - \frac{1}{RC}\right)\gamma \exp(-t/\tau_1) + B\gamma\left(\frac{1}{RC} - \frac{1}{\tau_2}\right)\exp(-t/\tau_2)$$

where $B = (V+a)\,K$, A, and τ_1 must be found from a fit to a rising portion of the data. For an approximate calculation, A = 0.4 to 0.7 times B and τ_1 is equal to 0.05 to 0.12 RC.

3. When the radiation pulse width is not short, Eq. 23 must be used.

REFERENCES

1. T. M. Flanagan and R. E. Leadon, "The Effects of Ionizing Radiation on Tantalum Capacitors," Summary Report, Part I, Gulf Rad Tech document Gulf-RT-10609, April 19, 1971.

2. "General Requirements for Solid Electrolite Tantalum Capacitors," drawing G657496 from Bell Telephone Laboratories, Whippany, New Jersey, and drawings G657119, G657120, G657121, G657315, 11300038, 11300041.

3. J. W. Harrity, "Radiation Effects in Dielectric Materials," Final Report on contract DA28-043-AMC-02446(E) for U.S. Army Electronics Command, Fort Monmouth New Jersey, TRECOM-02446-F, February 1969.

4. H. W. Holland, "Solid Tantalum Capacitor Failure Mechanism and Determination of Failure Rates," Kemet Engineering Bulletin F-2695, and Kemet detailed specification GR500/J.

5. K. Friedman, private communication.

6. "Accelerator Booster Program," Final Summary Report under contract DA49-146-XZ-411, Gulf General Atomic report GA-9209, June 23, 1969.

7. R. T. Baker, T. M. Flanagan, and R. E. Leadon, J. Appl. Phys. 44, 3, March 1973, p. 995.

8. R. T. Baker, "Photovoltaic Effects in Tantalum Capacitors," Technical Memorandum 71-2414-10, Bell Telephone Laboratories, Whippany, New Jersey, September 16, 1971.

9. H. K. Sugar, "Memorandum for File on Safeguards System Application of Tantalum Capacitors," Bell Telephone Laboratories, Whippany, New Jersey, November 15, 1972.

10. H. A. Boesch, private communication.

APPENDIX A

METHOD OF TEST

APPENDIX A

1. METHOD OF TEST

Ionization testing of Ta_2O_5 capacitors is performed using ~4-μsec pulses of electrons of 35 to 40 MeV from the Gulf Rad Tech electron linear accelerator (Linac) as an ionizing source. The dose delivered at the sample location is measured and controlled by the test engineer. Capacitors to be tested are mounted in the test fixture and individually cycled into position in the electron beam. The signal from each unit is amplified and displayed on an oscilloscope. This displayed signal is photographed, and it is also digitized into 30 discrete points and recorded in this form on magnetic tape. Data reduction is accomplished by computer manipulation of the digitized information or by visual scanning of the photographic records.

1.1 LINAC BEAM CALIBRATION AND CONTROL

The test configuration is shown in Figure A-1.

In the ionization tests, each Linac pulse is actively monitored through the use of a secondary-emission monitor (SEM). This consists of a 1-1/2-inch-diameter titanium-foil disk, 0.001 inch thick, mounted in an evacuated chamber positioned behind a lead-aluminum shield between the 1/4-inch aluminum scattering plate and the capacitor test chamber.

The evacuated chamber has 10-mil Mylar windows for entry and exit of the beam. The SEM foil is biased at -200 V to repel low-energy secondary electrons from the windows and walls of the chamber. As the high-energy electron beam passes through the SEM foil, secondary electrons are knocked from the foil proportional to the number of electrons in the primary beam. These electrons are replaced by current from ground, and the voltage developed by this replacement current through a resistance is amplified and transmitted to the data station. This signal is a measure of the beam current during the Linac pulse.

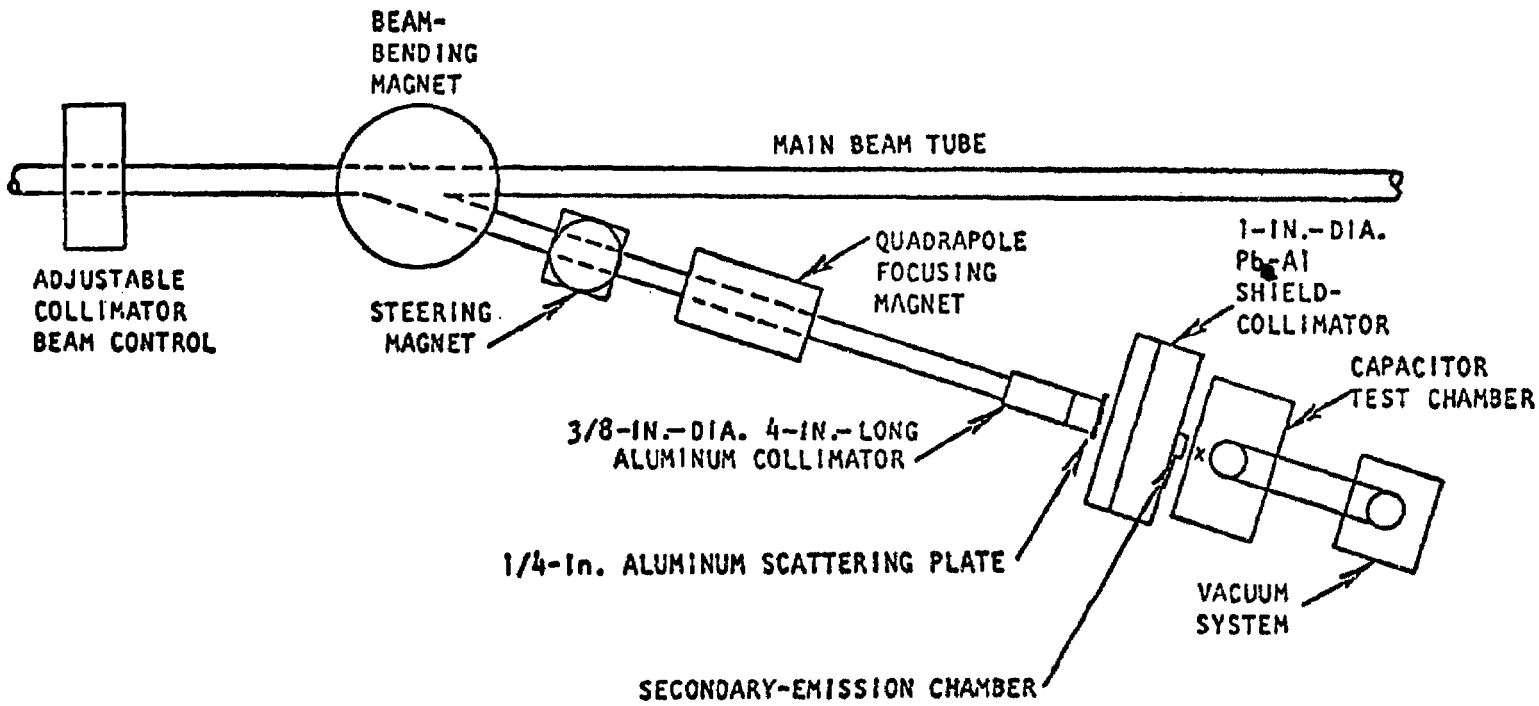

Figure A-1. Test configuration during testing of Ta_2O_5 capacitors

The correlation between this beam-current measurement and the dose deposited in the test specimen is established with the use of a secondary standard. The primary standard against which this has been calibrated is a standard Faraday cup.

This radiation standard is a thin copper-block calorimeter. This consists of a small copper block, mounted in a styrofoam block to provide good thermal isolation, to which is attached a fine copper-constantan thermocouple. This unit is positioned at the test location and the Linac pulsed. The temperature rise of the copper block is directly translatable to the dose deposited in the copper. Similar tests using other materials instead of copper as the calorimeter material have established the normalization factors for converting the copper dose to dose in other materials.

The amplified SEM signal is electrically integrated and displayed on the oscilloscope with each data trace. It is also fed to a sample-and-hold circuit and recorded on magnetic tape with the digitized data.

Control of the amplitude of the beam-current pulse is accomplished by use of a variable-collimator-stopping block located in the main beam tube following all accelerating stages. The motion of this variable collimator is controlled by the test engineer.

1.2 CAPACITOR TEST CIRCUIT

The capacitors to be tested are mounted on fiberglass wheels which can hold up to 60 single capacitors or parallel pairs or 36 back-to-back pairs. Diodes can be substituted for some capacitor positions.

The wheel is then mounted in a vacuum chamber which contains drive mechanism for positioning the wheel and electrical contact and switching mechanism to bring leads from the sample under test out to the measuring circuitry. A schematic of the measuring circuit used is shown in Figure A-2. Figures A-3 and A-4 show the method of installation of capacitors on the wheel.

The integrity of the wheels and test fixture are certified weekly when in continuous use, or prior to use when dormant for periods longer than one week.

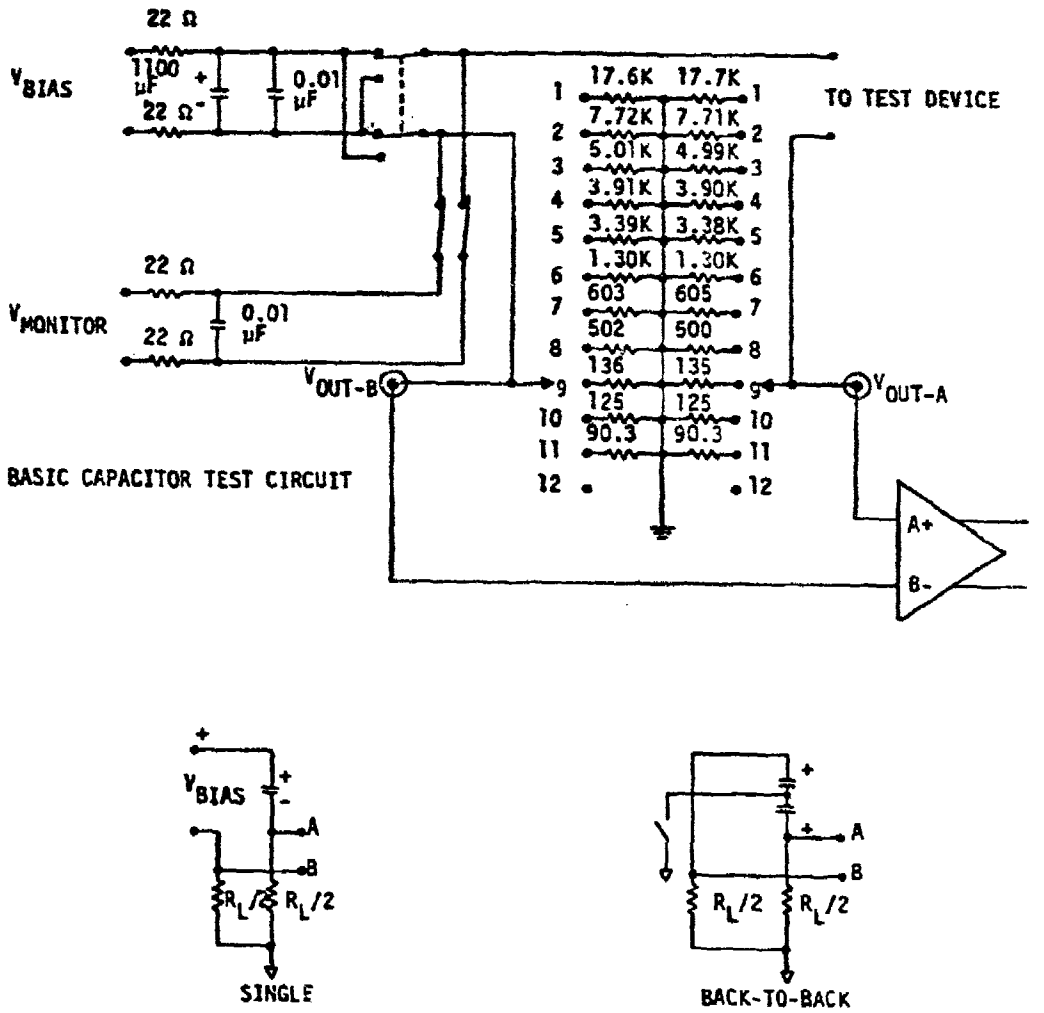

Figure A-2. Schematic of capacitor test circuit and simplified diagrams of test circuits

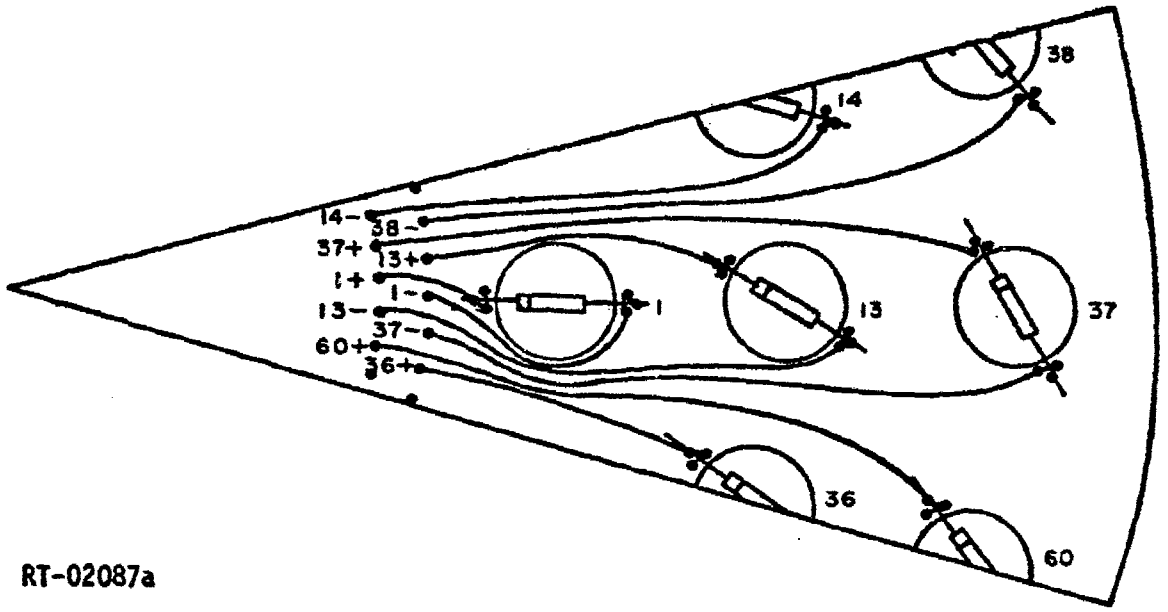

RT-02087a

Figure A-3. Capacitor positioning for biased single capacitor tests

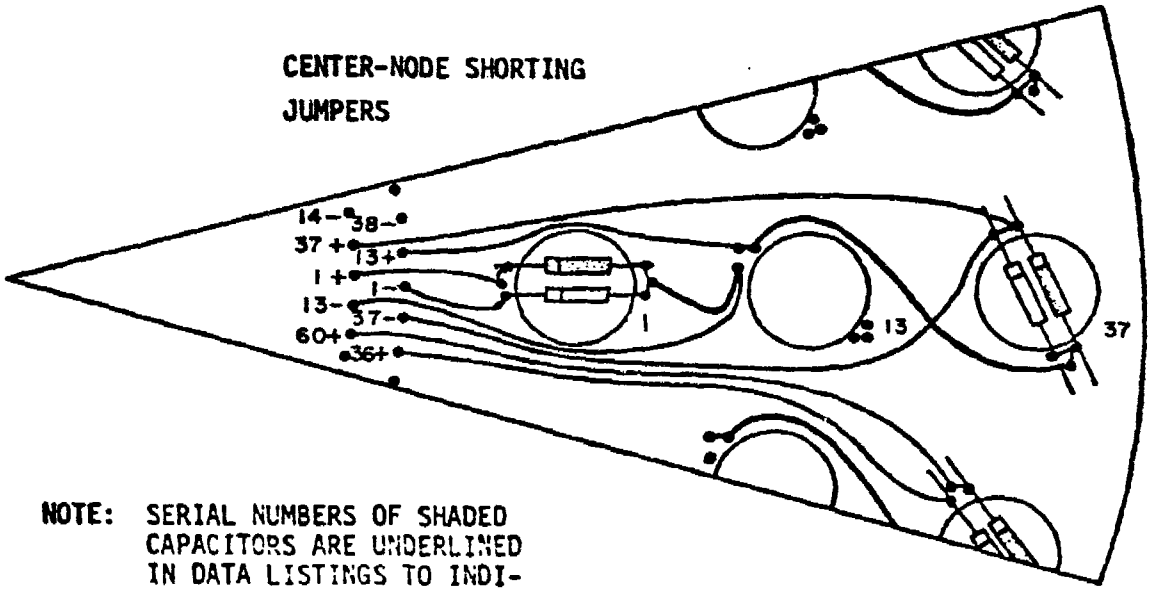

NOTE: SERIAL NUMBERS OF SHADED CAPACITORS ARE UNDERLINED IN DATA LISTINGS TO INDICATE CAPACITOR TIED TO -B AMPLIFIER UNIT.

RT-02088

Figure A-4. Capacitor positioning for back-to-back pairs

Corrected Pages AD-911497L

Table 9

NEUTRON RESPONSE EXPERIMENT

Capacitor Positions	Mfr.	C (μF)	W. V. V	dV/dγ mV / rad(CaF_2)	dV/dγ mV / rad(Ta_2O_5)	mV / n/cm^2	rad(Ta_2O_5)* / n/cm^2	rad(Ta_2O_5)** / n/cm^2
1	Sprague	100	10	0.050	0.032	7.8×10^{-12}	1.8×10^{-10}	1.4×10^{-11}
2	Sprague	100	10	0.050	0.032	8.5×10^{-12}	2.0×10^{-10}	3.8×10^{-11}
3	Sprague	100	10	0.050	0.037	9.4×10^{-12}	2.1×10^{-10}	9.1×10^{-11}
4	Sprague	100	10	0.053	0.034	8.5×10^{-12}	1.9×10^{-10}	1.4×10^{-11}
6	Sprague	100	10	0.050	0.032	7.4×10^{-12}	1.7×10^{-10}	1.6×10^{-11}
7	Sprague	100	10	0.055	0.035	8.9×10^{-12}	1.9×10^{-10}	1.6×10^{-11}
8	Kemet	39	35	0.031	0.020	4.6×10^{-12}	2.3×10^{-10}	1.7×10^{-12}

*Upper limit

**Based on calculation of γ-dose

If these numbers are used to calculate the fluence to dose conversion, the numbers in the last column of Table 9 are obtained.

Hence, the value from these experiments based on gamma yield calculations is about 1×10^{-11} rad(Ta)/n/cm^2 for the APFA spectrum. This is not too far from the predicted value. The upper limit (assuming the neutron-to-rad conversion for the TLD) is 2×10^{-10} rad(Ta)/n/cm^2.

6.2 CIRCUIT MODEL FOR TANTALUM CAPACITOR RADIATION RESPONSE

Circuit models have been developed to describe the radiation response of a tantalum capacitor by R. Leadon (Refs. 1,7) and R. Baker (Refs. 7,8). These models represent the capacitor in terms of circuit components which generate currents, store charge, etc., as required, and they represent the observed transient response with considerable accuracy. However, obtaining appropriate parameters for the models from experimental data is not straightforward and thus makes the models somewhat difficult to use. A simpler approach based on results from this program and from Baker's work (Ref. 8) was applied by H. Sugar (Ref. 9). Sugar's model describes the radiation response in terms of a single time-dependent current generator. This latter approach is somewhat easier to use and is an approach which will be pursued here.

In sugar's model, the initial conductivity is represented by an impulse function, followed by a current which decays as $\exp(-t/\tau_2)$. The final current generator expression appears as follows.

$$I(t) = CV_\rho/t_0 + V_\rho C \left(\frac{1}{RC} - \frac{1}{\tau_2}\right)\exp(-t/\tau_2) \qquad (10)$$

where

$$V_\rho = (V_0 + a)\,[1-\exp(-K\gamma)]\ , \qquad (11)$$

I = the current as function of time,

C = the capacitance,

t_0 = a time chosen to be shorter than RC (the precise value is not important),